UNIVERSITÀ DEGLI STUDI DI SALERNO
DIPARTIMENTO DI INGEGNERIA INDUSTRIALE
VIA PONTE DON MELILLO 84084, FISCIANO
SALERNO

DOTTORATO IN SCIENZE MATEMATICHE, FISICHE E INFORMATICHE
CURRICULUM FISICA DEI SISTEMI COMPLESSI E DELL'AMBIENTE
CICLO XI NUOVA SERIE

PhD Thesis in

Quantumness
of Gaussian and non-Gaussian states
in the optical domain

CANDIDATE:
Daniela Buono

SUPERVISOR:
Prof. Silvio De Siena

COORDINATOR:
Prof. Patrizia Longobardi

2012-2013

An 'Active': "I want to be free, free as a man.
As evolved man over which rises up with the intellect
that defies nature by undisputed force of the science
wearing the excitement of spacing without limits in the cosmos
and convinced that the power of thought is the only freedom "
An 'He does not know': "Freedom is not to be on a tree,
not even a action or an invention,
freedom is not free space,
Freedom is participation."

[Un 'Impegnato': "Vorrei essere libero, libero come un uomo.
Come l'uomo più evoluto che si innalza con la propria intelligenza
e che sfida la natura con la forza incontrastata della scienza,
con addosso l'entusiasmo di spaziare senza limiti nel cosmo
e convinto che la forza del pensiero sia la sola libertà"
Un 'Non so': "La libertà non è star sopra un albero,
non è neanche un gesto o un'invenzione,
la libertà non è uno spazio libero,
libertà è partecipazione."]
Giorgio Gaber, Libertà è partecipazione, Dialogo tra un impegnato ed un non so.

CONTENTS

LIST OF TABLES

LIST OF FIGURES

Part I

Preamble

0.1 *Introduction*

It is now ascertained that quantum mechanics is a powerful tool in the Information and Communication theory. The quantum properties of light radiation allow to implement, relatively easily and with high efficiency, large part of Quantum Information protocols, developed to make possible the transfer of information to a point arbitrarily far away. Many of the properties, which make the quantum theory an instrument so precious, are related to the linear nature of the theory. It is this linear nature the main cause of the existence of most of the quantum paradoxes, included the celebrated *EPR paradox*. As is well known, this paradox arises, in 1935, with the *interrogative*-paper [1] of Einstein-Podolsky and Rosen EPR *Can Quantum-Mechanical Description of Physical Reality Be Considered Complete?* Authors' aim was to demonstrate the incompleteness of Quantum Theory. The scientific history of the last seventy-eight years shows that EPR did not reach their goal, but they paved the way for the discovery of genuinely quantum correlations, which Schrodinger [2] called *entanglement*. Such correlations are the basis of most efficient protocols developed to date in the field of quantum mechanics. An entangled state is such that it cannot be factorized into pure local states of which it is composed. This is because the subsystems share quantum correlations. The Quantum Information theory exploits such nonclassical correlations to encode, to process and to distribute information by techniques that are impossible to implement, or that give very inefficient results, in the context of classical physics. For this reason, in the last decades, many efforts have been aimed at the production of entangled quantum states and at the study of the quantum properties that take a quantum state to become a efficient resource in the Quantum Information protocols. What is the best quantum resource to use depends on the protocol that we choose and on the purpose we want to achieve.

A protocol widely studied in Quantum Information is arguably the quantum teleportation. As is known, the no-cloning theorem, which is a direct consequence of the postulates of quantum mechanics, forbids, in agreement with the theorem of quantum non-discrimination, to create an exact duplicate of an unknown quantum state. However, it is possible to transfer the quantum state from a system to another system, provided, of course, the no-cloning theorem is respected.This implies that the information in the original system must be destroyed. The quantum teleportation is a technique that allows, under certain restrictions, to transfer a quantum state from one system to another one arbitrarily far away. This protocol is based on the fact that the two parts, called Alice and Bob, between which it must take place the transfer of the state, share an entangled state, that is the resource of the protocol.

Quantum states can be divided into two main categories: Gaussian states and non-Gaussian states. The state describing a system belongs to one either category depending on the statistical distribution of the observable of the state. Gaussian states play an exceptional role in Quantum Information theory. They are easy to

produce and control in the laboratory. Indeed they can be obtained in nonlinear processes such as parametric amplifiers, in which a nonlinear medium is allocated in an optical cavity providing an optical parametric oscillator OPO. Such systems, in a semiclassical approach, are described by bilinear Hamiltonians, thus realize the paradigm for the Gaussian state generation. In particular, below threshold a single continuous-wave OPO, generating squeezing in a fully degenerate operation can give rise to a pair of bright cv entangled beams in the nondegenerate case. It leads to states that represent robust resources for implementing different Quantum Information and Communication tasks. These states, however, also suffer from some limitations, both technical (which occurs if we try to generate states with very high degree of entanglement) and intrinsic properties of the quantum theory (*Extremality of Gaussian Quantum States* [3]). In this context, a appropriately sculptured non-Gaussianity can become a resource for the efficient implementation of the quantum protocols. All quantum states that can not be described by a Gaussian distribution function are non-Gaussian states. To identify the special features that bring a non-Gaussianity to be a resource in Quantum Information is not easy. In recent years many efforts have been made in the analysis of quantum properties of classes of non-Gaussian states and in the engineering of experimental schemes, making it possible to easily prepare and control non-Gaussian states in the laboratory. Many advances have been made both in terms of experimental and theoretical aspects. In the theoretical framework the features, whose must enjoy a quantum state to be an optimal resource of quantum teleportation, have been identified [4], in the context of continuous variables. A new class of states, the *Squeezed Bell states* [4], has been proposed. It is able to offer a probability of success of the teleportation protocol BKV greater than that provided by the main known Gaussian and non-Gaussian resources [4], [5]. In the experimental framework, some non-Gaussian quantum states have been implemented and, in parallel, some techniques which avoid the use of optical active means (such the OPO) have been developed. The crucial point of the experimental reality, at least with regard to the continuous variables cv quantum optics, is the impossibility to produce, realistically speaking, pure states. This occurrence leads to the new interpretations of many physical concepts and opens many questions in Quantum Information. For example, the definition of an entangled state is conceptually connected to pure states. The properties of these states are described by wave functions. All the gedanken experiments that we can think to realize for testing the different theoretical aspects of the entanglement lead to a same entanglement measure, but the pure entangled states, discussed in such experiments, are an idealization. The states we can prepare and manipulate in the laboratory are not pure but mixed, so we cannot expect to observe precisely the phenomenon introduced by the theory. The experimental entanglement tests, especially in the cv regime, are described in terms of density matrices rather than wave functions. It is necessary becouse the systems interact with the environment and/or observers,

therefore they undergo decoherence phenomena departing far from the ideal concept of pure states. In optics the most common process leading to decoherence is the phase-insensitive loss of photons through diffusion and absorption mechanisms. This process is described by a Lindblad equation for the evolution of the field operators that translates into a Master equation for the state density matrix.

This Dissertation collects my personal both theoretical and experimental contributions, in the context of the Quantum Information theory and, more generally, of the Quantum Optics in continuous variables. In this context, I have dealt with various issues related to the efficiency of realization of quantum information protocols. Much of the research has been aimed at identifying the resources that allow to realize quantum teleportation with a highest probability of success. For this reason we proceeded to the study of quantum quantities that influence the success rate of teleportation of a quantum state, in the protocol BKV.

The quantum resources, as we said so far, can be divided in two main classes: Gaussian resources and non-Gaussian ones. My research activity has been structured in which way to be able to proceed, in parallel, to the analysis of both classes.

This Dissertation is organized as follows.

After describing some basic concepts of the quantum theory (chapter 1) in order to clarify the context in which it was carried out the results of the research, in the chapter 2 we explore the concept of quantum state as resource. We investigate the properties that allow to distinguish between classical states and non-classical ones (§ 2.1). Then we analyze, in more detail, the features that define the *quantumness* of a state as, for example, the *mutual information* (§ 2.2) and the *quantum discord* (§ 2.3). We clarify the difference between entanglement measure and entanglement criteria. Then we describe, in the formalism of the characteristic function, the protocol of entanglement swapping, through which it is possible to transfer the entanglement from two couples of entangled modes to one couple of unentangled modes. Quantumness and nonlocality are two closely related concepts. So we try to clarify some aspects of this relationship. We complete the chapter with a description of the protocol of quantum teleportation. In the first two chapters we lay the foundations in order to proceed to the description of the original findings. We can divide such description into two main parts.

The first part (chapters 3 and 4) is dedicated to the results carried out on the pure and mixed Gaussian resources.

To date there isn't a single measure that quantifies the entanglement of mixed states and various measures have been suggested in the literature, they are not easy to apply and provide sometimes conflicting results. To assess the presence of entanglement in a quantum system it is possible to refer to the many criteria proposed in the literature. The criteria are often the most used tool, in the experimental Quantum Optics field, to evaluate the quality of entanglement of a

quantum-optical system. In chapter 3 we study some of the main criteria generally used for Gaussian bipartite mixed states. This study has allowed us to establish a hierarchy very useful for the evaluation of the entanglement [6]. Then we have discussed and experimentally analyzed the effects of the transmission over a lossy channel on the quantumness of bipartite Gaussian cv optical entangled states, focusing our analysis on the states generated by a type-II OPO [7]. The obtained results are reported in [6], [8]. Eventually, in chapter 4, it is reported the study of the Bell's inequality in terms of purity and entanglement for a bipartite Gaussian state. The need to begin such a study comes two considerations: the deterioration of the purity of a quantum state greatly affects the performance of the system associated with that state; the entanglement is not the only type of genuinely quantum correlation present in quantum systems. It becomes necessary, therefore, to investigate how the "quantumness" owned by a state, established by the violation of Bell's inequality, is related to the purity of the state and to the entanglement. The obtained results are reported in [9].

The second part (chapters 5, 6, 7 and 8) is dedicated to the results carried out on non-Gaussian resources. The study of non-Gaussian resources mainly related to a particular class of states: the squeezed Bell states. All the analysis carried out to date show that these states are one of the best possible resources for efficient cv quantum teleportation protocol BKV. We proceed as described below. In order to assess which quantum resource allows to have a higher probability of success in the quantum teleportation of a coherent state, have processed the following two theoretical tests:

1. In chapter 5 we report the study of the behavior of the Bell's inequality for the whole class of states obtained by the *squeezed Bell states*. Such study makes possible to determine what is the quantum resource that maximizes the violation of the inequality, i.e. which is the most "non-local resource" among all those considered. The results are collected in a paper of next submission [10].

2. In the chapter 6, we analyze the performances of teleportation provided by Bell squeezed resource, when it is subjected to two cascade protocols: at first the squeezed Bell undergoes a swapping process; then the swapped state is used as resource in a quantum teleportation protocol. The result is compared with that provided by the other main quantum swapped resources. The results are collected in a paper of next submission [11].

   to understand how a resource behaves after undergoing a process of swapping is very useful becouse error probability, in a transmission channel, scales with the length of the channel. However it is possible to divide the channel into segments of shorter length and applying a protocol of entanglement swapping to restore the lost entanglement. This test is particularly useful to reconfirm

the squeezed Bell states as one of the best resources suitable in quentum Information, implemented within quantum theory quantum information.

As a consequence of the positive results of the two studies conducted to investigate the "quantum qualities" of the class of the squeezed Bell states, we have proceeded (chapter 7) to the design of an experimental scheme of engineering, that is capable to produce bimodal state, similar to squeezed Bell one. The analysis of the ideal scheme has been expanded to the realistic case by introducing all possible contributions of losses, decoherence effects and detection for evaluating the actual "experimental feasibility" of the sculptured resource and to provide, with good approximation, the desired squeezed Bell state.The results are reported in a paper of next submission [12].

In the chapter 8 it is reported the study of different types of non-Gaussian states. In fact, the investigation of the technical limitations, that afflict the OPOs sources, for the generation of Gaussian states with a high degree of entanglement, has allowed us to understand that these "inconveniences", under appropriate conditions, can become a resource for the generation of non-Gaussian states . These considerations have led to the study of non-Gaussianity produced by fluctuations of pump beam in a sub-threshold OPO. We have assumed to use this particular non-Gaussian state as a resource for the teleportation of a coherent state. The obtained fidelity, i.e. the probability of success of the teleportation, is greater than that of a Gaussian resource. This result has allowed to discover a new type of non-Gaussian resource, capable of realizing quantum teleportation with a high probability of success.

Eventually, the conclusions of the entire Dissertation are drawn.

CHAPTER 1

PRELIMINARIES

In a outlook, that can be called *positivistic*, because it coincides with the attitude at first adopted by logical positivists, we can divide any physical theory into the following constituents: (*a*) the *formalism*, expressed in terms of primitive concepts; (*b*) the *rules of deduction*, enabling us to derive theorems by manipulating the symbols associated to the formalism; (*c*) the *dynamical law*, imposing additional restrictions on values which can be taken by some primitive concepts; (*d*) the *correspondence rules,* establishing the link between experience and theory [13].

In this chapter, we present some of these constituents in the context of the Quantum Theory. They are preliminaries and allow us to introduce concepts as continuous variables (see § 1.1.1), pure and mixed states (§ 1.1.2), Gaussian and non-Gaussian states (in § 1.1.2.1 and 1.1.2.2), and notations that will be frequently used throughout the Dissertation.

1.1 Observables and States

In this section we introduce the primitive quantum concepts of observable and state, by establishing the link between the mathematical formalism and the physical meaning [14].

1.1.1 Observables

An observable is rappresented by a self-adjoint operator on a Hilbert space with spectral representation

$$O = \sum_n o_n P_n,$$

where P_n are orthogonal projectors of O,

$$P_n = \sum_a |a, o_n\rangle \langle a, o_n|,$$

with o_n eigenvalues of O and the parameter a labels the degenerate eigenvectors belonging to the same eigenvalue of O. An observable has a complete orthogonal set of eigenvectors. An observable is a theoretical construct, whose domain of definition is a subset of a set of the real numbers, called *spectrum* of the observable, and which is associated, by means of given correspondence rules, with one or more *measurable quantities*.

The sums become integrals in the case of continuous spectra.

So the observables of quantum systems can posses either a discrete or a continuous spectra. The quantum electromagnetic fields have both the continuous and discrete degrees of freedom. For example, the photon number of the field gives discrete outcomes whereas measurements of the field's quadrature provide continuous outcomes. A physical model that takes advantage of both the degrees of freedom is called hybrid. In this dissertation we'll refers mainly to the continuos degrees of freedom of the quantum electromagnetic field.

1.1.2 The quantum state

The state of a physical system is the mathematical description of the knowledge one has of it. It is represented by a self-adjoint, non-negative definite, and of unit trace operator. This implies that any state operator, called also *density matrix* ρ, may be diagonalized in terms of its eingenvalues and eigenvectors,

$$\rho = \sum_n \rho_n \left| \phi_n \right\rangle \left\langle \phi_n \right|, \tag{1.1}$$

with $0 \leq \rho_n \leq 1$ and $\sum_n \rho_n = 1$. For a pure state, the statistical operator ρ is idempotent, $\rho^2 = \rho$, so there is exactly one non zero eigenvalue of ρ, i. e. $\rho_n = 1$, $\rho_{n'} = 0$ for $n \neq n'$. A pure state may be represented by wave vector $\left| \phi \right\rangle$ in the Hilbert space such as $\rho = \left| \phi \right\rangle \left\langle \phi \right|$. A generic state, which is not pure, is called mixed. Density matrix formalism encopasses the possibility of describing both pure and mixed states. In this context it becomes very important to introduce the parameter *purity* μ,

$$\mu = Tr[\rho^2], \tag{1.2}$$

such as

$$\frac{1}{N} \leq \mu \leq 1 \tag{1.3}$$

with N dimension of the Hilbert space, $\mu = 1$ only for pure states. In the context of the continuous variables $0 \leq \mu \leq 1$. The purity assumes a relevant role in quantum information protocols, indeed the fidelity, i.e. the rate of success of the protocol, depends critically on the purity of the all involved states.

An description, alternative to operatorial one, of the state is given in terms of the characteristic function $\chi(\boldsymbol{\lambda}) = Tr[\rho D(\boldsymbol{\lambda})]$, where $D(\boldsymbol{\lambda})$ is the displacement operator, that for n bosons is defined by

$$D(\boldsymbol{\lambda}) = \bigotimes_{k=1}^{n} D_k(\lambda_k),$$

where $\boldsymbol{\lambda}$ is the column vector $\boldsymbol{\lambda} = (\lambda_1, ..., \lambda_n)^T$, $\lambda_k \in \mathbb{C}$, $k = 1, ..., n$ and $D_k(\lambda_k) = exp\{\lambda_k a_k^\dagger - \lambda_k^* a_k\}$, with the field mode operator a such that $\left[a_k, a_l^\dagger \right] = \delta_{kl}$.

The characteristic function is also known as the moment-generating function, since its derivatives in the origin of the complex plane generate symmetrically ordered moments of the mode operators,

$$(-)^q \frac{\partial^{p+q}}{\partial \lambda_k^p \partial \lambda_l^{*p}} \chi(\boldsymbol{\lambda}) \bigg|_{\boldsymbol{\lambda}=\mathbf{0}} = Tr[\rho[(a_k^\dagger)^p a_l^q]_S], \tag{1.4}$$

where, for the first non trivial moments we have $\left[a^\dagger a\right]_S = \frac{1}{2}(a^\dagger a + aa^\dagger)$, $\left[aa^{\dagger 2}\right]_S = \frac{1}{3}(a^{\dagger 2}a + aa^{\dagger 2} + a^\dagger aa^\dagger)$, $\left[a^\dagger a^2\right]_S = \frac{1}{3}(a^2 a^\dagger + a^\dagger a^2 + a^\dagger a)$ [15].

The Fourier transform of the characteristic function is called *Wigner distribution*,

$$W(\boldsymbol{\alpha}) = \int_{\mathbb{C}^n} \frac{d^{2n}\boldsymbol{\lambda}}{\pi^{2n}} \exp\{\boldsymbol{\lambda}^\dagger \boldsymbol{\alpha} + \boldsymbol{\alpha}^\dagger \boldsymbol{\lambda}\} \chi(\boldsymbol{\lambda}). \tag{1.5}$$

1.1.2.1 Bipartite Gaussian State

A continuous-variable Gaussian bipartite state ρ_{ab} is two-mode state, on the Hilbert space $\mathcal{H} = \mathcal{H}_a \otimes \mathcal{H}_b$, that has a representation in terms of Gaussian characteristic function or, equivalently, Gaussian Wigner function

$$W(\mathbf{K}) = \frac{\exp\{-\frac{1}{2}\mathbf{K}^T \boldsymbol{\sigma}^{-1}\mathbf{K}\}}{2\pi\sqrt{Det[\boldsymbol{\sigma}]}}$$

where $\boldsymbol{\sigma}$ is the covariance matrix and $\mathbf{K} \equiv (X_a, Y_a, X_b, Y_b)$ is the vector of the amplitude and phase field quadratures for mode a and b respectively. We have considered null the first moments. In quantum optics, the quadrature operator assumes the role of the dimensionless variables position q and momentum p. It is defined as follow:

$$\widehat{X}_\vartheta \equiv \frac{\widehat{a}e^{i\vartheta} + \widehat{a}^\dagger e^{-i\vartheta}}{\sqrt{2}}. \tag{1.6}$$

For $\vartheta = 0$, $\widehat{X}_0 = \widehat{X}$, called *amplitude* quadrature, is identical to adimensional position operator $\widehat{q}$, whereas, for $\vartheta = \pi/2$, $\widehat{X}_{\pi/2} = \widehat{Y}$, called *phase* quadrature, is identical to the adimensional momentum operator $\widehat{p}$. From commutation relation $\left[a_k, a_l^\dagger\right] = \delta_{kl}$ results that $[X, Y] = i$.

All the quantum features of a Gaussian state can be retrieved experimentally by measuring the first and second order statistical momenta of the field quadratures, i.e. the covariance matrix (**CM**) $\boldsymbol{\sigma}$

$$\boldsymbol{\sigma} = \begin{pmatrix} \boldsymbol{\alpha} & \boldsymbol{\gamma} \\ \boldsymbol{\gamma}^\top & \boldsymbol{\beta} \end{pmatrix}, \tag{1.7}$$

with elements $\sigma_{hk} \equiv \frac{1}{2}\langle\{K_k, K_h\}\rangle - \langle K_k\rangle\langle K_h\rangle$, where $\{K_k, K_h\} \equiv K_k K_h + K_h K_k$ is the anti-commutator; $\boldsymbol{\alpha}$ and $\boldsymbol{\beta}$ are the covariance matrices associated to the

reduced state of the subsystems a and b, while $\boldsymbol{\gamma}$ describes the correlation between the two subsystems. For this reason they are of great practical relevance, being feasible to produce and control with linear optical elements. Moreover this state appears naturally in every quantum system which can be described or approximated by a quadratic Bosonic Hamiltonian. Important examples include vacua, coherent, squeezed, thermal, and squeezed-thermal states of the electromagnetic field.

To study the correlation between the two modes of the system it is convenient, at first, to transform the Gaussian state into some standard forms through local symplectic operations, that is transformations preserving canonical commutation relations of the quadratures. Any Gaussian state ρ_G can be trasformed, through symplectic transformations, into the standard form

$$\boldsymbol{\sigma} = \begin{pmatrix} n & 0 & c_1 & 0 \\ 0 & n & 0 & c_2 \\ c_1 & 0 & m & 0 \\ 0 & c_2 & 0 & m \end{pmatrix}. \tag{1.8}$$

The quantities n, m, c_1 and c_2 are determined by the four local symplectic invariants $I_1 \equiv \det(\boldsymbol{\alpha}) = n^2$, $I_2 \equiv \det(\boldsymbol{\beta}) = m^2$, $I_3 \equiv \det(\boldsymbol{\gamma}) = c_1 c_2$, $I_4 \equiv \det(\boldsymbol{\sigma}) = (nm - c_1^2)(nm - c_2^2)$. Hereafter, whenever we refer to **CM** we will intend the standard form covariance matrix (1.8) if not differently specified. As we mentioned above the purity of the state, and so also the condition Eq.(1.3), becomes a essential constraint to establish the physicity of the state under investigation.

For a Gaussian state Eq. (1.2) reads

$$\mu(\sigma) = \frac{1}{4\sqrt{Det\,[\sigma]}}. \tag{1.9}$$

From Eq. (1.3) we obtain the following constraint on the symplectic invariant I_4:

$$\sqrt{I_4} \geq \frac{1}{4}. \tag{1.10}$$

1.1.2.2 Non-Gaussian States

All states that do not have a Gaussian Wigner function are called non-Gaussian nG states. As we will see in the following of Dissertation, non-Gaussianity is revealing itself as a resource for continuous variable Quantum Information. For this reason there needs a measure able to quantify the non-Gaussian character of a quantum state.

Departures from Gaussian statistics may be noted by the observation of the higher moments than the second one. It is possible, for example, to measure the kurtosis, i. e. the fourth moment $\langle X^4 \rangle$ and to evaluate the kurtosys excess

$\mathcal{K} = \frac{\langle X^4 \rangle}{\langle X^2 \rangle^2} - 3$. The "minus 3", at the end of this formula, is added as a correction to make the kurtosis of the normal distribution equal to zero, so $\mathcal{K}$ is zero for a Gaussian random variable, while for most (but not all) non-Gaussian random variables it takes values different from zero. Moreover, random variables with negative kurtosis are called sub-Gaussian variables, while random variables with positive kurtosis are called super-Gaussian variables. Unfortunately, to use kurtosis as nG measure presents some drawbacks. Indeed, although it is easy to evaluate by a known probability density function, it becomes more complicated to estimate it by a measured sample, becouse kurtosys may strongly depend on only a few observations in the tails of the distribution. For this reason $\mathcal{K}$ is not considered a robust measure of nG [16].

Different nG measures have been proposed to quantify the non-Gaussian character of a state, as the Hilbert-Schmidt distance D_{HS} and the quantum relative entropy S. Although D_{HS} and S are based on different quantities, they share the same basic idea: to quantify the nG of a state ρ_{NG} in terms of its distinguishability from a reference Gaussian state τ, where τ is chosen in which way that it exhibits the same covariance matrix and the same vector $\mathbf{K}$ of the non-Gaussian state ρ_{NG}[16]. In the following we describe the main measures, introduced in leterature [17] ,[16], for evaluating the non-Gaussianity of ρ_{NG}:

nG using Hilbert-Schmidt distance [17]. Let

$$\delta_{HS}[\rho_{NG}] \equiv \frac{D_{HS}^2[\rho_{NG}, \tau]}{\mu(\rho_{NG})}, \tag{1.11}$$

with $D_{HS}^2[\rho_{NG}, \tau]$ the Hilbert distance between ρ_{NG} and τ,

$$D_{HS}^2[\rho_{NG}, \tau] = \frac{1}{2}Tr\left[(\rho_{NG} - \tau)^2\right] = \frac{\mu(\rho_{NG}) + \mu(\tau) - 2\kappa[\rho_{NG}, \tau]}{2},$$

where μ denotes the purity of the corresponding state and $\kappa[\rho_{NG}, \tau]$ is the overlap between ρ_{NG} and τ, $\kappa[\rho_{NG}, \tau] = Tr[\rho_{NG}\tau]$.

nG using quantum relative entropy. Let

$$\delta_S[\rho_{NG}] \equiv S(\rho_{NG}||\tau) = Tr[\rho_{NG}\ln\rho_{NG}] - Tr[\rho_{NG}\ln\tau] = S(\tau) - S(\rho_{NG}), \tag{1.12}$$

where $S(\rho_{NG}||\tau) \equiv Tr[\rho_{NG}(\ln\rho_{NG} - \ln\tau]$ is the quantum relative entropy, i. e. the quantum entropy relative to the Gaussian reference τ, and $S(\rho)$ is the von Neumann entropy of the state ρ, $S(\rho) = -Tr_{\mathcal{S}}[\rho_{\mathcal{S}}Log\rho_{\mathcal{S}}]$.

Although the two measures $\delta_{HS}[\rho_{NG}]$ and $\delta_S[\rho_{NG}]$ capture, in general, the same qualitative non-Gaussian behavior [16], they induce different ordering on the set of quantum states; that is, it is possible to obtain $\delta_{HS}[\rho_{NG1}] > \delta_{HS}[\rho_{NG2}]$ and $\delta_S[\rho_{NG1}] < \delta_S[\rho_{NG2}]$, or viceversa, with ρ_{NG1} and ρ_{NG2} two different non-Gaussian states. This is probably due to the fact that different measures correspond to different operational meanings of non-Gaussianity: δ_{HS} takes in account the higher

moments of the distribution, while δ_S is based upon the fact that Gaussian distributions maximize the von Neumann entropy at fixed covariance matrix.

However, the two measures are connected one to each other by means of the inequality $S(\rho_{NG}||\tau) \geq D^2_{HS}[\rho_{NG}, \tau]$, i.e. $\delta_S[\rho_{NG}] \geq \delta_{HS}[\rho_{NG1}]\mu(\rho_{NG})$, that for pure states becomes $\delta_S[\rho_{NG}] \geq \delta_{HS}[\rho_{NG1}]$.

1.2 Dynamical law

In this Section we review the suitable formalism [18], [19] to describe the transmission of an arbitrary quantum state between regions spatially separated.

Any physical operation that reflects the time evolution of the state of a quantum system can be regarded as a channel. In particular, the study of quantum channels is useful to understand how quantum states are modified when subjected to noisy quantum communication lines.

The evolution of an arbitrary two-mode state is an irreversible process, the study of which requires the use of the open systems theory. In this context, we can postulate an weak coupling g_j of the considered system S with a reservoir (bath) R made of large number of external modes. In particular we assume:

○ *Born approximation* - the coupling between system and environment is so weak that the density matrix ρ_R of the environment is negligibly influenced by the interaction. This approximation allows to write the state $\rho_{SR}(t)$ of the global system as $\rho_{SR}(t) \approx \rho_S(t) \otimes \rho_R$;

○ *Markov approximation* - the time development of the state of the system at time t only depends on the present state $\rho_S(t)$. This approximation is justified if the time scale τ over which $\rho_S(t)$ varies appreciably under the influence of the bath is large compared to the time scale τ_R over which the bath forgets about its past, $\tau \gg \tau_R$.

○ *Secular approximation (rotating wave approximation)*- the typical time scale τ_S of the intrinsic evolution of the system S is small compared to the relaxation time τ.

These assumptions are typically satisfied for quantum optical systems and allow to obtain the equation of the Kossakowski-Lindblad, that describes the time evolution in noisy channel of the bipartite quantum state ρ_S in the interaction picture

$$\dot{\rho}_S = \sum_{k=1,2} \frac{\Gamma_k}{2} \left\{ (N_k + 1)\mathcal{L}[a_k] + N_k\mathcal{L}\left[a_k^\dagger\right] - M_k^*\mathcal{D}[a_k] - M_k\mathcal{D}\left[a_k^\dagger\right] \right\} \rho_S \ ,$$

where Γ_k denotes the damping rate of the $k-$mode, $N_k \in \mathbb{R}$ and $M_k \in \mathbb{C}$ are, respectively, the effective photons number and the squeezing parameter of the reservoir b. $\mathcal{L}[O]$ is the Lindblad superatoroperator defined by $\mathcal{L}[O]\rho \equiv 2O\rho O^\dagger - O^\dagger O\rho - \rho O^\dagger O$ describing losses and linear, phase insensitive, amplification processes and $\mathcal{D}[O]\rho \equiv 2O\rho O - OO\rho - \rho OO$ takes in account phase de-

pendent fluctuations. We have considered that each mode evolves independently in its channel and there aren't correlations among noises in different channels.

In the chapter 3 we describe the our experimental implementation [6], [8] of a quantum channel. In such case, we had a thermal reservoir, i. e. $M_k = 0$. So, at the room temperature, i. e. $N_k \simeq 0$, the evolution of system S is described by the equation of motion

$$\dot{\rho} = \sum_{k=1,2} \frac{\Gamma_k}{2} \mathcal{L}\left[a_k\right] \rho, \tag{1.13}$$

where Γ_k is the damping rate of the trasmission channel of the $k-$mode ($k = 1, 2$). From now on, we consider that the damping rates don't depend of the channel, $\Gamma_k = \Gamma$ (for $k = 1, 2$).

In the formalism of the Wigner function Eq.(1.5), the Eq. (1.13) becomes the *Fokker-Planck equation*,

$$\partial_t W\left(\mathbf{R}, t\right) = \frac{\Gamma}{2}\left(\partial_{\mathbf{R}}^\top \mathbf{R} + \frac{1}{2}\partial_{\mathbf{R}}^\top \partial_{\mathbf{R}}\right) W\left(\mathbf{R}\right) \tag{1.14}$$

$$= \frac{\Gamma}{2}\left(\partial_{\mathbf{R}}^\top \mathbf{R} + \frac{1}{2}\nabla_{\mathbf{R}}^2\right) W\left(\mathbf{R}\right),$$

where $\partial_{\mathbf{R}}^\top = (\partial_{X_1}, \partial_{Y_1}, \partial_{X_2}, \partial_{Y_2})$ and $\nabla_{\mathbf{R}}^2 = \partial_{\mathbf{R}}^\top \partial_{\mathbf{R}} = \partial_{X_1}^2 + \partial_{Y_1}^2 + \partial_{X_2}^2 + \partial_{Y_2}^2$.

1.3 Uncertainty priciple

Let A and B be two hermitian, not compatible operators, i.e such that their commutator is not null. The condition $[A, B] \neq 0$ prevents the two operators have simultaneous eigenvectors. However, we can estimate how much the eigenvector of A is far from that of B. When $|\psi\rangle$ is eigenvector of A, the variance is zero, i.e. $\langle\psi| A^2 |\psi\rangle = \langle\psi| A |\psi\rangle^2$. So the variance is a measure of how close we are to an eigenvector. We can define the following operators: $a \equiv \Delta A = A - \langle A\rangle$ and $b \equiv \Delta B = B - \langle B\rangle$. They allow us to neglect the mean value without loss of generality[1],

$$\langle\Delta J\rangle = 0$$
$$\langle(\Delta J)^2\rangle = \langle J^2\rangle - \langle J\rangle^2 = \langle j^2\rangle,$$

with $J = A, B$ and $j = a, b$. We obtain

$$\Delta A \Delta B \equiv \sqrt{\langle\psi| A^2 |\psi\rangle \langle\psi| B^2 |\psi\rangle}$$
$$= \sqrt{\langle A\psi | A\psi\rangle \langle B\psi | B\psi\rangle}$$
$$\geq |\langle A\psi | B\psi\rangle|.$$

---

[1]the variances don't change.

In the last line, we have invoked the *Cauchy-Schwarz inequality*, in view of the which we obtain

$$\Delta A \Delta B \geq |\langle \psi| AB |\psi\rangle| .$$

Now, we consider the following operators $O_1 \equiv \frac{1}{2}[a,b]$ and $O_2 \equiv \frac{1}{2}\{a,b\}$, where the braces $\{...\}$ refer to the anti-commutator. They are antihermitian and hermitian, respectively,

$$
\begin{aligned}
O_1 &\equiv \frac{1}{2}[a,b] = -\frac{1}{2}(ba - ab) = -\frac{1}{2}(ab)^\dagger - \frac{1}{2}(ba)^\dagger = -O_1^\dagger, \\
O_2 &\equiv \frac{1}{2}\{a,b\} = O_2^\dagger,
\end{aligned}
$$

so it is clear that the eigenvalue of $O_1 + O_2 = ab$ is the sums of an pure immaginary number and pure real one. Since the magnitude of a complex number is greater than or equal to the magnitude of its imaginary part, we can write

$$\langle (\Delta A)^2 \rangle \langle (\Delta B)^2 \rangle \geq \frac{1}{4} \langle [A,B] \rangle^2 + \frac{1}{4} \langle \{a,b\} \rangle$$

with $\langle \{a,b\} \rangle \geq 0$. From which we obtain the following inequality

$$\langle (\Delta A)^2 \rangle \langle (\Delta B)^2 \rangle \geq \frac{1}{4} \langle [A,B] \rangle^2 , \tag{1.15}$$

that is the *uncertainty Heisenberg's principle*. Physically realizable quantum states must comply with this inequality. It then provides information on the *physicality* of the analyzed quantum state.

We note that the inequality Eq.(1.15) was obtained for pure states [20],[21]. It has been demonstrated to be valid also for mixed states [22]. However, in the case of pure states it is able to provide useful informations about the nature of the state under consideration. For example it can be shown that the state that minimizes the uncertainty, i. e. the state in which the inequality Eq. (1.15) is verified with the sign of equality, has Gaussian distribution. For mixed states, however, the inequality is, in general, strongly violated, so that it is not possible to extract useful information on the distribution. Moreover, in the mixed state case, also the purity Eq.(1.3) contributes to the *physicality*.

We have seen that the uncertainty principle is a direct consequence of the commutation relations for non-compatible observables. As a consequence, the inequality (1.15), applied to the quadrature operators, provides $\langle (\Delta X)^2 \rangle \langle (\Delta Y)^2 \rangle \geq \frac{1}{4}$.

Uncertainty relations among canonical operators impose a constraint on the covariance matrix, in according to which $\boldsymbol{\sigma}$ represents a physical state iff

$$\boldsymbol{\sigma} + \frac{i}{2}\boldsymbol{\Omega} \geq 0 , \tag{1.16}$$

where $\boldsymbol{\Omega} = \boldsymbol{\omega} \oplus \boldsymbol{\omega}$ is the two-mode symplectic matrix, with $\boldsymbol{\omega} \equiv \begin{pmatrix} 0 & 1 \\ -1 & 0 \end{pmatrix}$.
Moreover the Heisemberg uncertainty (1.16) can be written in terms of the four symplectic invariants

$$I_1 + I_2 + 2I_3 \leq 4I_4 + \frac{1}{4}. \tag{1.17}$$

The inequalities (1.16),(1.17) ensure that $\boldsymbol{\sigma}$ is a *bona fide* **CM,** *i. e.* it describes a physical state.

However, every covariance matrix is, by definition, real symmetric positive definite. These information are stored in the constraints (1.16), (1.3), but not in the (1.17). Therefore, the use of (1.17) requires more caution. It alone does not ensure the *physicality*. It must be accompanied by the condition of positivity of the density matrix, expressed, for example, by (1.3).

1.3.1 Squeezed states

A state is squeezed in respect to the observable A if $\langle (\Delta A)^2 \rangle < \frac{1}{2} \langle [A, B] \rangle^2$. So the squeezing is the reduction of quantum fluctuations in one observable below the standard quantum limit (vacuum fluctuation) at the expense of an increased uncertainty of the conjugate variable.

Squeezed states are an example of advantageous interchange between experiment and theory in quantum optics. To be able to discuss the characteristics it is not possible don't consider the process that generates them (described briefly in the following). The squeezed states are produced through a process of **O**ptical **P**arametric **G**eneration **OPG**, in which the pump beam (typically a laser beam, which emits radiation in the coherent state $|\beta\rangle$), at the frequency ω_p,impinges on a not center-symmetric crystal. At the output of the non linear crystal two signals a and b are produced, such that the pump energy is distributed between two output,

$$\omega_p = \omega_a + \omega_b,$$

and the total momentum is preserved. When the outputs a and b are degenerate in frequency (degenerate **OPG**), and with the same wave vectors, the interacting Hamiltonian reads

$$\mathcal{H}_{int} = i\hbar \, |\varsigma\beta| \, [e^{i\phi} a^\dagger b^\dagger - e^{-i\phi} ab], \tag{1.18}$$

where we have considered the average on the input coherent state $|\beta\rangle$, $\phi = \arg(\beta) + \arg(\varsigma)$ and ς is the coupling parameter.

In according to Hamiltonian $\mathcal{H}_{int}$ Eq. (1.18) the pure two-mode squeezed vacuum state reads

$$|\psi\rangle_{ab} \equiv e^{\frac{i}{\hbar}\mathcal{H}_{int}t} = e^{|\varsigma\beta|[e^{i\phi} a^\dagger b^\dagger - e^{-i\phi} ab]t} |00\rangle. \tag{1.19}$$

We note that putting $|\varsigma\beta|\,e^{i\phi}t = re^{i\phi} \equiv \xi$, with $\xi = re^{i\phi}$ arbitrary complex number, we obtain the expression of $|\psi\rangle$, Eq. (1.19), in terms of the squeezing operator $S(\xi)$,

$$|\psi\rangle_{ab} = S(\xi)\,|00\rangle_{12}\,, \qquad (1.20)$$

with $S(\xi) = e^{\frac{1}{2}(\xi^* ab - \xi a^\dagger b^\dagger)}$. We note the module r of ξ is linked to the intensity of the pump laser beam and the phase ϕ is manipulable through delay lines, so the parameter of squeezing ξ is completely under experimental control.

Tipically modes a and b generated by an **OPG** are weak, for this reason the active medium (nonlinear crystal) is put often into an optical cavity. Under appropriate conditions the parametric interaction can overcome the effects of possible losses (i.e. absorption, diffraction...). In this case the system undergoes an oscillation and intense output beams are obtained. Such a device is called an **O**ptical **P**arametric **O**scillator (**OPO**). The modes at the output of the **OPO** are thermal modes, but their linear combination is squeezed. We express the two-mode squeezing operator $S_{ab}(-r)$ in terms of single-mode squeezing operators $S_c(r)$, $S_d(-r)$. These are obtained by introducing the annichilation operators $\hat{c}$ and $\hat{d}$ made by the superpositions

$$\hat{c} = \frac{\hat{a} + \hat{b}}{\sqrt{2}},$$

$$\hat{d} = \frac{-\hat{a} + \hat{b}}{\sqrt{2}}.$$

We have

$$S_{ab}(-r)\,|00>_{ab} = S_c(-r)\,S_d(r)\,|00>_{cd}, \qquad (1.21)$$

where $\hat{S}_k(\xi) = \exp\left[-\frac{1}{2}\xi\hat{k}^{\dagger 2} + \frac{1}{2}\xi^*\hat{k}^2\right], (k = c, d)$ is the single-mode squeezing operator. Consequently, the characteristic function that describes the state $|\psi>_{cd}$ results

$$\chi_{cd}(\beta_c; \beta_d) = \mathrm{Tr}\left[\rho_{cd}\hat{D}_c(\alpha_c)\,\hat{D}_d(\alpha_d)\right],$$

where $\rho_{cd} = |\psi>_{cd\ cd}<\psi|$. We compute the variance of the modes c and d by the characteristic function (moment-generating function). Indeed, from the relation Eq. (1.4) we obtain the following variances

$$\Delta^2 X_c = \Delta^2 Y_d = \frac{e^{2r}}{2}, \qquad (1.22)$$

$$\Delta^2 X_d = \Delta^2 Y_c = \frac{e^{-2r}}{2}. \qquad (1.23)$$

These relationships show that the squeezing operator acts attenuating the quantum noise in one direction and amplifying it in the orthogonal direction.

CHAPTER 2

STATES AS RESOURCES

In this chapter we describe the properties that allow us to evaluate the quality of a quantum resource. At first, we briefly make a distinction between classical states and non-classical ones (§ 2.1). Then, since the protocols of quantum information and communication exploit the correlations between subsystems, we analyze the main types of correlations that may arise between subsystems of a bipartite system:

- the *mutual information*, which takes into account correlations of both classical and quantum nature (§ 2.2);

- the *quantum discord*, by which we can evaluate all the genuinely quantum correlations (§ 2.3);

- The *entanglement*, that is a particular type of genuinely quantum correlation (§ 2.4).

The discussion on the entanglement is very long and complex and some issues are still under discussion in the scientific community. To date, it is still a very hot topic in the literature. In this chapter we will try to limit the description only to the special aspects useful for understanding of the topics discussed during the Dissertation. In particular, we describe some properties, of which should enjoy a good entanglement measure and some measures very considered in the literature. These concepts we will help us understand the bound to which Gaussian resources can be considered extremal compared to non-Gaussian ones (§ 3.1). Moreover the entanglement criteria (§ 2.4.1) are some of the quantum markers, used in (§ 3.2), to determine the advantages of the use of a quantum resource compared to classical one.

We describe also the *entanglement swapping protocol* (§ 2.5), which allows us to establish entanglement between two beams that share not any common past. We will analyze the consequences of the application of this protocol in chapter 6.

The concept of entanglement inevitably deals to *non locality* (§ 2.6.2). This circumstance requires a brief discussion on different forms of non-locality in the quantum theory. Moreover, it allows us to introduce a particular example of Bell's inequality (§ 2.7): the inequality CHSH (§ 2.7.1), used in Chapters 4 and 6 to investigate some quantum properties of some quantum resources.

All the features listed so far can be helpful in identifying resources actually useful quantum teleportation. It constitutes one of the central cores of the entire

Dissertation. For this reason, we conclude this chapter by describing just the continuous variables teleportation protocol (§ 2.8).

2.1 Non classicality

To express the density operator in terms of c-number functions is very useful, because it makes possible to give a representation in phase space of all operators. This approach allows a direct comparison between the classical and quantum physics.

In classical statistical physics we evaluate the averages of functions $O_{cl}(q,p)$ that depending from the phase space variables q and p with the help of the classical probability distribution $W_{cl}(q,p)$ through the relation

$$\langle O_{cl}(q,p)\rangle = \int_{-\infty}^{\infty} dq \int_{-\infty}^{\infty} dp O_{cl}(q,p) W_{cl}(q,p). \tag{2.1}$$

The role of the probability distribution of the classical phase space is taken from the quasi-probability distributions, which allow to calculate the average of an operator $\widehat{O}$ in the following way

$$\left\langle \widehat{O}(\widehat{X},\widehat{Y})\right\rangle = \int_{-\infty}^{\infty} dX \int_{-\infty}^{\infty} dY O(X,Y) W(X,Y), \tag{2.2}$$

where $\widehat{X}$ and $\widehat{Y}$ are the quadrature operators Eq. (1.6) and $O(X,Y)$ is the *c-number* representation of the operator $\widehat{O}$. Eq. (2.2) is similar to Eq. (2.1). In general, it isn't trivial to find this representation. Indeed there exist many classical forms of the same operator depending on we choose to order the noncommuting operators $\widehat{X}$ and $\widehat{Y}$, before we replace them by c-numbers. For the expectation values of simmetrically ordered operators in $\widehat{X}$ and $\widehat{Y}$, the distribution function $W(X,Y)$ is precisely the Wigner function Eq. (1.5). The Wigner function allows to describe physical systems in the phase-space without referring to the density matrix. Quantum dynamics is described by the evolution of the phace-space quasi-distribution. The main difference between $W_{cl}(q,p)$ and the Wigner function $W(X,Y)$ is that the Wigner function is only a quasi-distribution, i. e. it is bounded and normalized just like a distribution function, but it may be at negative values. All of the above explains the statistical nature of operator ρ describing the quantum state.

This border between classical and quantum states is of high importance for the cv quantum information processing since it turns out that *resource* states that belong to the "classical" regime are incapable of executing quantum protocols beating the performance of classical protocols [[23]].

It should establish a method to distinguish between classical and quantum correlations.

2.2 Mutual Information

Both the classical and quantum correlations can give an effective contribution to the information theory.

The mutual information quantifies the amount of information that one random variable contains about another random variable. In classical regime, let $\mathcal{X}$, $\mathcal{Y}$ two random variables associated to the probability distributions $p_{\mathcal{X}=x}$ and $p_{\mathcal{Y}=y}$ respectively, where x and y are the possible values that $\mathcal{X}$ and $\mathcal{Y}$ can assume, the mutual information is given by [24]

$$\mathcal{J}(\mathcal{X}:\mathcal{Y}) = H(\mathcal{X}) - H(\mathcal{X}|\mathcal{Y}), \tag{2.3}$$

where $H(\mathcal{X}) = -\sum_x p_{\mathcal{X}=x} Log p_{\mathcal{X}=x}$ is the classical Shannon entropy and $H(\mathcal{X}|\mathcal{Y})$, i.e. the entropy of $\mathcal{X}$ conditional on knowing $\mathcal{Y}$ is given by

$$\begin{aligned} H(\mathcal{X}|\mathcal{Y}) &= -\sum_y p_{\mathcal{Y}=y} H(\mathcal{X}|\mathcal{Y}=y) \\ &= -\sum_y p_{\mathcal{Y}=y} \sum_x p_{\mathcal{X}|\mathcal{Y}=y} \log p_{\mathcal{X}|\mathcal{Y}=y} \end{aligned}$$

By Eq. (2.3) we deduce that the mutual information is the reduction in the uncertainty of one random variable due to the knowledge of the other.

Using the Bayes rule

$$p_{\mathcal{X}|\mathcal{Y}=y} = \frac{p_{\mathcal{X},\mathcal{Y}=y}}{p_{\mathcal{Y}=y}}$$

it is shown that $H(\mathcal{X}|\mathcal{Y}) = H(\mathcal{X},\mathcal{Y}) - H(\mathcal{Y})$, where $H(\mathcal{X},\mathcal{Y})$ is joint entropy of the pair of random variables $(\mathcal{X},\mathcal{Y})$ with a joint distribution $p(x,y)$, so the Eq. (2.3) can be written as

$$\mathcal{I}(\mathcal{X}:\mathcal{Y}) = H(\mathcal{X}) + H(\mathcal{Y}) - H(\mathcal{X},\mathcal{Y}). \tag{2.4}$$

Now, we translate the concept of mutual information in the quantum context. We consider a quantum physical system $\mathcal{S}$ composed by the two subsystems $\mathcal{S}_1$ and $\mathcal{S}_2$.

The mutual information $\mathcal{I}$ is obtained replacing the classical probability distributions with the density matrices $\rho_{\mathcal{S}_1}$, $\rho_{\mathcal{S}_2}$, $\rho_{\mathcal{S}_1,\mathcal{S}_2}$, and the Shannon entropy with the von Neumann entropy

$$H(\rho_{\mathcal{S}}) = -Tr_{\mathcal{S}}[\rho_{\mathcal{S}} Log \rho_{\mathcal{S}}].$$

In this way, we obtain

$$\mathcal{I}(\mathcal{S}_1:\mathcal{S}_2) = H(\mathcal{S}_1) + H(\mathcal{S}_2) - H(\mathcal{S}_1,\mathcal{S}_2), \tag{2.5}$$

where $H(\mathcal{S}_1) + H(\mathcal{S}_2)$ is the uncertainty of the two subsystems, each treated separately, and $H(\mathcal{S}_1,\mathcal{S}_2)$ is the uncertainty of the joint system.

We have generalized the concept of mutual information $\mathcal{I}$ to quantum systems. However, the generalization of the expression $\mathcal{J}$ Eq. (2.3) is not as automatic, since the conditional entropy $H(\mathcal{S}_1|\mathcal{S}_2)$ requires to specify the state of $\mathcal{S}_1$ given the state of $\mathcal{S}_2$, i. e. conditional information depends on the observer finding out about one of the subsystems. This statement is ambiguous in quantum theory until the to–be–measured observables on $\mathcal{S}_1$ are selected so that the conditional state of $\mathcal{S}_2$ can be defined. It necessarily involves the conditional state of a subsystem after a measurement performed on the other one. Then the conditional entropy is non so trivial in the quantum context. Indeed, in general, in order to find out $H(\mathcal{S}_1|\mathcal{S}_2)$ one must choose a set of projection operators $\Pi_j^{\mathcal{S}_2}$ and define the conditional density matrix given by the outcome corresponding to $\Pi_j^{\mathcal{S}_2}$ through $\rho_{\mathcal{S}_1|\Pi_j^{\mathcal{S}_2}} = Tr_{\mathcal{S}_2} \Pi_j^{\mathcal{S}_2} \rho_{\mathcal{S}_1\mathcal{S}_2}$. This leads to the following quantum generalization of $\mathcal{J}$:

$$\mathcal{J}(\mathcal{S}_1 : \mathcal{S}_2)_{\{\Pi_j^{\mathcal{S}_2}\}} = H(\mathcal{S}_1) - H(\mathcal{S}_1|\{\Pi_j^{\mathcal{S}_2}\}), \qquad (2.6)$$

that represents the information gained about the system $\mathcal{S}_1$ as a result of the measurement $\{\Pi_j^{\mathcal{S}_2}\}$.

2.3 Quantum Discord

As we see in the previous section, the two classically identical expressions for the mutual information Eqs (2.3),(2.4) are profoundly different in the quantum case.

The amount of genuinely quantum correlations, called Quantum Discord $\mathcal{D}$, is the difference $\mathcal{D}$,

$$\mathcal{D} = \mathcal{I}(\mathcal{S}_1 : \mathcal{S}_2) - \mathcal{J}(\mathcal{S}_1 : \mathcal{S}_2)_{\{\Pi_j^{\mathcal{S}_2}\}}. \qquad (2.7)$$

It depends both on $\rho_{\mathcal{S}_1\mathcal{S}_2}$ and on the projectors $\{\Pi_j^{\mathcal{S}_2}\}$, i.e. also by the choice of which observable is measured on $\mathcal{S}_2$. In classical physics all observables commute, so there is no such dependence. Thus, non-commutation of observables in quantum theory is a source of information. The obvious use for the discord is to employ it as a measure of how non-classical the underlying correlation of two quantum systems is. In particular, when there exists a set of states in one of the two systems in which the discord disappears, the state represented by $\rho_{\mathcal{S}_1\mathcal{S}_2}$ admits a classical interpretation of probabilities in that special basis. Moreover, unless the discord disappears for trivial reasons (which would happen in the absence of correlation, i.e., when $\rho_{\mathcal{S}_1\mathcal{S}_2} = \rho_{\mathcal{S}_1} \rho_{\mathcal{S}_2}$), the basis which minimizes the discord can be regarded as "the most classical". For $\mathcal{D} = 0$ the states of such preferred basis and their corresponding eigenvalues can be treated as effectively classical [25].

2.4 Entanglement

The pillar correlation of quantum mechanics is undoubtedly the entanglement. It was the first genuinely quantum correlation to be theorized [1], [2]. Its discov-

ery involved an aglow debate about the nature of the quantum theory. To date, paraphrasing Horodechi [26], we can say that it is still difficult to *understand fully what entanglement is*: we know *its manifestations like violation of Bell's inequalities, teleportation or quantum computation* and *its mathematical description,* but it is still more difficult to understand the phenomenon. Nevertheless, to date, entanglement is the primary tool of the main protocols in Quantum Information theory. For this reason it is necessary to establish unequivocally a method for quantifying the content of entanglement in a state.

From the mathematical definition we know that, given the bipartite density matrix ρ_{AB} acting on a composite Hilbert space $\mathcal{H}_{AB} = \mathcal{H}_A \otimes \mathcal{H}_B$, the state ρ_{AB} is called separable if it can be represented as a convex sum of tensor products of single states,

$$\rho_{AB} \text{ separable} \Rightarrow \rho_{AB} = \sum_k p_k \rho_A^k \otimes \rho_B^k, \qquad (2.8)$$

with $p_k \geq 0$, $\sum_k p_k = 1$, $\rho_A^k \in \mathcal{H}_A$ and $\rho_B^k \in \mathcal{H}_B$ are density operators describing the Alice's and Bob's subsystems. Conversely, the state is entangled.

The first papers about the entanglement were based on the pure states. How to quantify the entanglement of such states is also well established unequivocally [27]. However, in practice, the experimentally producted states are mixed: the [28] problem to quantify the entanglement becomes complicated for such states.

In general there exist different possible subdivisions:

1. **finite/asymptotic regime**. According to finite regime, we quantify the entanglement of a single system. In the second case (asymptotic) we are interested in entanglement of a sequence of systems, or quantum source. A quantum source is a family of compatible states ρ_n, i.e. such as $Tr_{\mathcal{H}_n}\rho_n = \rho_{n-1}$. The simplest example of source is memoryless, for which $\rho_n = \rho^{\otimes n}$. In this case all the subsequently emitted systems are completely uncorrelated, and the state of each system is the same. Given the entanglement measure E in finite regime, we obtain its *density* E^∞ for the source $Q = \{\rho_n\}$:

$$E^\infty(Q) = \lim_{n \to \infty} \frac{E(\rho_n)}{n}.$$

2. **operational/abstract approach**. The operational approach is based on the better achievement of some operational task. For example a faithful teleportation is possible using the state $|\psi_+\rangle = (1/\sqrt{2})(|00\rangle + |11\rangle)$ as resource. A mixed state cannot achieve the same result. However, if we have many copies of the mixed state ρ, say n, it is possible, by use of local operation and classical communication (LOCC), to transform them in a smaller number, say m, of states $|\psi_+\rangle$. The number

$$E_D(\rho) = \lim_{n \to \infty} \frac{m}{n},$$

is the entanglement distillation. It is based on an infinite set of copies of the analysed state and assumes an optimization over all possible LOCC protocols. Through this measure we quantify the entanglement with respect to rate of teleportation. There are entangled states, for which it is not possible to obtain E_D. This type of entanglement is called entanglement bound (see Appendix A). The second approach is based on the identification of the natural properties that a good entanglement measure must comply. For example the entanglement between two systems cannot increase without quantum interaction.

Over the years, many entanglement measures have been proposed, but they are often incommensurate among them. In fact, different entanglement measures give different ordering[1] in the set of all states, i.e. $E(\rho) > E(\sigma)$ doesn't imply $E'(\rho) > E'(\sigma)$, with E different entanglement measure by $E\prime$ and ρ, σ two mixed states.

In the general confusion of the different measures (arising by the different approaches), also only to establish the proprierties that an appropriate entanglement measurement $E(\rho)$ should satisfy is an open problem [28], [29].

Many axioms have been suggested in the literature to clarify the quantification of the entanglement, i.e. the question whether a given density operator is separable or inseparable.

In the following we report some of the basic axioms that any potential measure $E(\rho)$ should satisfy

- *Monotonicity.* For any proper[2] *LOCC* Λ and any state, it is ρ $E(\Lambda(\rho)) \leq E(\rho)$.

- Monotonicity implies invariance under reversible operations.

---

[1]One can interpret this lack of single ordering as follows: there are many different types of entanglement (in particular, we have seen that the entanglement bound is different from the entanglement distillation), so it is possible that in one state we have more entanglement of one type, while in the other state there is more entanglement of some other type.

[2]In according to [26] all possible physical operations can be divided into two main calsses:

1. state-to-ensamble operations;

2. ensemble-to-state operations (mixing);

A special class of the operation 1. is the state-to-state operation, called *proper operartion.* It is described by trace preserving completely positiv map. The operations 2 are made on an ensemble, ie a set of states $\{\rho_i\}$ with ascribed probabilities $\{p_i\}$, taking the convex combination

$$\{p_i, \rho_i\} \rightarrow \rho_{out} = \sum_i p_i \rho_i.$$

The action of mixing corresponds to erasure the information about the member of ensemble [29].

Let an LOCC operation produce ensemble $\{p_i, \rho_i^{out}\}$ out of initial state ρ_{in}. In this circumstance, the montonicity implies

$$\sum_i p_i E\left(\rho_i^{out}\right) \le E\left(\rho_{in}\right). \qquad (2.9)$$

We obtain a stronger condition if we require also non increasing under mixing. In this case, to the condition (2.9) is added the condition of convexity.

- *Convexity.* $E(\sum_i p_i \rho_i) \le \sum_i p_i E\left(\rho_i\right)$.

  We note that entropy is a concave function of its argument: mixing of pure states increases their von Neumnn entropy, but it decreases their entanglement.

- *Discrimince.* $E(\rho) = 0$ *if and only if* ρ *is separable.*

  This condition is very strong. There exist many types of entanglement. It is possible that an entanglement measure vanishes for some entangled state becouse the state does not contain the type of entanglement quantified by that particular measure; for example any measure quantifying the distillable entanglement does not respect this axiom, due to existence of bound entangled states. For this reason, sometimes it is required the weaker property:

  Weak discrimince. If ρ is separable then $E(\rho) = 0$.

  The quantities that satisfy these postulates are called entanglement monotones, in according to which the quantum entanglement cannot be created locally.

- *Asymptotic continuity.* Let ρ_m and σ_m sequences of states acting on m copies of the composite Hilbert space, $(\mathcal{H}_N \otimes \mathcal{H}_K)^{\otimes m}$

$$\text{If } \lim_{m \to \infty} \|\rho_m - \sigma_m\|_1 = 0 \text{ then } \lim_{m \to \infty} \frac{E(\rho_m) - E(\sigma_m)}{m \ln NK} = 0.$$

  Two neighbouring states should be characterized by similar entanglement.

- *Additivity.* $E(\rho \otimes \sigma) = E(\rho) + E(\sigma)$ for any $\rho, \sigma \in \mathcal{M}_{NK}$.

  This property is extremely difficult to prove for two arbitrary density matrices. However one can require the easier subadditivity

  Subadditivity. $E(\rho \otimes \sigma) \le E(\rho) + E(\sigma)$,

  or superadditivity,

  Superadditivity. $E(\rho \otimes \sigma) \geqslant E(\rho) + E(\sigma)$

  The additivity requires both of them.

- *Normalization.* For the maximally entangle state $|\psi^-\rangle$, E is $E\left(|\psi^-\rangle\langle\psi^-|\right) = 1$;

- *Computability.* There exists an efficient method to compute E for any ρ.

These we have listed are just some of the basic axioms reported in the literature. The complete list is very demanding, so it is not surprising that instead of one ideal measure of entanglement fulfilling all required properties, there is a plethora of measures, each of them satisfying some axioms only [28].

In the following we describe two different exemples of measures. At first, we consider an operational measure. This type of measure takes in account the entanglement that may also be quantified in an abstract manner by considering the minimal resources required to generate a given state or a given maximal entanglement. It is based on an infinite set of copies of the analysed state and assume an optimization over all possible LOCC protocols. A type of operational measure is the *distillable entanglement* [29].

Distillable entanglement is a measure of a fundamental importance, that estimates how much entanglement one may extract out of a state ρ and use,

$$E_D(\rho) = \lim_{n \to \infty} \frac{m}{n},$$

where m is the maximal number of singlets $\left| \psi^- \right\rangle$ obtained out of n copies of ρ by an optimal LOCC conversion protocol. It is rather difficult to compute.

Moreover it is not likely to be convex, although it satisfies the weaker condition of the *pure state convexity*.

At second, we introduce an algebraic measure, the Negativity.

Negativity. If a partial transpose of a state ρ is not positive then ρ is entangled. The partial transpose[3] preserves the trace, so if $\rho^{T_A} \geq 0$ then $\left\| \rho^{T_A} \right\|_{Tr} = Tr[\rho^{T_A}] = 1$. Hence we can use the trace norm to characterize the degree, to which the positivity of ρ^{T_A} is violated. Negativity [30],

$$\mathcal{N}(\rho) \equiv \left\| \rho^{T_A} \right\|_{Tr} - 1,$$

is easy to compute, convex (partial transpose is linear and the trace norm is convex) and monotone [30]. It is not additive, but this drawback may be cured by defining the *logaritmic negativity*[4]. However, the major deficiency of the negativity is its failure to satisfy the *Discrimince*. Moreover, it isn't super additive.

In the Chapter 3 we will see that the existence of these two different measures is reason of debate about the extremality of the Gaussian states.

2.4.1 Entanglement criteria

We have seen that it is not possible to define a single, universal entanglement measure for mixed states, i.e. to quantify uniquely the amount of entanglement of

---

[3]partial transpose indicates the transposition of the density matrix with respect to only one of the two subspaces of Hilbert.

[4]The logaritmic negativity is additive but it isn't convex.

a mixed quantum state. However we can use some criteria to evaluate the quality of the entanglement in the quantum systems.

In the following we report a brief description of two different criteria: the *Peres-Horodechy-Simon* (*PHS*) and the *Duan* criterion. They, in general, represent conditions only necessary (*PHS*) or only sufficient (DUAN) to entanglement. However, both these criteria, in some specific cases, become necessary and sufficient conditions to ascertain the presence of entanglement in a given state.

Let ρ_{AB} the density matrix of the bipartite system that we want to analyze,

$$\rho_{AB} = \sum_k p_k \rho_A^k \otimes \rho_B^k, \tag{2.10}$$

with $p_k \geq 0$, $\sum_k p_k = 1$, $\rho_A^k \in \mathcal{H}_A$ and $\rho_B^k \in \mathcal{H}_B$. For establishing if ρ_{AB} is entangled or not, we can use one of the following two criteria:

- *Peres Horodechi-Simon PHS Criterion.*

If $\left(\rho^J\right)^T \not\geq 0$, $J = A, B$, the state is entangled.

With the symbol T we have indicated the trasposition operation, that is applied to any one of the two subsystems. As it makes use of the partial transposition operation, the criterion is sometime referred to as the *ppt* criterion (*positivity* under *partial transposition*).

It is a necessary and sufficient condition for entanglement in the 2×2 and 2×3 dimensional cases [31]. and for Gaussian states [32], but ceases to be a sufficient condition in higher dimensions [31].

By definition, it seems that to use this test on the state ρ, we must perform the partial transposition of the density matrix ρ, diagonalize, and check if all eigenvalues are non-negative. In fact if this circumstance is verified, it means that the two subsystems are described by two indipendent density matrices ρ_A and ρ_B, so it is separable. However, with increasing Hilbert space dimension, the partial transposition operation will be expected to become more and more difficult to implement it in practice. Fortunately, it was shown by Simon [32] that in the limit of infinite dimension, corresponding to continuous variable bipartite states, the criterion translates into a test that is extremely easy to implement. The key concept of the work [32] is the observation that the partial transpose operation, which acts on ρ and gives its transpose ρ^T, in the continuous case,becomes mirror reflection in the Wigner phase space,

$$\rho \to \rho^T \iff W(X, Y) \to W(X, -Y).$$

Then the criterion reads as follow:

if ρ is separable, then its Wigner distribution W necessarily goes over into a Wigner distribution W_Λ under the phace mirror reflection Λ, $\Lambda = diag(1, 1, 1, -1)$

for a bipartite system [32]. Roughly speaking, local time reversal, defined by Λ, is a symmetry in the subspace of separable states.

The criterion can be expressed as a restriction on the second moments. Indeed, when the Wigner distribution undergoes mirror reflection, under partial transpose, it follows that the variance changes from σ to $\widetilde{\sigma}$, so $\sigma \to \widetilde{\sigma} = \Lambda\sigma\Lambda$. For this reason, the condition, in according to which W_Λ has to be a Wigner distribution for separable states, translates into the following constraint on the second moments:

$$\widetilde{\sigma} + \frac{i}{2}\Omega \geq 0, \quad \widetilde{\sigma} = \Lambda\sigma\Lambda,$$

or equivalently

$$\sigma + \frac{i}{2}\widetilde{\Omega} \geq 0, \quad \widetilde{\Omega} = \Lambda\Omega\Lambda,$$

as a necessary condition for separability. This restriction is generally stronger than the usual uncertainty principle Eq.(1.16).

- *Duan Criterion.*

The Duan criterion is based on the idea that a maximally entangled continuous variable state can be expressed as a co-eigenstate of a pair of EPR type operators, i. e. of a couple of operators that represent correlated δ observables[5], such that their total variance reduces to zero for maximally entangled states. The operators $X_d = X_a - X_b$ and $Y_c = Y_a + Y_b$, associated to the modes introduced in § (1.20) can be considered examples of cv EPR type operators. However the variances $\Delta^2 X_d = \Delta^2 Y_c = \frac{e^{-2r}}{2}$ tend to zero only in the limit of infinite energy, so, in this context, maximally entangled continuous variable states are not physical.

Nevertheless the variances will rapidly tend to zero by increasing the degree of squeezing. It is possible to find [33] that for separable states, there exists a lower bound to the total variance. This limit is obtained introducing the following pair of EPR–like conjugate operators defined by

$$\hat{u} = |a|\, X_1 - \frac{1}{a}X_2 \text{ and } \widehat{v} = |a|\, Y_1 + \frac{1}{a}Y_2 \;, \tag{2.11}$$

with a an arbitrary non–zero real number and the subscript 1 (2) refers to the entangled subsystems. By calculating the total variance of such a pair of operators on ρ, a separable state of the form of Eq.(2.8), it can be proven [33] that

$$\left\langle (\Delta\widehat{u})^2 \right\rangle_\rho + \left\langle (\Delta\widehat{v})^2 \right\rangle_\rho \geq a^2 + \frac{1}{a^2} \;, \tag{2.12}$$

setting a lower bound for separable states. Contrarily to the PHS criterion, inequality (2.12) has been formulated as a necessary condition for separability so that it is a sufficient condition for entanglement of a generic cv state.

---

[5]The physical means of this concept will be explained in § 2.6.1.

It can become (under some condition, see §3.2) a necessary and sufficient for characterizing the entanglement of cv Gaussian states.

In Appendix A we report some considerations about the different physical nature of the two introduced criteria.

2.5 Entanglement Swapping

The entanglement swapping protocol establishes entanglement between two beams that share not any common past, i. e. through this protocol it is possible to transfer the entanglement from two couples of entangled modes to one couple of unentangled modes. To date, thanks to its ability to transfer entanglement, the swapping is a standard tool in Quantum Communication. It, e.g., plays a relevant role in the quantum repeaters implementation. Indeed the error probability scales with the length of the channel. The swapping protocol allows to distribute entanglement between the nodes of shorter segments, wherein the channel can be divided. Naturally, the degree of success of the entanglement swapping process depends on the original couples of entangled states.

In the following we decribe the entanglement swapping using the formalism of the characteristic function.

A schematic picture of the cv such protocol is depicted in Fig. 2.1.

The initial state $\rho_0 = \rho_{12}^A \otimes \rho_{34}^B$ is a biseparable four-mode state, composed by two indipendent couples of entanlged states: **A**, the two-mode entangled input state ρ_{12}^A, and **B**, the two-mode entangled resource ρ_{34}^B; the corresponding overall characteristic function reads

$$
\begin{aligned}
\chi_0(\alpha_1; \alpha_2; \alpha_3; \alpha_4) &= Tr[\prod_{j=1}^4 D_j(\alpha_j)\rho_0] \\
&= \chi_{12}(\alpha_1; \alpha_2)\, \chi_{34}(\alpha_3; \alpha_4)\,, \qquad (2.13)
\end{aligned}
$$

where Tr denotes the trace operation, $D_j(\alpha_j)$ denotes the displacement operator of mode j $(j = 1, \ldots, 4)$, χ_{12} is the characteristic function of the input state ρ_{12}^A, and χ_{34} is the characteristic function of the resource ρ_{34}^B.

By introducing the usual quadrature operators $\widehat{X}_j = \frac{1}{\sqrt{2}}(a_j + a_j^\dagger)$ and $\widehat{Y}_j = \frac{i}{\sqrt{2}}(a_j^\dagger - a_j)$, and the corresponding phase space variables $X_j = \frac{1}{\sqrt{2}}(\alpha_j + \alpha_j^*)$ and $Y_j = \frac{i}{\sqrt{2}}(\alpha_j^* - \alpha_j)$, such a state is described, in the phase space $(X_i, Y_i)\,, i = 1, \ldots 4$, by the characteristic function $\chi_0(X_1, Y_1; X_2, Y_2; X_3, Y_3; X_4, Y_4)$:

$$\chi_0(X_1, Y_1; X_2, Y_2; X_3, Y_3; X_4, Y_4) = \chi_{12}(X_1, Y_1; X_2, Y_2)\, \chi_{34}(X_3, Y_3; X_4, Y_4). \quad (2.14)$$

First step: *Bell measurement.* The Bell measurement is made by mixing the beams 2 and 3 in a beam splitter and performing a homodyne measurement on the outgoing beams:

1. E*ntangler beam splitter.* The mode 2 of the input two-mode entangled state is mixed to mode 3 of the entangled resource at a balanced beam splitter. The mixing makes entangled the modes at the output. Therefore the modes 1 and 4 become entangled.

2. *Homodyne measurement.* It is performed on the state at the output of the beam splitter. The effects of the inefficiencies of the photodetectors and of the photon losses are simulated by two additional fictitious beam splitters [34], with transmissivity T_j^2 (reflectivity $R_j^2 = 1 - T_j^2$), $j = 2, 3$, placed in front of the detectors. We denote by $\widetilde{X}$ and $\widetilde{Y}$ the results of the homodyne measurements of the first quadrature of the mode 3 and of the second quadrature of the mode 2, respectively. The realistic Bell measurement is described in full details, by using the formalism of the characteristic function, in Ref. [5]. Here we give the final expression of the characteristic function $\chi_{Bm}(X_1, Y_1; X_4, Y_4)$ associated with the whole measurement process:

$$
\begin{aligned}
\chi_{Bm}(X_1, Y_1; X_4, Y_4) \;=\; & \frac{\mathcal{P}^{-1}(\widetilde{X}, \widetilde{Y})}{(2\pi)^2} \int d\xi\, dv\, e^{i\xi\widetilde{Y} - i\widetilde{X}v} \\
& \times \chi_{12}\left(X_1, Y_1; \frac{T_2\xi}{\sqrt{2}}, \frac{T_3 v}{\sqrt{2}}\right) \chi_{34}\left(\frac{T_2\xi}{\sqrt{2}}, -\frac{T_3 v}{\sqrt{2}}; X_4, Y_4\right) \\
& \times \exp\left[-\frac{R_2^2}{4}\xi^2 - \frac{R_3^2}{4}v^2\right],
\end{aligned}
\tag{2.15}
$$

where the function $\mathcal{P}(\widetilde{X}, \widetilde{Y})$ is the distribution of the measurement outcomes $\widetilde{X}$ and $\widetilde{Y}$, i.e.

$$
\begin{aligned}
\mathcal{P}(\widetilde{X}, \widetilde{Y}) \;=\; & \frac{1}{(2\pi)^2} \int d\xi\, dv\, e^{i\xi\widetilde{Y} - i\widetilde{X}v} e^{-\frac{R_2^2}{4}\xi^2 - \frac{R_3^2}{4}v^2} \\
& \times \chi_{12}\left(0, 0; \frac{T_2\xi}{\sqrt{2}}, \frac{T_3 v}{\sqrt{2}}\right) \chi_{34}\left(\frac{T_2\xi}{\sqrt{2}}, -\frac{T_3 v}{\sqrt{2}}; 0, 0\right).
\end{aligned}
\tag{2.16}
$$

Third step: *Propagation in a lossy channel.* After the realistic Bell measurement, the result is transmitted to the locations of modes 1 and 4 through classical channels. It is assumed that both the input state and the resource are produced close to the Charlie's location (Bell measurement), and far from Alice's and Bob's locations (remote users). Therefore, it is supposed that the modes 2 and 3 are not affected by the decoherence due to propagation; on the contrary, the modes 1 and 4 propagate through noisy channels, e.g. optical fibers, towards Alice's and Bob's locations, respectively. The dynamics of a multimode system subject to decoherence is described, in the interaction picture, by the following master

equation for the density operator ρ [35], [36]:

$$\partial_t \rho = \sum_{i=1,4} \frac{\Upsilon_i}{2} \left\{ n_{th,i} L[a_i^\dagger]\rho + (n_{th,i} + 1) L[a_i]\rho \right\}, \tag{2.17}$$

where the Lindblad superoperators are defined as $L[\mathcal{O}]\rho \equiv 2\mathcal{O}\rho\mathcal{O}^\dagger - \mathcal{O}^\dagger\mathcal{O}\rho - \rho\mathcal{O}^\dagger\mathcal{O}$, Υ_i is the mode damping rate, and $n_{th,i}$ is the number of thermal photons of mode i. Because of the effect of decoherence due to propagation in the noisy channels, the characteristic function (2.15) rewrites:

$$
\begin{aligned}
\chi_t(X_1, Y_1; X_4, Y_4) \quad &= \\
&\chi_{Bm}(e^{-\frac{1}{2}\Upsilon_1 t}X_1, e^{-\frac{1}{2}\Upsilon_1 t}Y_1; e^{-\frac{1}{2}\Upsilon_4 t}X_4, e^{-\frac{1}{2}\Upsilon_4 t}Y_4) \\
&\times e^{-\frac{1}{2}\sum_{i=1,4}(1-e^{-\Upsilon_i t})\left(\frac{1}{2}+n_{th,i}\right)(X_i^2+Y_i^2)}.
\end{aligned} \tag{2.18}
$$

Being related to the technical specifics of the experimental apparatus, e.g. the efficiency of the photodetectors, the characteristics as the length of the channels (fibers), the temperature of the environment, we will assume to possess full knowledge on the following quantities: T_j (equivalently R_j, $j = 2, 3$), Υ_i and $n_{th,i}$ ($i = 1, 4$). Therefore, we will consider T_j, Υ_i and $n_{th,i}$ fixed to certain values. In the last step of the protocol, two displacements λ_1 and λ_4 are performed at Alice's and Bob's locations; a displacement $\lambda_1 = -g_1(\widetilde{X} - i\widetilde{Y})$ is performed on mode 1, and a displacement $\lambda_4 = g_4(\widetilde{X} + i\widetilde{Y})$ is performed on mode 4. The real parameters g_1 and g_4 are the gain factors of the displacement transformations [37]. After such transformations, the characteristic function writes:

$$
\begin{aligned}
\chi_D(X_1, Y_1; X_4, Y_4) \quad &= \quad e^{-i\sqrt{2}\tilde{x}(g_1 Y_1 - g_4 Y_4) - i\sqrt{2}\tilde{p}(g_1 X_1 + g_4 X_4)} \\
&\times \chi_t(X_1, Y_1; X_4, Y_4).
\end{aligned} \tag{2.19}
$$

At these locations, according to the result of the Bell measurement, unitary displacements are performed on mode 1 of the input state and on mode 4 of the resource. The resulting two-mode swapped (entangled) state of modes 1 and 4 is the output state of the protocol.

Last step: *the swapped entangled state.* Finally, the output characteristic function $\chi_{out}(X_1, Y_1; X_4, Y_4)$ describing the output state of the entanglement swapping protocol, it is obtained taking the average of all the possible outcomes $\widetilde{X}$ and $\widetilde{Y}$ of the Bell measurements. It is given by:

$$\chi_{out}^{(swapp)}(X_1, Y_1; X_4, Y_4) = \int d\tilde{x}d\tilde{p}\mathcal{P}(\widetilde{X}, \widetilde{Y})\chi_D(X_1, Y_1; X_4, Y_4), \tag{2.20}$$

where $\tau_i = \Upsilon_i t$. The above integral yields the final expression (2.21) for the

characteristic function associated with the swapped resource.

$$
\begin{aligned}
\chi_{out}^{(swapp)}(X_1, Y_1; X_4, Y_4) \;=\;& \chi_{12}\big(e^{-\frac{\tau_1}{2}}x_1, e^{-\frac{\tau_1}{2}}p_1; T_2(g_1 x_1 + g_4 x_4), T_3(-g_1 p_1 + g_4 p_4)\big) \\
& \chi_{34}\big(T_2(g_1 x_1 + g_4 x_4), -T_3(-g_1 p_1 + g_4 p_4); e^{-\frac{\tau_4}{2}}x_4, e^{-\frac{\tau_4}{2}}p_4\big) \\
& e^{-\frac{1}{2}(1-e^{-\tau_1})\left(\frac{1}{2}+n_{th,1}\right)(x_1^2+p_1^2)-\frac{1}{2}(1-e^{-\tau_4})\left(\frac{1}{2}+n_{th,4}\right)(x_4^2+p_4^2)} \qquad (2.21) \\
& e^{-\frac{R_2^2}{2}(g_1 x_1 + g_4 x_4)^2 - \frac{R_3^2}{2}(-g_1 p_1 + g_4 p_4)^2}, \qquad\qquad\qquad\qquad (2.22)
\end{aligned}
$$

where τ_i denotes the dimensionless time $\tau_i = \Upsilon_i t$.

In the instance of ideal protocol ($R_i = 0$, $T_i = 1$, $\tau_i = 0$) and for $g_1 = 0$, $g_4 = 1$, Eq. (2.21) reduces to:

$$
\chi_{out}^{(swapp)}(X_1, Y_1; X_4, Y_4) = \chi_{12}(X_1, Y_1; X_4, Y_4)\chi_{34}(X_4, -Y_4; X_4, Y_4) . \qquad (2.23)
$$

This last formula offers a clear interpretation of the task of the swapping protocol. For instance, assuming the entangled resource to be a twin beam with squeezing parameter r_{34}, in the limit of large r_{34} the function $\chi_{34}(X_4, -Y_4; X_4, Y_4)$ tends to one; correspondingly, the output characteristic function χ_{out} coincides with χ_{12}, with the complete swapping of mode 2 with the mode 4.

2.6 EPR correlation, entanglement and Bell's inequality

The phenomenon of entanglement was noted from the seminal work of Einstein, Podolsky and Rosen EPR [1]. As is known, the aim of the authors was to demonstrate the incompatibility between the local causality and completeness of quantum mechanics. They left the following premise [38]:

necessary condition for completeness. *Every element of the physical reality must have a counterpart in the physical theory*;

where the *physical reality* satisfies the following

sufficient condition for reality. *If, without in any way disturbing a system, we can predict with certainty (i. e. with probability equal to unity) the value of a physical quantity, then there exists an element of physical reality corresponding to this physical quantity.*

Then they argumented that if a system is in an eigenstate of an operator A, with eigenvalue a, by the criterion for the reality, there must be an element of physical reality corresponding to the physical quantity A. On the other hand, if the state of the system is a superposition of eigenstates of A, it is no possible to assign an element of reality to the physical quantity A. From this EPR deduced that either (1) the quantum-mechanical description of reality given by the wave function is not complete or (2) when the operators corresponding to two physical quantities do not commute the two quantities cannot have simultaneus reality.

Then they imagined an ideal experiment involving a bipartite system $S = S_A + S_B$ and two non-commutating operators $\widehat{O}_1$ and $\widehat{O}_2$, whose bases eigenstates

of the subsystem S_A are indicated as $\{|\psi_n\rangle_A\}$ and $\{|\phi_s\rangle_A\}$ respectively. Depending on the quantity that is to be measured, $\widehat{O}_1$ or $\widehat{O}_2$, it is preferable to consider one or the other following expansion of the overall bipartite state (that, in hindsight, we call entangled)

$$
\begin{aligned}
|\psi\rangle &= \sum_n c_n |\psi_n\rangle_A \otimes |u_n\rangle_B, \\
|\psi\rangle &= \sum_s c'_n |\phi_s\rangle_A \otimes |v_s\rangle_B,
\end{aligned}
$$

where $|u_n\rangle_B$ and $|v_n\rangle_B$ denote some states of S_B. They deduced that *as a consequence of two different measurements performed upon the first system, the second system may be left in states with different wave functions*[6]. EPR took for granted the *locality*, i. e. that no real change can take place in the second system in consequence of anything that may be done to the first system[7]. Based on this assumption it is possible to assign two different wave functions to the same reality in the presented model, in contraddiction of the sufficient condition for reality. This implies, if we refer to the initial dilemma $(1) - (2)$, that the sentence (2) is false, therefore the quantum mechanics is not-complete. They put forward the idea of the existence of a set of local hidden variables (LHVs) underlying quantum systems which should be able to reproduce the statistics of the results, and, at the same time, to restore locality.

At the EPR argumentations Schrodinger tried to find a solution [2], that save the quantum mechanics [38]. He was, probably, the first to define the scenario described by EPR in [1] as *EPR paradox*. Indeed he didn't believe to the quantum mechanics incompletenesses, but neither saw a flaw in the EPR argumentation. At first, he defined the entanglement: *If two separated bodies, each by itself known maximally, enter a situation in which occurs regularly... [an] entanglement of our knowledge of the bodies,* and the disentanglement, *After establishing one representative by observation, the other one can be inferred simultaneously... this procedure will be called the disentanglement.* Then he described the EPR paradox as the *obvious but very disconcerting fact that even though we restrict the disentangling measurement to one system, the representative obtained for the other system is by no means independent of the particular choise of the observation which we select for the purpose and which by the way are entirely arbitrary.*

Schrodinger called *steering* this ability to affects the state of the remote subsystem. However, both EPR's and Schrodinger arguments can not be tested in

---

[6]If we make a measurement of $\widehat{O}_1$ obtaining as result $|\psi_k\rangle_A$, the overall state will become $|\psi\rangle = c_k |\psi_k\rangle_A \otimes |u_k\rangle_B$, so the subsystem S_B will be described by $|u_k\rangle_B$, if we measure $\widehat{O}_2$ obtaining $|\phi_r\rangle_A$, the state of S_B will collapse into $|v_r\rangle_B$. This phenomenon is just what Schrodinger later termed *steering*

[7]They never used the term locality, but the previous sentence is to all effects a necessary condition for locality.

the laboratory because they involve perfect correlations and pure states. Such states are unobtainable in pratice due to unavoidable inefficiency in preparation and detection of real pysical systems.

So the ability to manipulate a subsystem acting appropriately on the other one wasn't proved in laboratory until 1989. In such year, Reid et al worked out an (of more general validity) useful criterion.

2.6.1 *EPR-Reid Criterion*

The essential difference between EPR-Reid criterion and the original EPR argument is in the concept of realty [38]:

Reid's extension of EPR's sufficient condition of reality. If, without in any way disturbing a system, we can predict with some specified uncertainty the value of a physical quantity, then there exists a stochastic element of physical reality which determines this physical quantity with at most that specific uncertainty.

Moreover, the original version was formulated by EPR in terms of two spatially separated particles with higly correlated positions and momenta, instead in [39] the paradox is formulated in terms of the field quadratures at the output of an ideal **OPO**. Indeed the conjugate quadrature phase amplitude of signal and idler are higly correlated and, in principle, provide an example of EPR couple.

For the rest, the scenario is the same. The paradox describes the ability to infer the expectation value of an observable (the position in EPR scenario, quadrature in EPR-Reid one) on a sub–system by measuring the EPR companion observable (momentum in the first scenario, conjugate quadrature in the second one) on the second sub–system. However, as we said in § 2.4.1, the observables "quadrature" aren't maximally correlated, so the EPR-Reid must take in account an error of inference. It is still possible to obtain the paradox providing if the error is small compared to the uncertainty predicted by the Heisenberg uncertainty principle.

Therefore the EPR-Reid criterion can be verified calculating the conditional variance for an observable on sub–system A given the result of a measurement on sub–system B and comparing it with the standard quantum limit (i. e. with the vacuum fluctuations).

We consider that Alice makes a measurement of the quadrature $\widehat{X}_A$, on the subsystem A, and Bob measures the quadrature $\widehat{X}_B$ on the subsystem B. We call unconditional probabilities the quantities of the type $P(J_A)$, $P(J_B)$ $J = X$, Y while the conditional probability $P(J_B|J_A)$, indicates the probability that Bob obtains J_B in a measurement of $\widehat{J}_B$ given the Alice's outcome J_A. Alice and Bob measure such conditional probabilities and obtain distributions with variances $\Delta^2(X_B|X_A)$, $\Delta^2(Y_B|Y_A)$. Based on her results, Alice can estimate the results of

Bob, from which she obtains an optimal average inference variances

$$\Delta_{\text{inf}}^2 X_B = \int dX_A dX_B P(X_A) \Delta^2(X_B|X_A),$$

$$\Delta_{\text{inf}}^2 Y_B = \int dY_A dY_B P(Y_A) \Delta^2(Y_B|Y_A).$$

Reid showed that the violation of the inequality

$$\Delta_{\text{inf}}^2 X_B \Delta_{\text{inf}}^2 Y_B \geq \frac{1}{4} \tag{2.24}$$

implies the experimental demostration of the EPR paradox. This is the EPR-Reid criterion. The subsystems that violate the inequality (2.24) are called EPR-correlated and the corresponding operator (e.g. $\widehat{X}_B$ and $\widehat{Y}_B$ that give $\Delta_{\text{inf}}^2 X_B$ and $\Delta_{\text{inf}}^2 Y_B$ in (2.24)) form an EPR couple.

The EPR-Reid criterion represents only a sufficient condition to the entanglement. Indeed it is a distinct form of nonlocality in respect to the entanglement, as we will see in the next subsection.

2.6.2 Distinct forms of non-locality: Bell's inequality, Entanglement, EPR-Steering correlation

As we saw in § 2.6, the concepts of *entanglement, steering,* and *nonlocality* were born together, in confused attempts to find an answer to the EPR question [1]: "Can Quantum-Mechanical Description of Physical Reality Be Considered Complete?". Moreover, in 1969, Bell formulated mathematically the EPR's idea about the existence of some local hidden variables LHV [40].

In the light of the historical-scientific journey which took place from 1935 to today, we can say that quantum mechanics is nonlocal and that different forms of nonlocality exist. This concept has been clearly formalized in [41] and then in [38]. According to the authors, let consider the usual spatially separated observes Alice and Bob. Let $\mathcal{D}_\alpha$ the set of all observables on the Alice's Hilbert space, whose generic element is A, $\mathcal{M}_\alpha \subseteq \mathcal{D}_\alpha$ denotes the meaurements that Alice can perform. Analogues symbols are used for Bob (by the replacement $\alpha \to \beta$). The set of ordered pairs $\mathcal{M} \equiv \{(A, B) : A \in \mathcal{M}_\alpha, B \in \mathcal{M}_\beta\}$ represents a measurement strategy. Alice and Bob perform measurements on systems prepared by a reproducible preparation procedure c[8]. In this way it is possible to consider that all the measures are performed on systems with the same state matrix w. Such measurements provide the eigenvalues $\{a\}$ $\{b\}$. So $P(a|A; w)$ represents the probability that Alice will obtain a as result of a measurement of the observable A on the state w, while the joint probability that the Alice' s measurement gives a and the

---

[8]c represents all those variables which are explicitly known in an experimental situation.

Bob's measurement gives b reads

$$P(a, b | A, B; w) = Tr[(\Pi_a^A \otimes \Pi_b^B) w],$$

where Π_j^J $J = A, B$, $j = a, b$ is the projector satisfying $J\Pi_j^J = j\Pi_j^J$ (we are restricting to projective measurements).

Bell's nonlocality. The so-called Bell's nonlocality emerged from the mathematical formulation [40] of the hidden variables theory suggested by EPR. Its understanding is likely more immediate if we refer to the the example advocated by Bohm [42] for describing the EPR paradox. We consider a pair of spin-half particles in the singlet spin state, on the select components of the spins $\widehat{\sigma}_1$ and $\widehat{\sigma}_2$. The particles are free to move in opposite directions. We suppose to measure the components along the direction $\overrightarrow{v}$, with $\overrightarrow{v}$ unit vector, in the hypoteses that the measurements are made at places remote from one another and that the orientation of one magnet doesn't influence the result obtained with the other. Following the formalism introduced above, if the measurement of the observable $A = \widehat{\sigma}_1 \cdot \overrightarrow{v}$ gives the value $a = +1$, then $B = \widehat{\sigma}_2 \cdot \overrightarrow{v}$ gives $b = -1$ and viceversa. r.

We see that it is possible to predict the the result of any chosen component of $\widehat{\sigma}_2$ by a previous measurement of the same component of $\widehat{\sigma}_1$. This predetermination is not present in the wave function. This circumstance suggested to EPR that the wave function may be better specified by means of additional parameters ξ and that introducing such parameters the system becomes again describable by classical physics. Bell provided a mathematical formulation, in which the result of measure $A = \widehat{\sigma}_1 \cdot \overrightarrow{v}$ depends on both $\overrightarrow{v}$ and ξ, and the result of measure $B = \widehat{\sigma}_2 \cdot \overrightarrow{u}$ depends on both $\overrightarrow{u}$ and ξ, i. e.

$$a(\overrightarrow{v}, \xi) = \pm 1, \quad b(\overrightarrow{u}, \xi) = \pm 1,$$

with the *vital assumption* that the result of B for particle 2 doesn't depend on the setting $\overrightarrow{v}$ of the magnet for particle .

Let $\mathfrak{p}(\xi)$ the normalized probability distribution of ξ, then the expectation value of the product of the two components A and B is

$$P(a, b | A, B; w) = \sum_{\xi} \mathfrak{p}(\xi) \mathfrak{p}(a | A, \xi) \mathfrak{p}(b | B, \xi). \tag{2.25}$$

Following quantum mechanics, the expectation value is given by

$$\langle \widehat{\sigma}_1 \cdot \overrightarrow{v} \; \widehat{\sigma}_2 \cdot \overrightarrow{u} \rangle = -\overrightarrow{v} \cdot \overrightarrow{u}. \tag{2.26}$$

If there are variables ξ for which Eq. (2.25) gives the same result of Eq. (2.26), then quantum mechanics coincides with classical mechanics.

Bell showed that there exist systems for which the two quantities give different results [40]. The local additional variables, introduced to restore causality and locality in the quantum mechanics, are incompatible with the statistical predictions of the quantum mechanics.

The Bell nonlocality is exhibited in any experiment on the state w iff the correlation between a and b cannot explained by a LHV model, i. e. iff the statistical prediction aren't described by Eq. (2.25).

By Eq. (2.25) it is possible to establish some inequalities, called Bell's inequalities, that are violated by the quantum mechanics. In the following sections we will see that such inequalities put a limit between systems that exibit quantum nonlocality and systems that admit descriptions in terms of hidden variables (i. e. admit a classical description).

The violation of the Bell's inequality (2.24) is a sufficient condition to ascertain the presence of entanglement (see chapter 4).

However although the entanglement represents correlation witnessing the nonlocality of quantum mechanics, it is a distint form of nonlocality in respect to Bell's nonlocality [38]

Nonlocality of the entanglement. Bell inequality is obtained introducing some hidden variable in the description of the observables that define the measurement strategy. However such variables can be *hidden* in the description of the state too.

A state w is nonseparable if it is impossibile to express it as a convex combination of product states,

$$w = \sum_{\xi} \sigma_\xi \otimes \rho_\xi \mathfrak{p}(\xi). \tag{2.27}$$

where $\sigma_\xi \in \mathcal{D}_\alpha$, $\rho_\xi \in \mathcal{D}_\beta$ are (positive, normalized) quantum states. We suppose that Alice and Bob measure a quorum of local observables to reconstruct the state w by tomography: Alice measures the eigenvalue a for recostructing σ_ξ, while Bob measures the eigenvalue b for recostructing ρ_ξ. In analogy to Bell nonlocality Eq. (2.25), we say that w is nonseparable iff it isn't possible to express the expectation values of the observales, nessary to tomography, as

$$P(a, b | A, B; w) = \sum_{\xi} \mathfrak{p}(a | A, \sigma_\xi) \mathfrak{p}(b | B, \rho_\xi) \mathfrak{p}(\xi), \tag{2.28}$$

Any constraint on the set of the possible phenomena derived by Eq. (2.28) is called *separability criterion* or *entanglement criterion*. This definition is of course equivalent to the definition that involves product states Eq. (2.27). Indeed, if there is a separable model for all possible measurement settings, then the joint state can be given. Conversely, if the state is given by a convex sum of the product state Eq. (2.27), the joint probabilities for each pair of measurements are given by Eq. (2.28).

Non-locality of the steering. Although the two introduced forms of nonlocality are conceptually very different, the scenarios introduced to describe they are similar. In fact, in both circumstances, Alice and Bob try to act, each on its own subsystem, independently of one another. There is a third part, outside the

system, that we can call Charlie, which analyzes the results and establishes the nonlocal character (see Fig 2.2).

This scenario is completely different from the nonlocality by steering[9], which describes an asymmetrical situation: one of two parts, e.g. Alice in Fig 2.3, prepares the bipartite state and gives a subpart to Bob. In this context, the steering describes the ability of Alice, to steer the results of Bob. The Alice's choise to measure A can cause the collapse of Bob's system into different types of states in the different ensambles $\mathfrak{e}^A \equiv \left\{ \widetilde{\rho}_a^A : a \in \lambda(A) \right\}$, the tilde denotes that the state $\widetilde{\rho}_a^A \equiv Tr_\alpha[w(\Pi_a^A \otimes \mathbf{I})] \in \mathcal{D}_\beta$ is unnormalized. The state w exhibits steering iff it is not valid

$$P(a, b | A, B; w) = \sum_\xi \mathfrak{p}(a | A, \xi) \mathfrak{p}(b | B, \rho_\xi) \mathfrak{p}(\xi)$$

Of course, Alice cannot affect Bob's unconditioned state $\rho = Tr_\alpha[w] = \sum_a \widetilde{\rho}_a^A$ that would allow superluminal signaling. Bell nonlocality and entanglement are both symmetric concepts between Alice and Bob. However, steering in inherently asymmetric. The violation of the LHV model by only one of the two parts, for example Bob, is a demonstration of EPR steering introduced by Schrodinger to refer to the EPR paradox.

It means that Bob's outcomes are described by some quantum state, but Alice's outocomes are free to be arbitrarly determined by ξ.

It is possible to verify that, for Gaussian states, the EPR-Reid correlation (described in § 2.6.1) occurs under precisely the same conditions of EPR-steering correlation.

2.7 Bell's Inequality

In the same year (1969) of the Bell's paper [40] Clauser, Horne, Shimony and Holt presented a generalization of Bell's theorem which applies to realizable experiments [43].

Tipically, the experiment involves three distant parties, Sophie, Alice, and Bob. Sophie (the source) prepares a bipartite state and distribute it to Alice and Bob (the two usual partners). Then, Alice and Bob randomly and independently decide between one of two possible quantum measurements A_1 or A_2 (B_1 or B_2), which should have only two possible outcomes $+1$, or -1. The experimental setup should be arranged in such a way that Alice and Bob do their measurements in a causally disconnected manner. Thereby, Alice's measurement cannot influence Bob's one, and vice-versa.

To summarize what has already been said in other words, *local realism* implies two assumptions:

---

[9]introduced by Scrodinger in [2]

(1) *Realism.* The physical properties A_1, A_2, B_1, B_2 have definite values a_1, a_2, b_1, b_2, which exist independently of their observation. This implies the existence of a probability distribution $P(a_1, a_2, b_1, b_2)$ dependent on how Sophie generates the bipartite state.

(2) *Locality.* Alice's measurement choice and outcome do not influence the result of Bob's measurement, and vice-versa. The measurement events are separated by a spacelike interval.

If we consider the local realism as the correct description of the physical world, then we obtain the *Bell-**CHSH*** *inequality*

$$\mathcal{B} = |\langle a_1 b_1 \rangle + \langle a_1 b_2 \rangle + \langle a_2 b_1 \rangle - \langle a_2 b_2 \rangle| \leq 2,$$

where $\langle a_j b_k \rangle$ denotes the average over the subset of experimental data where Alice measured a_j and, simultaneously, Bob measured b_k. An experimental test of Bell-CHSH inequalities where a violation of $\mathcal{B} \leq 2$ is observed disproves any classical (local realistic) description of Nature.

Now, if we consider that Sophie generates and distributes an entangled pair of qubits, the Bell operator $\mathcal{B}$ reads

$$
\begin{aligned}
\widehat{\mathcal{B}}_{qubit} & = (\mathbf{a}_1 \cdot \sigma_1) \otimes (\mathbf{b}_1 \cdot \sigma_2) + (\mathbf{a}_1 \cdot \sigma_1) \otimes (\mathbf{b}_2 \cdot \sigma_2) \\
& + (\mathbf{a}_2 \cdot \sigma_1) \otimes (\mathbf{b} \cdot \sigma_2) - (\mathbf{a}_2 \cdot \sigma_1) \otimes (\mathbf{b}_2 \cdot \sigma_2),
\end{aligned}
$$

where σ_j, is the Pauli matrix for the *jth* $(j = 1, 2)$ qubit and $\mathbf{a}_1$, $\mathbf{a}_2$, $\mathbf{b}_1$, $\mathbf{b}_2$ ar for unit three-dimensional vectors.

Quantum mechanics predicts $\mathcal{B}_{qubit} = \left\langle \widehat{\mathcal{B}}_{qubit} \right\rangle = 2\sqrt{2}$, which is in contradiction with local realism.

2.7.1 Continuous variable *Bell-**CHSH*** *inequality*

Many experimental Bell tests have been performed, observing the violation of Bell's inequalities predicted by quantum mechanics. The most of the experimental schemes used optical setups because, it allows to generate and distribute entangled particles (photons) at a distance in order to make Alice's and Bob's measurements causally disconnected.

However, the available single-photon detectors suffer from a low efficiency η, which can be exploited by a local realistic model to yield a violation. Thus, to reject local realism, it is necessary to make the extra assumption that the registered pairs form a fair sample of the emitted pairs. So, from a logical point of view, these experiments do not succeed in ruling out a local realistic model; this is the so-called detector-efficiency loophole. This loophole has been closed in a recent experiment with trapped ions, thanks to the high efficiency of the measurement of the ion states. However, the measurement events were not spacelike separated, opening in turn the so-called locality loophole.

Many alternative schemes have been proposed, but they are experimentally very challenging. An interesting alternative to the atom-based approaches consists of all-optical schemes based on continuous variables of light. Indeed, the balanced homodyne detection used in these schemes can exhibit a high detection efficiency, sufficient to close to detection loophole, and the optical beams can be can be transported at a distance from each other avoiding the problem of locality loophole.

There are two different methods to test the Bell's inequalities for the continuous variable **cv** bipartite state. Following the first method (that incorporates pseudo-spin [44] and homodyne approaches) one converts the problem of the **cv** inequality Bell into the well known **dv** inequality Bell mapping the modes into two-qubit system. The other one developes some test for specifically continuous variable system.

2.7.2 Pseudo-spin approach

In [44] the following operators for photons, for a single-mode light field, are introduced:

$$
\begin{aligned}
s_z &= \sum_{n=0}^{\infty} \left[|2n+1\rangle \langle 2n+1| - |2n\rangle \langle 2n| \right], &\quad (2.29) \\
s_- &= \sum_{n=0}^{\infty} |2n\rangle \langle 2n+1| = (s_+)^{\dagger},
\end{aligned}
$$

where $|n\rangle$ are the usual Fock state. The operator s_z is the parity operator, whereas s_+ and s_- are the "parity-flip" operators. They are called *pseudospin* operators becouse their commutation relations of these operators are identical to those of the spin-1/2 systems,

$$
[s_z, s_{\pm}] = \pm 2 s_{\pm}, \quad [s_+, s_-] = s_z. \qquad (2.30)
$$

This circumstance allows to establish a direct analogy to the discrete-variable case introduced in 2.7, in which the pseudospin operators $\widehat{\mathbf{s}} \equiv (s_x, s_y, s_z)$, with $s_x \pm s_y \equiv 2 s_{\pm}$, can be regarded as a cv counterpart of the spin operator σ. As the pseudospin operators act upon the parity space of photons, they are called the "parity spin" of photons.

Now let $\mathbf{a} = (\sin \vartheta_a \cos \varphi_a, \sin \vartheta_a \sin \varphi_a, \cos \vartheta_a)$ an arbitrary vector on the surface of a unit sphere, we obtain

$$
\mathbf{a} \cdot \widehat{\mathbf{s}} = s_z \cos \vartheta_a + \sin \vartheta_a \left(e^{i \varphi_a} s_- + e^{-i \varphi_a} s_+ \right).
$$

The commutation relations in Eq. (2.30) lead to

$$
(\mathbf{a} \cdot \widehat{\mathbf{s}})^2 = I, \qquad (2.31)
$$

that means that the outcome of the measurement of the Hermitian operator $\mathbf{a} \cdot \widehat{\mathbf{s}}$ (with eigenvalues ± 1) is $+1$ or -1. The above observations show that there exists a perfect analogy between the cv systems and the usual spin-1/2 systems. Using the Eqs. (2.29), (2.30), (2.31) we can write

$$\mathcal{B} = \left\langle \widehat{\mathcal{B}} \right\rangle = E\left(\vartheta_a, \vartheta_b\right) + E\left(\vartheta_a, \vartheta_{b'}\right) + E\left(\vartheta_{a'}, \vartheta_b\right) - E\left(\vartheta_{a'}, \vartheta_{b'}\right), \qquad (2.32)$$

with

$$E\left(\vartheta_a, \vartheta_b\right) = \left\langle s_{\vartheta_a}^{(1)} \otimes s_{\vartheta_b}^{(2)} \right\rangle$$

and

$$s_{\vartheta_a}^{(j)} \equiv s_{jz} \cos \vartheta_a + s_{jx} \sin \vartheta_a.$$

In the phace space the poseudospin operators correspond to the following Wigner functions

$$W_x = \frac{1}{\pi} sgn\left[\text{Re}\left[\alpha\right]\right], \quad W_z = -\frac{1}{2}\delta^{(2)}\left(\alpha\right), \quad W_y = -\frac{1}{2\pi}\delta\left(\text{Re}\left[\alpha\right]\right)\mathcal{P}\frac{1}{\text{Im}\left[\alpha\right]},$$

where $\mathcal{P}$ denotes the Cauchy principal value [45].

2.7.3 Homodyne approach

In this case [46] one discretizes the measured quadrature X assuming as outcome $+1$ when, for example, $X \geq 0$ and -1 otherwise. The violation of Bell's inequality is achieved as usual when $|\mathcal{B}| > 2$,

$$\mathcal{B} = E\left(\vartheta_1, \varphi_1\right) + E\left(\vartheta_1, \varphi_2\right) + E\left(\vartheta_2, \varphi_1\right) - E\left(\vartheta_2, \varphi_2\right),$$

where ϑ_j and φ_j are tha phases of the homodyne measurements at the modes a and b respectively, and

$$E\left(\vartheta_j, \varphi_k\right) = \int_{\mathbb{R}^2} dx_{\vartheta_j} dx_{\varphi_k} sgn\left[x_{\vartheta_j} x_{\varphi_k}\right] P\left(x_{\vartheta_j}, x_{\varphi_k}\right),$$

$P\left(x_{\vartheta_j}, x_{\varphi_k}\right)$ beeing the joint probability to obtain the two outcomes x_{ϑ_j} and x_{φ_k}.

Unfortunately, the Gaussian two-mode state cannot be directly employed to test Bell's inequalities with the homodyne technique. Indeed, as noted by Bell himself, this state is described by a positive-definite Gaussian Wigner function [47] [48], which thus provides a local realistic model that explains all correlations between quadrature measurements (carried out by balanced homodyne detectors). Thus, as the homodyne is a Gaussian measure, to use this approach we need to go beyond the Gaussian states.

2.7.4 Space phase approach. Non locality in the Wigner representation

The starting point is the observation that the two-mode Wigner function $W(\alpha, \beta)$ can be expressed as the quantum expectation value of a product of displaced parity operators,

$$W(\alpha, \beta) = \frac{4}{\pi^2} \Pi(\alpha, \beta), \tag{2.33}$$

with

$$\Pi(\alpha, \beta) = \widehat{D}_1(\alpha)(-1)^{\widehat{n}_1} \widehat{D}_1^\dagger(\alpha) \otimes \widehat{D}_2(\beta)(-1)^{\widehat{n}_2} \widehat{D}_2^\dagger(\beta), \tag{2.34}$$

where $\widehat{D}_j$ $j = 1, 2$ denotes the unitary phase-space displacement operator for the subsystems 1 and 2. As the measurement of the parity operator yields only one of two values $+1$ or -1 there exists an apparent analogy between the measurement of the parity operator and of the spin-$1/2$ projectors. The solid angle defining the direction of the spin measurement is now replaced by the coherent displacement describing the shift in phase space. By Eq. (2.34) we see that the correlation functions measured in such experiments are given by the joint Wigner function of the system, up to a multiplicative constant. As a consequence we have the fundamental relation

$$E(a, b) \equiv \Pi(\alpha, \beta).$$

If the correlation function $\Pi(\alpha, \beta)$ is measured for four possible combinations of the displacement amplitudes $\alpha_1, \alpha_2, \beta_1, \beta_2$, we can write the quantity $\mathcal{B}$,

$$\mathcal{B} = \Pi(\alpha_1, \beta_1) + \Pi(\alpha_1, \beta_2) + \Pi(\alpha_2, \beta_1) - \Pi(\alpha_2, \beta_2), \tag{2.35}$$

that for local theories satisfies the CSHS inequality

$$|\mathcal{B}| \leq 2. \tag{2.36}$$

2.8 cv QuantumTeleportation protocol

In this section we discuss the quantum teleportation protocol in continuous variable. Quantum teleportation was first proposed by Bennett et al. in the discrete variable regime. The idea of cv teleportation was put forward by Vaidman, but quantum-optical protocol for the teleportation of quadrature amplitudes of a light field was introduced by Braunstein and Kimble [49].

The cv protocol is developed in complete analogy with the one for discrete variables.

The key points of the teleportation, shown in a pictorial way in Fig 2.4, of an unknown state $|in\rangle$ from position A, Alice, to position B, Bob, are

1. **Initial Condition**. Alice and Bob share a quantum channel (resource) given by two modes a and b perfectly EPR correlated, such that

$$X_a - X_b = Y_a + Y_b = 0. \tag{2.37}$$

The Eq. (2.37) describes an ideal EPR couple. In cv regime, it is obtained only as a limit of infinite squeezing, whereas the realistic quantum channel has a finite amount of squeezing.

2. **cv Bell Measurement.** Alice performs a version of the cv Bell measurement through two subsequent operations:

   (a) mixing of the modes $|in\rangle$ and a through a balanced beam splitter BS, performing the following bilinear transformation on the quadratures

   $$X_\pm = \frac{X_a \pm X_{in}}{\sqrt{2}}, \quad Y_\pm = \frac{Y_a \pm Y_{in}}{\sqrt{2}},$$

   where $X_\pm$ and $Y_\pm$ are the quadratures of the output modes $+$ and $-$.

   (b) Homodyne detection of the quadratures. Alice detects the quadratures X_- and Y_+ obtaining the results $\widetilde{X}_-$ and $\widetilde{Y}_+$. Her meausurements cause the collapse

   $$X_a = X_{in} + \sqrt{2}\widetilde{X}_-, \qquad Y_a = -Y_{in} + \sqrt{2}\widetilde{Y}_+.$$

   Due the EPR property Eq. (2.37), Bob's quadratures are, instantaneously, prjected in

   $$X_b = X_{in} + \sqrt{2}\widetilde{X}_-, \qquad Y_b = Y_{in} - \sqrt{2}\widetilde{Y}_+.$$

3. **Classical communication**. Alice gives the results of its measurements (the two quadratures $\widetilde{X}_-$ and $\widetilde{Y}_+$) to Bob through a classical channel.

4. **Unitary transformation**. Bob uses the received classical information to perform a conditional dispacement on mode b, so he reconstructes the input state and complete the teleportation process,

$$X_b \rightarrow X_b' \equiv X_b - \sqrt{2}\widetilde{X}_- = X_{in}, \qquad Y_b \rightarrow Y_b' \equiv Y_b + \sqrt{2}\widetilde{Y}_- = Y_{in}$$

The use of continuous variables offers many advantages over the use of discrete ones [50], e.g. one of the key points of difficulty of the discrete variable protocol is the Bell measurement in order to couple the input qubit with the quantum channel. Until now, in all the real experimental setups, such a measurement has not been implemented in a clear and precise way. On the contrary, the cv version of the Bell measurement is realized via linear passive optics and homodyne measurements, whose outcomes can be discriminated with high precision (perfectly discriminated in the asymptotic sense).

2.8.1 Check the success of teleportation: fidelity

As can be seen from the description of the protocol, the teleported state can remain unknown to both Alice and Bob. That is a third party, e.g. the verificator, called often Victor, can prepare the quantum state $|in\rangle$ and give it to Alice, asking to teleport it to another station (the Bob's station). We suppose that Victor doesn't reveal any information about the initial state.

The field teleported ρ_{out}, emerging from the Bob's station, is analyzed by the same Victor, that can establish the "quality" of the teleportation through the evaluation of the overlap between the input state (which we assume pure) and the (obviously mixed) output state,

$$\mathcal{F} = \langle in| \, \rho_{out} \, |in\rangle.$$

$\mathcal{F}$ is called teleportation fidelity.

When the input state is a coherent state, the value of fidelity 0.5 marks the boundary between classical and quantum physics, i.e. $\mathcal{F} > 0.5$ is possible only with the help of the quantum strategy (with the use of entangled resource) [23].

2.8.2 Teleportation protocol in the formalism of characteristic function

We want to express the protocol in the characteristic function formalism. This formalism is particularly suited when we treat with non-Gaussian states and resources, because it greatly simplifies the calculational strategies.

Let ρ_{in} the single mode input state to be teleported. Its characteristic function is given by $\chi_{in}(\gamma) = Tr[\rho_{in}D(\alpha')]$, where $D(\alpha')$ is the usual displacement operator with complex amplitude α'. The complex amplitude γ of the input state can be expressed in terms of the quadratures:

$$\gamma = \frac{X_{in} + iY_{in}}{\sqrt{2}}.$$

In a similar way we define the characteristic function of the resource ρ_{ab} as $\chi_{ab}(\alpha, \beta)$, or, equivalently, $\chi_{ab}(X_a, Y_a; X_b, Y_b)$. The total initial state $\rho_{in} \otimes \rho_{ab}$ is described by

$$\chi_{ab}(\alpha, \beta, \gamma) = \chi_{in}(\gamma)\chi_{ab}(\alpha, \beta).$$

Alice mixes the input mode with her mode a in the balanced (lossless) BS performing the following transformation on the complex amplitudes

$$\nu_{\pm} = \frac{\alpha \pm \gamma}{\sqrt{2}},$$

with $\nu_{\pm} \equiv (X_{in} + iY_{in})/\sqrt{2}$ the complex amplitudes of the output modes $\pm$. Then alice detect the quadratures X_- and Y_+ obtaining the results $\widetilde{X}_-$ and $\widetilde{Y}_+$, i.e. she

obtains $\widetilde{\gamma} \equiv -\widetilde{X}_- + i\widetilde{Y}_+$, with probability $\mathcal{P}(\widetilde{\gamma})$. Due Alice's measurements, Bob has the following conditionated state

$$\chi(\beta|\widetilde{\gamma}) = \mathcal{P}^{-1}(\widetilde{\gamma}) \int d^2\gamma \chi_{in}(\gamma) \chi_{ab}(\gamma^* - (\widetilde{\gamma}^*, \beta).$$

Alice communicates her result $\widetilde{\gamma}$ to Bob through a classical channel and, consequently, Bob performs a displacement. If the two-mode resource χ_{ab} is an ideal EPR couple (i.e. Eq. (2.37) is satisfied), then the Bob's displacement is $\beta \to \beta' = \beta + \widetilde{\gamma}$, but in the realistic circumstances the Bob's displacement is given by

$$\beta \to \beta' = \beta + \widetilde{\gamma} + \widetilde{\delta}, \tag{2.38}$$

where $\widetilde{\delta} \equiv \widetilde{\delta}_D + \widetilde{\delta}_I$ takes in account the inefficiencies of the detection $\widetilde{\delta}_D$ and the non ideal initial correlation $\widetilde{\delta}_I$; $\widetilde{\delta}$ depends on the first moments of the resource. In according to the displacement Eq. (2.38) the final state at the Bob's station is given by

$$\chi(\beta' - \widetilde{\gamma} - \widetilde{\delta}|\widetilde{\gamma}) = \mathcal{P}^{-1}(\widetilde{\gamma}) \int d^2\gamma \chi_{in}(\gamma) \chi_{ab}(\gamma^* - \widetilde{\gamma}^*, \beta' - \widetilde{\gamma} - \widetilde{\delta}). \tag{2.39}$$

If we want to know how much, on average, this state is similar to the input state, we must average over all possible results $\widetilde{\gamma}$,

$$\chi_{out}(\beta', \widetilde{\delta}) = \int d^2\widetilde{\gamma} \mathcal{P}(\widetilde{\gamma}) \chi(\beta' - \widetilde{\gamma} - \widetilde{\delta}|\widetilde{\gamma}).$$

By Eq. (2.39) we obtain

$$\chi_{out}(\beta', \widetilde{\delta}) = \int d^2\gamma \mathcal{K}(\beta' - \gamma, \widetilde{\delta}) \chi_{in}(\gamma),$$

where the kernel $\mathcal{K}$ is given by

$$\mathcal{K}(\beta' - \gamma, \widetilde{\delta}) = \int d^2\widetilde{\gamma} \chi_{ab}(\gamma^* - \widetilde{\gamma}^*, \beta' - \widetilde{\gamma} - \widetilde{\delta})$$

In this formalism, the teleportation fidelity $\mathcal{F} = Tr[\rho_{in}\rho_{out}]$, i.e. the success probability of the teleportation protocol, reads

$$\mathcal{F} = \frac{1}{2\pi} \int d^2\lambda \chi_{in}(\lambda) \chi_{out}(-\lambda). \tag{2.40}$$

2.8.3 Teleportation protocol for Gaussian resources

Let us consider the particular case of Gaussian states, i.e. a pure Gaussian state as input, described by the covariance matrix $\mathbf{V}_{in}$, and a two-mode Gaussian

state as resource, described by the block matrix Eq. (1.7) [50]. With a suitable chosen of the dispacements $\widetilde{\delta}_D$ and $\widetilde{\delta}_I$ the teleportation fidelity reads

$$\mathcal{F} = \frac{1}{\sqrt{\det \mathbf{\Gamma}}},$$

where $\mathbf{\Gamma} \equiv 2\mathbf{V}_{in} + \mathbf{Z}\boldsymbol{\alpha}\mathbf{Z} + \boldsymbol{\beta} - \mathbf{Z}\boldsymbol{\gamma} - \boldsymbol{\gamma}^T\mathbf{Z}^T$ and $\mathbf{Z} = diag\{1, -1\}$, that for a coherent input state becomes

$$\mathcal{F} = \frac{1}{1 + e^{-2r}}.$$
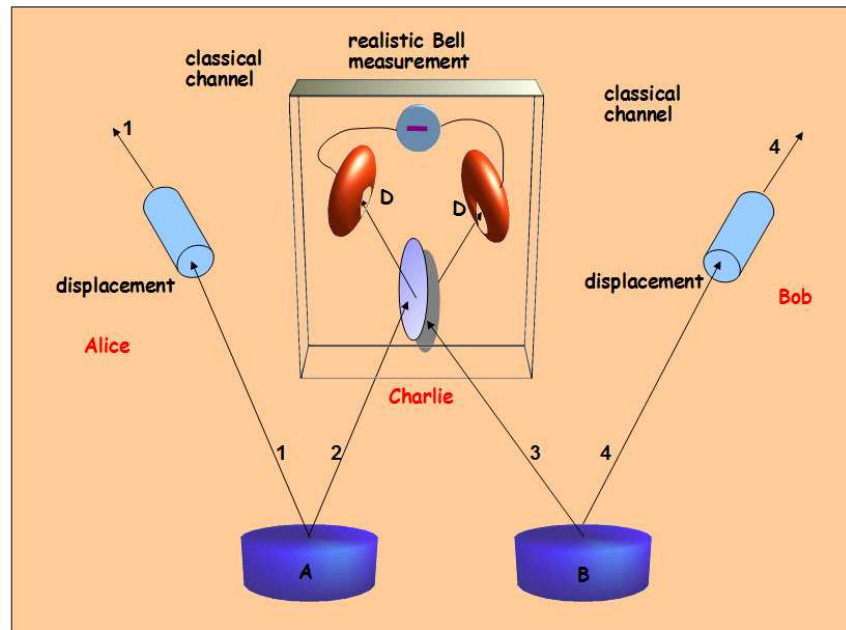
Figure 2.1: (Color online) Schematic picture of the non-ideal cv entanglement swapping protocol, in which two indipendent couples, **A** and **B,** of two-mode entanlged states $(1 - 2$ shared by Alice and Charlie, $3 - 4$ shared by Bob and Charlie) are used for producing the final swapped entangled state (composed by 1 and 4 modes), shared by the two final users Alice and Bob. See text for more details.
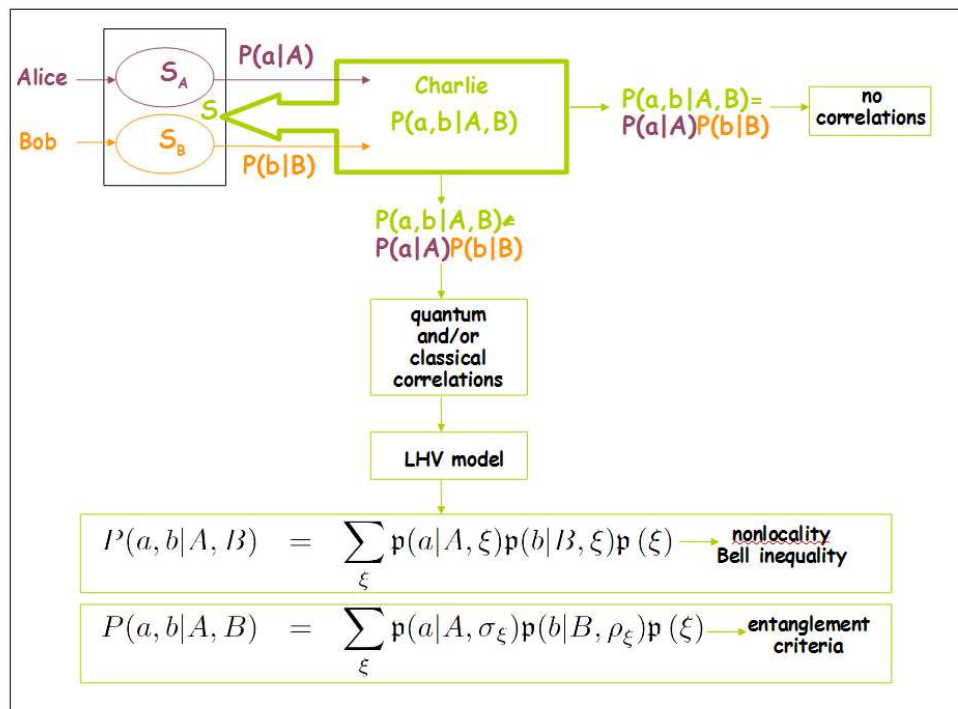
Figure 2.2: Pictorial representation (*color online*) of the scenario describing two possible test of nonlocality: Bell inequality and entanglement criteria. Alice makes a measurement on the subystem S_A, while Bob, indipendently, realizes a measurement on the subystem S_B. Charlie is the only acting on the joint system S. He compares the quantum expectation value (obtained considering whole system) with the product of the Alice's and Bob's results. If there isn't coincidence the system is correlated. To discriminate the quantum correlations from the classical ones Charlie applies the hidden variables theory LHV. For more details see text.
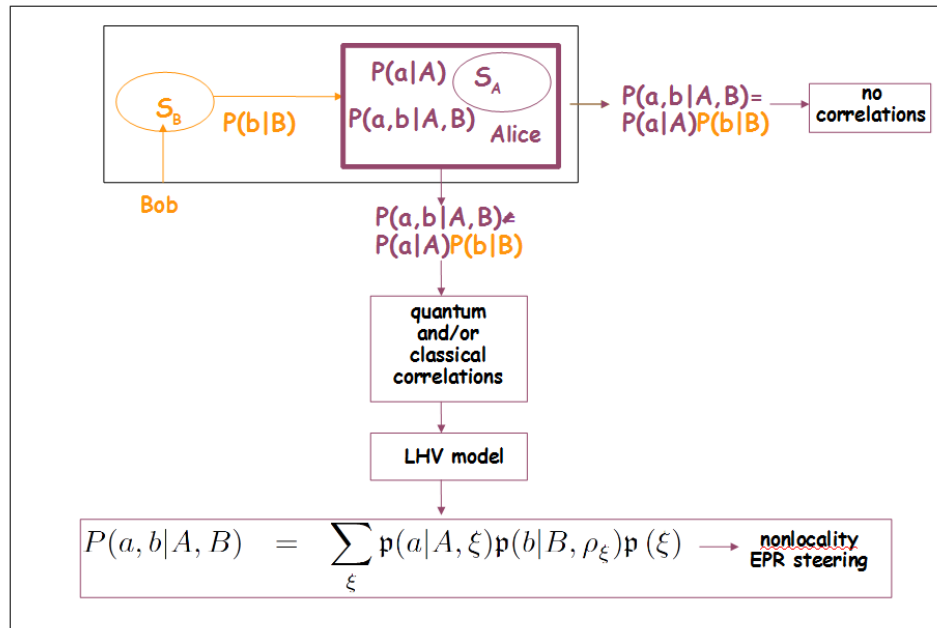
Figure 2.3: Pictorial representation (*color online*) of the scenario describing a possible test of nonlocality: EPR-steering. Alice prepares the whole bipartite state. Then she gives the subpart S_B to Bob. If two subsystems are correlated, then Alice can infer the Bob's quantum state by measurements made on S_A. To discriminate the quantum correlations from the classical ones Alice applies the hidden variables theory LHV. For more details see text.
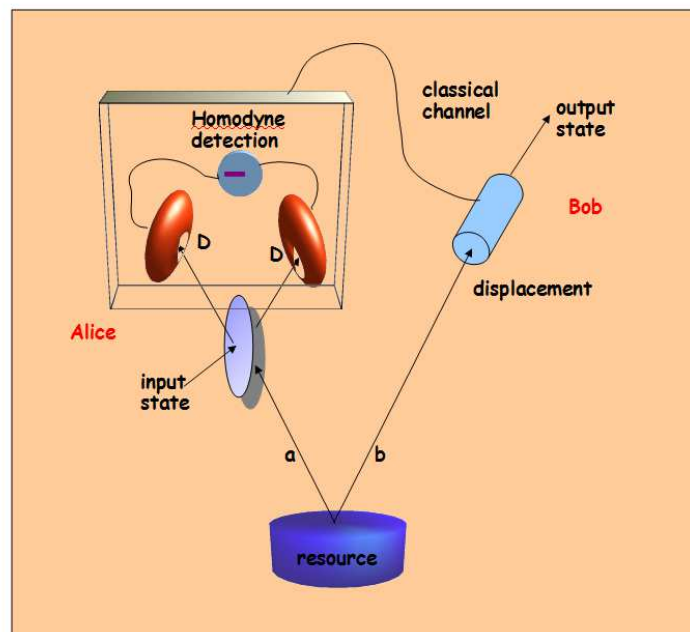
Figure 2.4: Schematic picture (*color online*) of the teleportation protocol, in which the resource (a two-mode entanlged state *a-b*), shared by Alice and Bob, is used for teleporting the input state from Alice's position to Bob's position. See text for more details.

Part II

Gaussian Resources

CHAPTER 3

GAUSSIAN STATES

The use of Gaussian states as resource in Quantum Information and Communication protocols is currently much debated. Although such states are of great pratical relevance, the non classical effects not always manifest themselves. Consider, for example, that the distribution function of Wigner is positive everywhere, so it can be used to construct a local hidden variable correlation and accordingly the Bell's inequality is never violated [47].

In this chapter, we explore the question of how useful is the use of a Gaussian resource in Quantum Information. At first we give some considerations on the extremality of the Gaussian states (§ 3.1). Then we specialize the markers introduced in the chapter 2 (e.g. mutual information, quantum discord, entanglement, teleportation fidelity) to Gaussian case, in order to identify indicators of non-classicality. Eventually, we study their evolution in a Gaussian channel. Gaussian channel plays a quite central role in Quantum Information and Communication, because it is a good model for the transmission of light through fibers, for random classical noise, introduced by Gaussian random displacements in phase space and losses that can be modelled as a beam splitter like interaction with the vacuum or a thermal mode.

We report some experimental tests carried out in the laboratory of Quantum Optics of the University of Naples *Federico II*.

The results reported in this chapter are shown in [6], [8].

3.1 Are Gaussian states extremals?

Gaussian states play a "particular" role in Quantum Information, besides their pratical relevance. They tend to be extremal within all continuous variable states with respect to different quantum properties [3]. For example, they minimize the content of entanglement in respect with the non-Gaussian states (at fixed covariance matrix). Precisely becouse of this particular property of extremality, in recent time the Gaussian states began to take a more marginal role compared to the increasing interest in the non-Gaussian states. However some clarifications are necessary.The extremality is demonstrated in [3] also over the entanglement measures taking in account the following lemma

Lemma 1 *Let $f : \mathcal{B}(\mathcal{H}^{\otimes N}) \to \mathbb{R}$ be a continuos functional, which is strongly superadditive and invariant under local unitaries U, $f(U^{\otimes N} \rho U^{\dagger \otimes N}) = f(\rho)$. Then for every density operator ρ describing an N-partite system with finite first and*

second moments, we have that

$$f(\rho) \geq f(\rho_G),$$

where ρ_G is the Gaussian state with the same first and second moments as ρ

Grouping the N parties of the Lemma 1 into $M \leq N$ ones and remembering that every entanglement measure is invariant, by definition, under local unitaries, the authors yield the following proposition

Proposition 2 *Let E be a continuous entanglement measure which is strongly superadditive. Then, for every density operator ρ describing an M-partite system with finite **CM** (and arbitrary, finite, number modes per site) we have that any Gaussian state ρ_G with same **CM** provides a lower bound*

$$E(\rho_G) \leq E(\rho). \tag{3.1}$$

Obviously, the estremality exists only for measures that verify the requirements of the Lemma.

Distillable entanglement E_D fulfills all the requirements. But the logarithmic negativity E_N that, among all the measures, is the most popular one as it is easy to calculate, fails the requirements. Moreover, doesn't satisfy Eq. (3.1), as shown in [3] by a simple counterexample:

Example 3 *For the state $|\varphi\rangle = \sqrt{1 - \lambda^2}\,|00\rangle + \lambda\,|11\rangle$, with $\lambda = 1/4$, we have $E_N(\varphi) = 0.57$ whereas $E_N(\varphi_G) \simeq 0.64$.*

We conclude that the issue is not trivial. What is the best resource to be used in quantum information depends on the type of protocol you want to use and on the particular quantum features it needs to give the best possible performance.

3.2 Quantum Markers

The markers of quantumness, described in the chapter 2, assume a feasible form for the Gaussian states. Indeed, since the Gaussian states are completely characterized by the first and second moments of the quadratures, all quantum markers are completely expressible as **CM**'s functions.

3.2.1 Mutual Information and Quantum Discord for Gaussian States

For Gaussian states, the Mutual Information Eqs. (2.5), (2.6) reads

$$\mathcal{I}(\boldsymbol{\sigma}) = f(\sqrt{I_1}) + f(\sqrt{I_2}) - f(d_+) - f(d_-), \tag{3.2}$$

where $f(x) = (x + 1/2)\log(x + 1/2) - (x - 1/2)\log(x - 1/2)$ and $d_\pm$ are the **CM** symplectic eigenvalues. In terms of the symplectic invariants read

$$\sqrt{2}d_\pm = \left[I_1 + I_2 + 2I_3 \pm \sqrt{(I_1 + I_2 + 2I_3)^2 - 4I_4} \right]^{1/2}.$$

Tha Quantum Discord Eq. (2.7) becomes

$$\mathcal{D}(\boldsymbol{\sigma}) = f(\sqrt{I_2}) - f(d_+) - f(d_-) + f\left(\frac{\sqrt{I_1} + 2\sqrt{I_1 I_2} + 2I_3}{1 + 2\sqrt{I_2}} \right). \tag{3.3}$$

3.2.2 Entanglement Criteria for Gaussian states

PHS Criterion for Gaussian states. The PHS criterion is a necessary and sufficient condition for separability, for all bipartite Gussian states.

Moreover, for a Gaussian state, described by the **CM** Eq. (1.8), it reads

$$n^2 + m^2 + 2\,|c_1 c_2| - 4\left(nm - c_1^2 \right)\left(nm - c_2^2 \right) \leq \frac{1}{4}. \tag{3.4}$$

In terms of symplectic invariants, the Ineq. (3.4) becomes

$$I_1 + I_2 + 2\,|I_3| - 4I_4 \leq \frac{1}{4}.$$

Duan Criterion for Gaussian states.

We note that, as proved in Ref. [33], any Gaussian state can be transformed, by local linear unitary Bogoliubov operations, *i.e.* by acting independently on one or both the subsystems by applying local squeezing and/or rotations, into the standard form

$$\boldsymbol{\sigma} = \begin{pmatrix} n_1 & 0 & c_1 & 0 \\ 0 & n_2 & 0 & c_2 \\ c_1 & 0 & m_1 & 0 \\ 0 & c_2 & 0 & m_2 \end{pmatrix}, \tag{3.5}$$

with the matrix elements satisfying the constrains

$$\frac{n_1 - 1/2}{m_1 - 1/2} = \frac{n_2 - 1/2}{m_2 - 1/2},$$
$$|c_1| - |c_2| = \sqrt{(n_1 - 1/2)(m_1 - 1/2)} - \sqrt{(n_2 - 1/2)(m_2 - 1/2)}. \tag{3.6}$$

In this case the EPR operators pair of Eq. (2.11) are written as

$$\widehat{u} = a_0 X_1 + (c_1)\frac{1}{a_0}X_2 \text{ and } \widehat{v} = a_0 Y_1 - (c_2)\frac{1}{a_0}Y_2 ,$$

where $a_0 = \sqrt{\frac{m_1 - 1/2}{n_1 - 1/2}} = \sqrt{\frac{m_2 - 1/2}{n_2 - 1/2}}$.

The sufficient and necessary Duan criterion is given by

$$a_0^2 \left(n_1 + n_2 - 1\right) + \frac{m_1 + m_2 - 1}{a_0^2} - 2\left(|c_1| - |c_2|\right) < 0 \ . \tag{3.7}$$

In a more general contest it is possible to write the sufficient but not necessary for a generic **CM** in the standard form of Eq. (1.8) as

$$\left(2n - 1\right) a^2 + \frac{\left(2m - 1\right)}{a^2} - 2\left(c_1 - c_2\right) < 0 \ , \tag{3.8}$$

where a can be set by $a^2 = \sqrt{\frac{m - 1/2}{n - 1/2}}$ to minimize the left hand side of the inequality:

$$\sqrt{\left(2n - 1\right)\left(2m - 1\right)} - \left(c_1 - c_2\right) < 0 \ . \tag{3.9}$$

We note that, while for symmetric states $(m = n)$ $|a| = 1$ and the EPR pair consists of two orthogonal field quadratures, this is not true, in general.

EPR-Reid Criterion for Gaussian states.

In terms of **CM** elements:

$$n^2 \left(1 - \frac{c_1^2}{nm}\right)\left(1 - \frac{c_2^2}{nm}\right) < \frac{1}{4} \ . \tag{3.10}$$

We note that, being based on conditional variances (and thus on conditional states) this criterion is not symmetric under the exchange of the two sub-systems. So that the criterion itself can be recast if sub–system A is measured and the conditional variance on B is given

$$m^2 \left(1 - \frac{c_1^2}{nm}\right)\left(1 - \frac{c_2^2}{nm}\right) < \frac{1}{4} \ . \tag{3.11}$$

The two statements (3.10), (3.11) of the EPR-Reid criterion can make it ambiguous if one of the relations are not satisfied. This is not the case of balanced systems $(m = n)$. Moreover, it can be proved that no pure state can asymmetrically violate the EPR criterion. It is easy to see that the above two expressions for the EPR criterion are invariant for symplectic transformations like the PHS one. In particular,

$$\frac{I_4}{I_2} < \frac{1}{4} \ \left(\frac{I_4}{I_1} < \frac{1}{4}\right)$$

For a pure state $I_4 = 1/16$ so that by (3.10), (3.11) we obtain

$$I_2 \ > \ \frac{1}{4},$$

$$I_1 \ > \ \frac{1}{4} \ .$$

3.2.3 Entanglement Witness

According to what is stated by the following lemma [51]

Lemma 4 *For any inseparable state $\rho \in \mathcal{H}_1 \otimes \mathcal{H}_2$ there exists Hermitian operator W such that $Tr(W\rho) < 0$ and $Tr(W\sigma) \geq 0$, for any separable σ, where the operator W is called entanglement witness.*

For any entangled state ρ there exists entanglement witness W.

Now we define three different entanglement witness, one each for the three criteria,

$$
\begin{aligned}
w_{PHS} &= 4\left(nm - c_1^2\right)\left(nm - c_2^2\right) + \frac{1}{4} - \left(n^2 + m^2\right) - 2\left|c_1 c_2\right| , \\
w_{DUAN} &= 2\sqrt{\left(n - \frac{1}{2}\right)\left(m - \frac{1}{2}\right)} - (c_1 - c_2) , \\
w_{EPR} &= n^2\left(1 - \frac{c_1^2}{nm}\right)\left(1 - \frac{c_2^2}{nm}\right) - \frac{1}{4} .
\end{aligned}
\tag{3.12}
$$

In summary, for a Gaussian bi–partite state the three criteria (see Eqs. (3.4), (3.9), and (3.10)) reduce to

$$
\rho \text{ is entangled} \left\{
\begin{aligned}
&\Longleftrightarrow w_{PHS} < 0 \\
&\Longleftarrow \left\{
\begin{aligned}
w_{DUAN} &< 0 \\
w_{EPR} &< 0
\end{aligned}
\right.
\end{aligned}
\right. .
\tag{3.13}
$$

The three witnesses don't satisfy the requirements for being a measure of entanglement. For example they don't verify the basic axiom stating that a good measure should be equal to 0 for any separable state [52].

However, once the state ρ is entangled w_{PHS}, w_{DUAN} and w_{EPR} provide suitable markers for evaluating how far the state is from being separable. Somehow they measure the robustness of the entanglement.

We note that for *diagonal* fully symmetric states ($n = m$ and $c_1 = -c_2 = c$ in Eq. (1.8)), i. e. described by the following **CM** matrix

$$
\widetilde{\boldsymbol{\sigma}} = \begin{pmatrix}
n & 0 & c & 0 \\
0 & n & 0 & -c \\
c & 0 & n & 0 \\
0 & -c & 0 & n
\end{pmatrix} ,
\tag{3.14}
$$

w_{PHS}, w_{DUAN} and w_{EPR} read

$$
\begin{aligned}
w_{PHS} &= 4\left(n^2 - c^2\right)^2 + \frac{1}{4} - 2n^2 - 2c^2 ,
\tag{3.15}
\end{aligned}
$$

$$
w_{DUAN} = 2\left(n - c\right) - 1 ,
\tag{3.16}
$$

$$
w_{EPR} = n^2\left(1 - \frac{c^2}{n^2}\right)^2 - \frac{1}{4} ;
\tag{3.17}
$$

and the two bounds $(c > n - 1/2)$ for w_{PHS} and w_{DUAN} coincide while the bound for w_{EPR} is $c > \sqrt{n\left(n - \frac{1}{2}\right)}$ so that the EPR-Reid criterion is stricter than the PHS and Duan ones for any allowed value of n.

3.2.4 An extra marker: the purity

The purity of the composite system cannot be considered a general entanglement marker [53]. As a matter of fact, any pair of physical systems in a pure state has $\mu = 1$ even if they are disentangled. Nevertheless, it is useful to introduce the purity (1.9) as an extra marker that tells how far the analysed state is from a pure one, i.e. the extent to which the experimental entanglement tests, especially in cv regime, must be described in terms of density matrices rather than wavefunctions. In fact, the states that it is possible to prepare and to manipulate in the laboratory are mixed. This is due to the circumstance that even when the state is born pure, it decoheres into a mixture by interacting with the external world [18] and the quantumness can be completely lost. In this context the purity becomes a crucial marker.

The experimental data presented in this chapter refer to cv entangled state, generated by a type-II sub–threshold OPO [7]. In this specific case, we have a precise hypothesis on the ideal state: it is a pure twin–beam diagonal state, described by the **CM** (3.14). Since the state, at the birth ($t = 0$), is pure, by Eqs. (1.3) with $N = \infty$ (cv) and (1.9), we obtain that the correlation parameter c is equal to $c = \sqrt{\left(n^2 - \frac{1}{4}\right)}$. At the outing of the OPO crystal, the state starts to loose its purity becoming mixed, by Eqs. (1.3), (1.9), we have

$$c \leq \sqrt{\left(n^2 - \frac{1}{4}\right)}, \tag{3.18}$$

with the equal sign valid only for pure states. This allows us to consider μ as a measure of the total decoherence that has affected the state.

3.2.5 Teleportation fidelity with Gaussian resources

If we imagine to teleport a coherent state $|\beta\rangle$ and use, for this purpose, a two-mode pure squeezed vacuum state as a resource, the fidelity of teleportation reads [50]

$$\mathcal{F} = \frac{1}{e^{-2r} + 1}. \tag{3.19}$$

We can see that only in the limit of infinite squeezing, the fidelity is equal to one, i.e. there is perfect coincidence between the initial state and the state actually teleported. However, this is impossible to obtain because it is need to infinite energy (unphysical resource). The relationship (3.19) seems to leave it to say

that a very large value of r, but still finite (finite energy), the fidelity may be one, i.e. it seems that the only obstacle to a teleportation with complete success (probability of success equals to one) is technical: to arrange an experimental setup that produces a squeezed vacuum state with a high parameter of squeezing r. Instead, there is an impediment of physical nature which manifests itself most clearly when we express the fidelity in terms of the **CM** elements.

The relation Eq. (3.19) is obtained when the resource is a pure Gaussian state. More generally, we have a (pure or mixed) Gaussian state described by the matrix $\boldsymbol{\sigma}$ Eq. (1.7). The success of teleportation $\mathcal{F}$ of a coherent state with such state (1.7) is given by [50]

$$\mathcal{F} = (\det \boldsymbol{\Gamma})^{-\frac{1}{2}}, \tag{3.20}$$

where

$$\boldsymbol{\Gamma} \equiv 2\boldsymbol{\sigma} + \mathbf{Z}\boldsymbol{\alpha}\mathbf{Z} + \boldsymbol{\beta} - \mathbf{Z}\boldsymbol{\gamma} - \boldsymbol{\gamma}^T Z^T,$$

with $\mathbf{Z} \equiv diag\{1, -1\}$. To make easier the algebra, we assume that the state is described by the **CM** Eq. (3.14), so the teleportation fidelity Eq. (3.20) reads

$$\mathcal{F} = \frac{1}{1 + 2(n - c)}. \tag{3.21}$$

The Eq. (3.21) shows that to be completely successful teleportation is necessary that $n = c$, but this circumstance is prohibited by the Eq. (3.18), i.e. it is impossible to have $\mathcal{F} = 1$ with Gaussian resource, also if the state is pure. However, for $n \to \infty$, $\sqrt{n^2 - 1/4} \to n$, i.e. once again we find that in the limit of infinite energy the fidelity goes to one.

3.3 Teleportation fidelity and Entanglement

As we have said in the chapter 2 $\mathcal{F} = 0.5$ sets [23] a boundary for entrance into the quantum domain in the sense that Alice and Bob can exceed this value only making use of entanglement. So entanglement is a sufficient condition to *quantum fidelity*, but not necessary.

By the Eq. (3.19) it is evident that a pure squeezed vacuum state, used as resource in a teleportation protocol of a coherent state, gives $\mathcal{F} = 0.5$ for $r = 0$, while exceeds this value as soon as we turn on the entanglement ($r > 0$).

A similar relation can be found also on the mixed resource. In fact, for a state described by the matrix (3.14), the fidelity can be easily expressed in terms of the Duan witness (3.16) as

$$\mathcal{F} = \frac{1}{2 + w_{DUAN}}. \tag{3.22}$$

We can see again that in absence of entanglement ($w_{DUAN} = 0$), the maximum is given by $\mathcal{F} = 0.5$.

In this sense teleportation fidelity appears as an entanglement indicator.
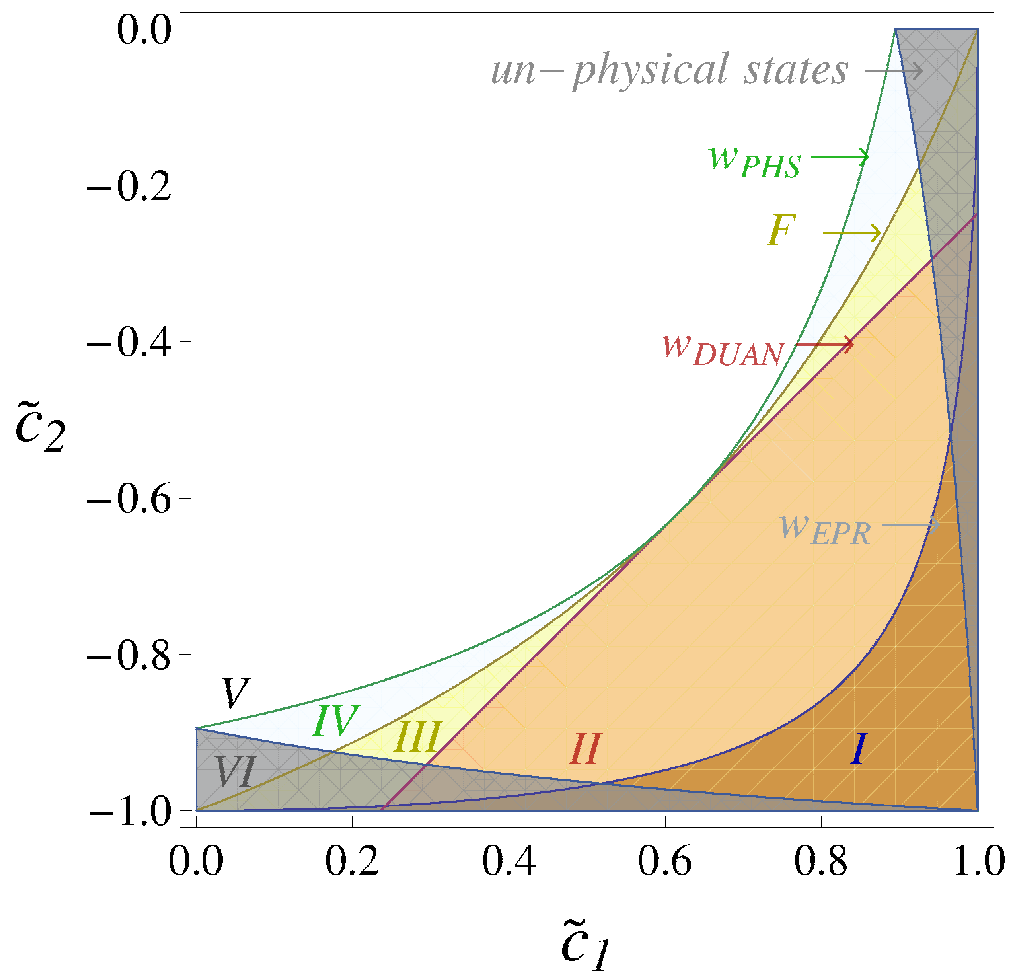
Figure 3.1: Region plot (*color online*) of the different entaglement witnesses of Eqs. (3.12) and teleportation fidelity (Eq. (3.21)) as an entanglement marker. The *light gray* (labelled with (VI)) areas indicate un-physical **CM**s (*i.e.* violating inequality (1.16). The different criteria show different regions of entanglement (see text for details).

In Fig. 3.1 we have visualized the different region plots set by the three entanglement witnesses Eqs. (3.15), (3.16), (3.17) and the region for which $\mathcal{F} > 1/2$ (see Eq. (3.21)). The regions have been identified considering a **CM** in the form of Eq. (1.8) with $m = n$ (balanced system). The axes report the value of $\tilde{c}_1$ (below) and $\tilde{c}_2$ (left), the two correlation terms of the covariance matrix normalized to $c_{MAX} = \sqrt{n^2 - 1/4}$ so that $\tilde{c}_1 = -\tilde{c}_2 = 1$ will represent a pure maximally entangled state (*i.e.* the state showing the maximum quantum correlation for a given total energy of the system, see subsection ...). We note that the fully symmetric states, described by the **CM** (3.14), that we indicated as *diagonal* states, lay on the plot diagonal (top–left to bottom–right).

The *light gray* (labelled with (*VI*)) area indicates un–physical states *i.e.* **CM** violating inequality (1.16).

The state lying on the diagonal starting in $\tilde{c}_1 = -\tilde{c}_2 = 1$ satisfy the conditions (see Eq. (3.6)) for which the Duan criterion becomes also necessary so that the coincidence between the Duan and the PHS bounds, along the diagonal, is not a surprise. Being both necessary and sufficient they coincide. For these *diagonal* states entanglement (seen as non–separability property) implies $\mathcal{F} > 1/2$, so we can see that, in the plot, along the diagonal, the three bounds $\mathcal{F} > 1/2$, $w_{PHS} < 0$ and $w_{DUAN} < 0$ coincide.

There are two pairs of interesting regions in the plot that deserve some comments. The first one, encompassing area labelled as (*III*) and (*IV*) in the plot (*light green* and *yellow*), represents areas where the states violate the PHS bound ($w_{PHS} < 0$) while they do not the Duan one ($w_{DUAN} \geq 0$). This apparent ambiguity can be solved noting that the **CM** represented by these regions do not respect the condition (3.6) so that the non–negativity of w_{DUAN} does not imply a separability of the state. On the other hand for such states $w_{PHS} < 0$ implies that they are effectively entangled. By transforming by local squeezing operations, as outlined in Ref. [33], these **CM** into a form that respect conditions (3.6) it is possible to see that the transformed states show $w_{DUAN} < 0$. We have numerically done a few tests on such *odd* matrices, verifying that once taken into that form, the states violate the Duan bound (3.7) as well, so confirming that the Duan and PHS criterion are equivalent. We note that, being the latter written in a more general form, it is more useful from the practical point of view. Moreover, such a matrix transformation take states lying outside of the diagonal on the plot, completely out from the plot itself. Indeed, the transformed **CM** have the form given in Eq. (3.5) different from the one in Eq. (1.8) and represented in the plot. We also note that the referred transformation change also the EPR operators pair (see Eq (2.11)).

The second interesting region, labelled with (*IV*) (*light green*) in Fig. 3.1, represents states that, although entangled, cannot be used for teleporting coherent states, **CM** lying inside this area will not give $\mathcal{F} > 1/2$. It is interesting to note that such states fall also inside the region for which the Duan criterion (3.9) is

not fulfilled. As above mentioned, once the relative **CM** is transformed into the form (3.5) by local squeezing the transformed state will fulfill the Duan criterion in the form (3.7) so that, in this new scenario, the system is surely entangled. At the same time, if this novel state is used as a quantum resource for teleportation of a coherent state it will give $\mathcal{F} > 1/2$ [50] so that the local squeezing acts as entanglement unveiling. The initial state lying in this area is entangled for PHS, being $w_{PHS} < 0$, but, form the point of view of teleportation, entanglement manifests itself in an useless way. This entanglement can be made useful by locally transforming the two subsystems.

We can see that the EPR criterion (region (I), *light brown*) offers a more restrictive condition with respect to the other two criteria even for diagonal states.

Region (II) (*salmon*) represents the bound fixed by the Duan criterion as a sufficient but not necessary condition. While region (V) (*white*) represents separable states.

3.4 Quantum markers evolution

We can see that the evolution, Eq. (1.14), preserves the Gaussian character of the initial state and in terms of the **CM** $\boldsymbol{\sigma}$ reads

$$\boldsymbol{\sigma}(t) = \left(1 - e^{-\Gamma t}\right) \frac{1}{2}\mathbb{I} + e^{-\Gamma t}\boldsymbol{\sigma}(0), \tag{3.23}$$

where $\boldsymbol{\sigma}(0)$ is the covariance matrix at $t = 0$.

This form is in all equal to the effects of a fictitious beam–splitter (BS) that mimics the channel losses and couples into the system the vacuum quantum noise through its unfilled port. Being $U_k\left(\zeta\right) = \exp\left\{\zeta\left(a_k^\dagger v_k - v_k^\dagger a_k\right)\right\}$ the $SU(2)$ transformation induced by the BS on the k–mode ($k = 1,\ 2$, with v_k the modal operator for the vacuum) and $T = e^{-\Gamma t}$ the power transmission of the beam splitter ($\tan\zeta = \sqrt{(1-T)/T}$), the above equation becomes:

$$
\begin{aligned}
\boldsymbol{\sigma}_T &= (1 - T)\frac{1}{2}\mathbb{I} + T\boldsymbol{\sigma}_1 \\
&= \begin{pmatrix} \boldsymbol{\alpha}_T & \boldsymbol{\gamma}_T \\ \boldsymbol{\gamma}_T^\top & \boldsymbol{\beta}_T \end{pmatrix},
\end{aligned} \tag{3.24}
$$

In this form we can drop the temporal dependence and label the **CM** of the initial state as $\boldsymbol{\sigma}_{T=1} \equiv \boldsymbol{\sigma}_1$. For states in the form of Eq. (1.8) the different elements evolve as

$$
\begin{aligned}
j_T &= \frac{1}{2} + T\left(j - \frac{1}{2}\right), \\
c_{i,T} &= c_i T
\end{aligned} \tag{3.25}
$$

with $j = n$, m and $i = 1, 2$. For $\Gamma \rightarrow \infty$ (corresponding to an infinite transmission channel) $T \rightarrow 0$ and $\boldsymbol{\sigma}_T \rightarrow \frac{1}{2}\mathbb{I}$ *i.e.* the covariance matrix of the vacuum state.

The quantum markers introduced in the § 3.2 are **CM** function, so they evolve consequently.

Henceforth the subscript $_T$ will indicate the quantity undergone to a lossy transmission described by Eq.(3.24).

We note that the vacuum state obtained for $T = 0$ is a pure one *i.e.* $\mu_0 = 1$. Moreover, in the ideal case (no loss), the OPO would generate a pure state as well. Being $\mu_{0<T<1} < \mu_{0,1}$ the evolution of μ_T in T is not monotonic. This is another indication that the purity of the composite system cannot be considered a general entanglement marker.

It is easy to see that $\mathcal{F}_T$, $w_{PHS,T}$, and $w_{DUAN,T}$ describe properties very robust under decoherence. Once they are $\mathcal{F} > 1/2$, $w_{PHS} < 0$ and $w_{DUAN} < 0$ for $T = 1$ they will keep breaking the respective bounds for every level of loss. Both mutual information and quantum discord show, with respect to loss, the same feature even if decoherence affects their amount. On the contrary a state that show EPR–like correlation ($w_{EPR} < 0$) for $T = 1$ will not keep this property along the propagation so that some particular protocol based on this property cannot be reproduced. Under a total loss greater than 50% any state looses this correlation property.

3.5   The Experiment

The transmission over a Gaussian channel is described by Eq. (1.14). This evolution is in all equivalent to a fixed amount of loss introduced by a fictitious beam–splitter. The actual experimental apparatus is made of the cv entangled state source, a variable attenuator (mimicking the BS), and a state characterization stage. A block diagram of the experimental setup is presented in Fig. 3.2

3.5.1   The cv entangled state source

The [7] state source relies on a CW internally frequency doubled Nd:YAG laser (*Innolight Diabolo*) whose outputs @532nm and @1064nm are respectively used as the pump for a non degenerate optical parametric oscillator (OPO) and the local oscillator (LO) for the homodyne detector. The OPO is set to work below the oscillation threshold and it provides at its output two entangled thermal states (the signal, a and the idler b).

The OPO is based on an α-cut periodically poled KTP non linear crystal (PPKTP, *Raicol Crystals Ltd.* on custom design) which allows implementing a type II phase matching with frequency degenerate and cross polarized signal and idler beams, for a crystal temperature of $\approx 53°$C. The transmissivity of the
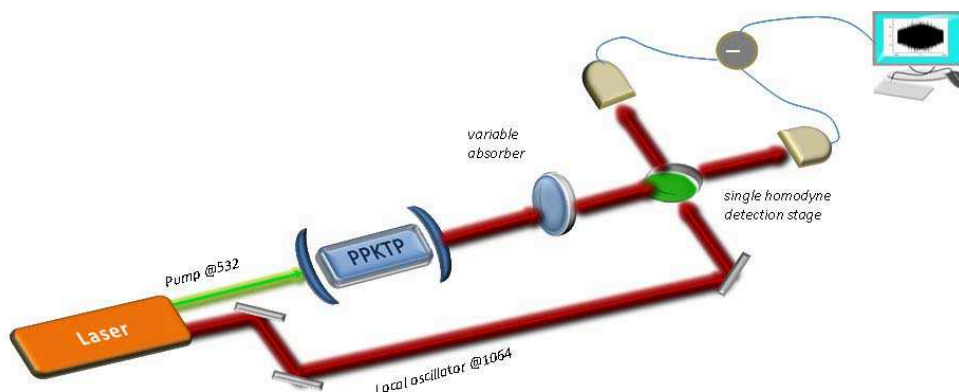
Figure 3.2: *(color online)* Block diagram of the experimental setup, able to implement the Eq. (3.23). The details on the OPO source are given §3.5.1 [54], while the characterization stage, based on a single homodyne detector, is fully described in Ref. [56, 58].

cavity output mirror, T_{out}, is chosen in order to guarantee, together with crystal losses (κ) and other losses mechanisms (T_{in}), an output coupling parameter $\eta_{out} = T_{out}/(T_{in} + \kappa)$ @1064 nm of ≈ 0.73, corresponding to an experimental linewidth of 15 MHz @1064 nm. In order to obtain a low oscillation threshold, OPO cavity geometry is set to warrant simultaneous resonance on the pump, the signal and the idler: pump resonance is guaranteed by servo-assisting the OPO cavity with a Drever Pound Hall system, while the resonance of other beams is induced by exploiting the natural birefringence of the KTP to tune the optical path of each beam inside the cavity, through a fine control of the crystal temperature and tilts [54]. Measured oscillation threshold is around 50 mW; during measurement runs the system has been operated at $\approx$60% of the threshold power to avoid unwanted non–Gaussian effects [55].

The two beams outing the OPO are transmitted through a filter of variable optical density. The loss level introduce by the filter is polarization independent and can be tuned from a few percent up to more than 99%.

3.5.2 The state characterization stage

The laser beam used for the experiment is emitted at the wavelenght $\lambda = 532$ *nm*. It is obtained by the Nd:YAG laser *Innolight Diabolo* through a second harmonic generation process. The beam is sent to the Type-II sub-threshold OPO described in § 3.5.1, that produces two beams athe the wavelenght $\lambda = 1064$ *nm*: the signal and the idler modes. A polarization system at the output of the OPO allows to choose the beam to be detected with a standard homodyne detector. The polarization system is made of an half-wave plate ($\lambda/2$) followed

by a polarizing beam splitter (PBS); the different wave-plate orientations allow choosing the beam to be transmitted by the PBS: the signal (a), the idler (b) or their combinations $c = \frac{1}{\sqrt{2}}(a + b)$ or $d = \frac{1}{\sqrt{2}}(a - b)$. Two other combinations, $e = \frac{1}{\sqrt{2}}(ia+b)$ and $f = \frac{1}{\sqrt{2}}(ia-b)$, can be obtained by inserting before the PBS an additional quarter wave plate ($\lambda/4$) [56, 57]. Acquisition times are considerably short thank to pc-driven mechanical actuators that allow setting the $\lambda/2$ and $\lambda/4$ positions in a fast and well calibrated manner.

Once a beam is selected, it goes to an homodyne detector put downstream the PBS. This exploits, as local oscillator, the laser output @1064 nm, previously filtered and adjusted to match the geometrical properties of the OPO output: a typical interferometer visibility is 0.98. The LO oscillator phase θ is spanned by a piezo-mounted mirror, linearly driven by a ramp generator who is, in turns, adjusted to obtain a 2π variation in 200 ms. In order to avoid low frequency noise in the homodyne current, it is demodulated at Ω=3 MHz and low-pass filtered (B=300 KHz). Then it is sampled by a PCI acquisition board (Gage 14100) obtaining 10^6pts/run, with 14-bit resolution. The electronic noise floor is 16 dBm below the shot noise level, corresponding to the a SNR $\approx$40. Data are analysed by a ©Mathematica routine that extract from the six homodyne traces the relevant quadrature variances necessary for reconstructing the whole covariance matrices [56].

3.6 Experimental results in the range $0.01 \leq T \leq 0.63$

We have performed different sets of measurement under lossy transmission in order to investigate different loss regime. Each experimental **CM** comes from seven homodyne traces: the shot noise calibration trace, obtained by obscuring the OPO output, six traces each for one of the six modes required for a full state characterization. Contrarily to other previous experiments, where quantum tomographic routine were used in order to retrieve experimental **CM**s without any *apriori* hypothesis on the measured state [58], we have evaluated **CM**s by a simpler ©Mathematica routine that calculates relevant second order moments of homodyne distributions in a faster way without enhancing the experimental indeterminacy on the **CM** elements. We have tested on a few **CM**s that this procedure gives results in all compatible with quantum tomography. We have also checked, with the standard procedure outlined in [59], that the states under scrutiny were effectively Gaussian.

Once a **CM** is obtained the different entanglement witnesses (w_{PHS}, w_{DUAN}, and w_{EPR} Eq. (3.12)), state purity (μ Eq. (1.9)), teleportation fidelity ($\mathcal{F}$ Eq. (3.21)), quantum discord ($\mathcal{D}$ Eq. (3.3)), and mutual information ($\mathcal{I}$ Eq. (3.2)) are calculated. Then, the overall decoherence, *i.e.* the total level of loss that includes OPO cavity escape efficiency, propagation loss, filter absorption, homodyne efficiency, is assigned as a label to the measurement. This expected level

of decoherence is then compared to the theoretical one obtained by inverting Eq. (3.24) and solving for T under the condition $\det(\boldsymbol{\sigma}_1) = 1/16$; thus requiring that $\boldsymbol{\sigma}_1$ represents a pure state (see the discussion at the end of Sect.3.2.4). We have verified that, even if experimental **CM**s do not reproduce exactly *diagonal* states, all of them respect the Duan conditions (3.6) within experimental indeterminacies. So that for the analysed matrix the Duan witness w_{DUAN} represent a sufficient and necessary condition for entanglement.

In all the reported plots we have considered the less decohered datum (obtained for $T = 0.63$) as a reference so that all the reported theoretical curves are obtained imposing that Eqs. (3.25) and the quantum markers as function of the Eq. (3.25) evaluted for $T = 0.63$ give the measured values.

The total losses we have measured span the interval $37 - 99\%$ ($0.01 \leq T \leq 0.63$). We note that $T = 0.63$, having a cavity escape efficiency of ≈ 0.73 implies an overall state detection efficiency of ≈ 0.86 in agreement with an homodyne visibility of 0.98 ± 0.01, a photodiode (nominal) efficiency of 0.90 ± 0.01 and residual transmission loss between the OPO output mirror and the detector surface of 0.01 ± 0.01.
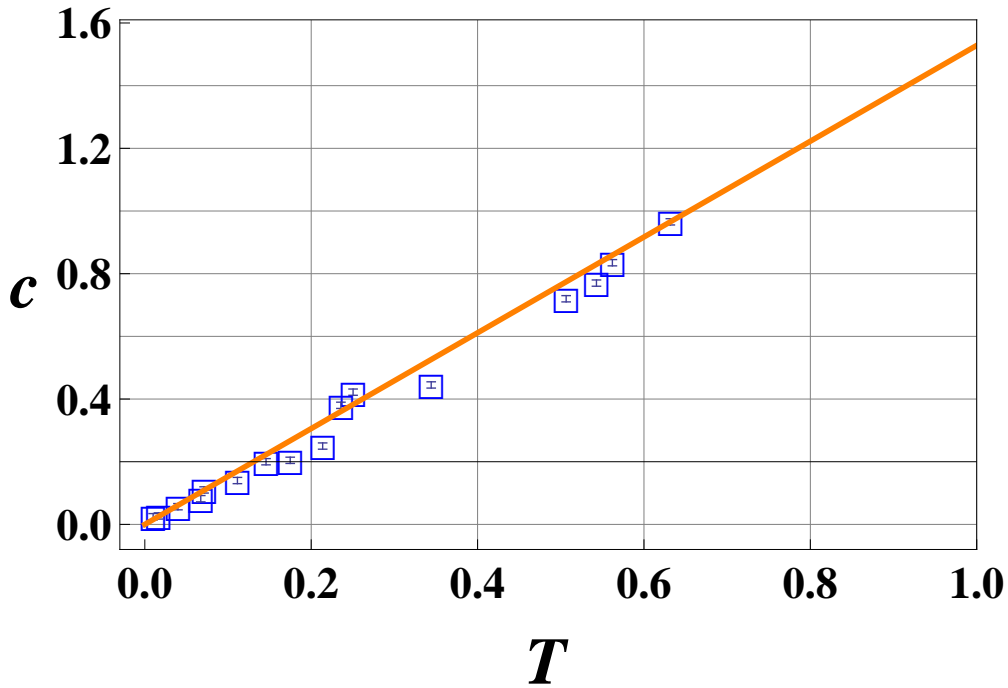
Figure 3.3: *(color online)* Behavior of $c = |c_{1,T}| + |c_{2,T}|/2$ in Eq. (3.24). The full (*dark orange*) line represents the theoretical behaviour calculated starting from the first experimental point we have measured ($T = 0.63$); the experimental points (*blue color*) follow the theoretical line, i.e., as expected, the correlation reduces linearly with T.

In Fig. 3.9 we report the behavior of $c = \left(|c_{1,T}| + |c_{2,T}| \right) / 2$, i.e. the averaged correlation terms see Eq. (3.25)). As expected the correlation between the two sub–systems degrades linearly with the total loss ($T \to 0$). The expected behavior (full *dark orange* line), obtained by considering the less absorbed **CM** ($T = 0.63$) as a reference, follows quote well the reported data. Actually, setting the less absorbed datum as a reference can be seen as assuming that the actual state outing the OPO is the same over the complete acquisition run. This is a strong hypoyhesis that cannot be exactly fulfilled for tehcnical reasons. Thus, the scattering of the point around that line is more due to source long–term dynamics then to actual deviation from the Lindblad model. At the same time the fact that the points are reasonably close to that line prove that the long term stability of the source can be considered quite good.
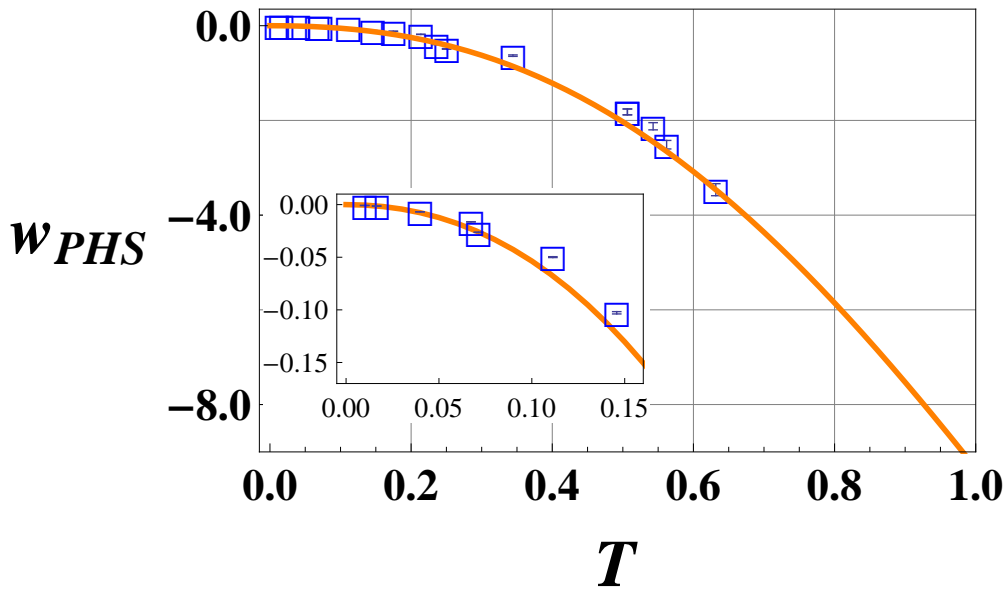
Figure 3.4: *(color online)* w_{PHS} vs.T. The full (*dark orange*) line represents the theoretical behavior, calculated starting from the first experimental point at $T = 0.63$. Error bars are obtained by propagating the experimental uncertainty on the **CM** elements in the expression of w_{PHS} in Eq. (3.12). The inset is a magnification of the plot in the high loss regime ($T < 0.15$). We see that the un–separability persists, as witnessed by w_{PHS}, even in presence of strong decoherence.

As already mentioned, w_{PHS} and w_{DUAN} describe a physical property of the state that is strong under decoherence. This can be seen in Figs. 3.10 and 3.5 where w_{PHS} and w_{DUAN} are plotted vs. T. We have also enlarged, in the insets the region for strong loss ($T > 0.85$) to prove that, even if the analysed state is very close to a two-mode vacuum (the total average number of photon $\left((n + m - 1) / 2 \right)$
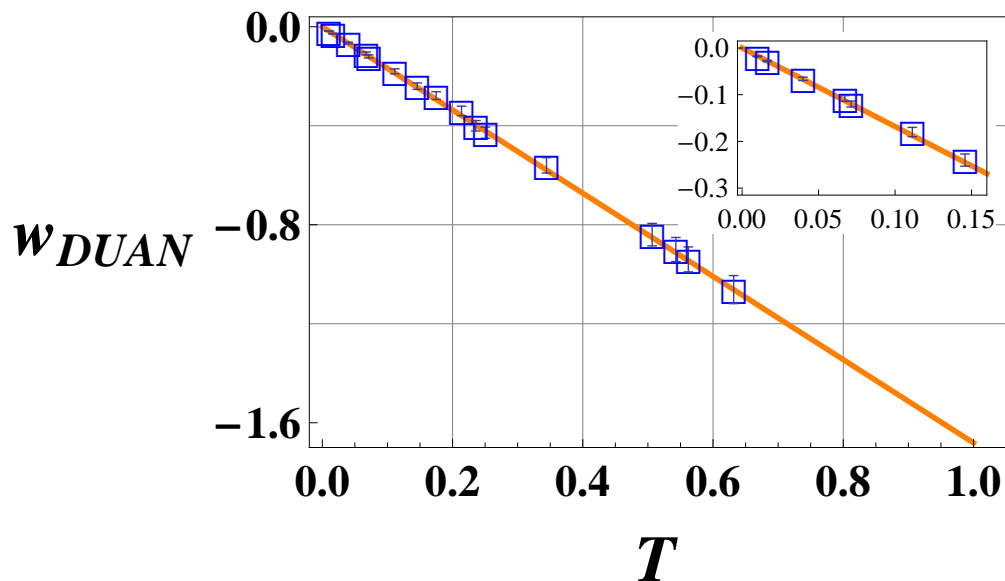
Figure 3.5: *(color online)* w_{DUAN} vs.T. The full (*dark orange*) line represents the expected behavior calculated starting from the first experimental point we have measured ($T = 0.63$). Error bars on the experimental points (*blue*) are obtained by propagating the uncertainty on the measured **CM** elements in Eq. (3.12). The inset is a magnification of the plot in the high loss regime ($T < 0.15$) in order to stress the persistence of entanglement, as witnessed by w_{DUAN}, even in presence of strong decoherence.

reduce to 0.02 ± 0.01) it is still experimentally possible to prove that the state is non–separable. It has to be noted that, while for $T \to 0$, w_{PHS} approaches its classical limit non–linearly, w_{DUAN} is linear. Thus, in the very high loss regime it becomes more reliable to assess entanglement using the latter than the former.
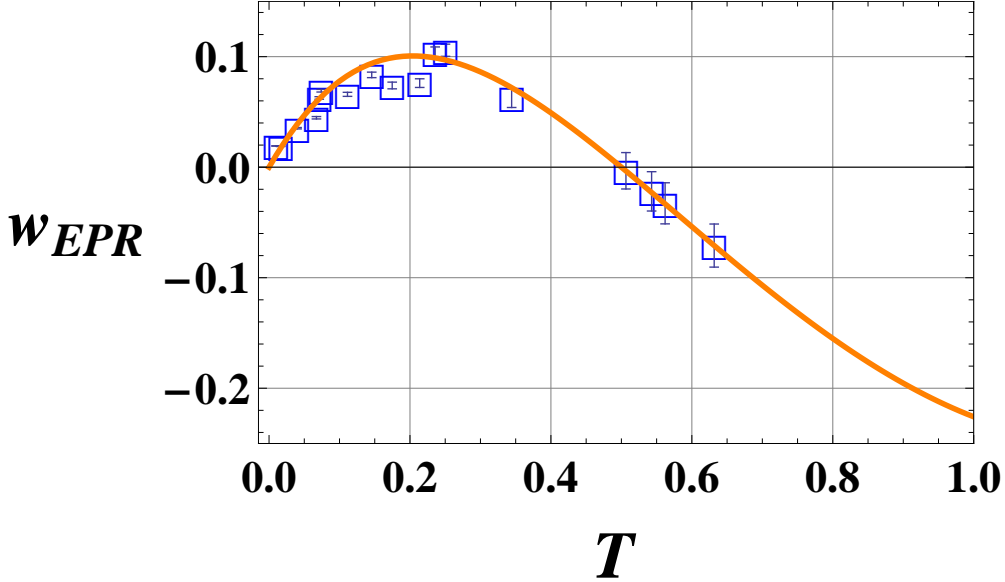
Figure 3.6: *(color online)* w_{EPR} vs.T. The full *(dark orange)* line represents the expected behaviour calculated starting from the first experimental point we have measured ($T = 0.63$). Error bars are obtained by propagating the uncertainty on the **CM** elements in Eq. (3.12). They are considerably larger for point at low loss.

$w_{EPR} < 0$ indicates that the state exhibits EPR–like correlation so that it is possible to gain information on the expectation value of one observable on one sub–system with a precision better than the standard quantum limit once the EPR companion is measured on the other sub–system. These feature is by far the most fragile under decoherence: for $T < 0.5$ no state can keep this quantum feature. This can be understood from the fact that loss, a stochastic process, affects directly the degree of correlation between the two sub–systems while the system representation (*i.e.* its un–separability) is only smoothed by this process. It is relevant to note that $T = 0.5$ also coincide with the minimum state purity μ. So that, loosing the EPR character coincides with the maximum mixedness for the state during its propagation. In Fig. 3.6 we report the experimental behavior found for w_{EPR} for our state. Measured **CM**s for $T < 0.5$ all show $w_{EPR} > 0$. A positive w_{EPR} indicates that, for these states, any attempt to gain information on one sub–system by measuring the other would result less precise than the standard quantum limit.
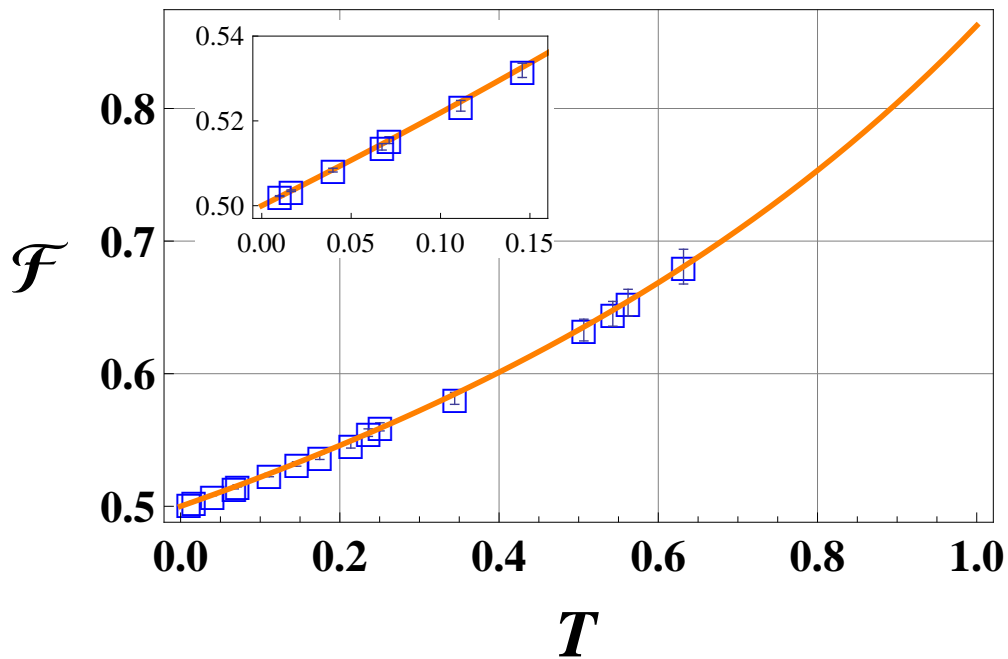
Figure 3.7: *(color online)* $\mathcal{F}$ vs.T. The full *(dark orange)* line represents the expected behavior calculated starting from the first experimental point we have measured ($T = 0.63$). The inset is a magnification of the plot in the high loss regime ($T < 0.15$) in order to underline the persistence of a quantum teleportation regime even in presence of strong decoherence (high loss).

An important signature for an entangled cv state is its ability of acting as a quantum resource in the cv teleportation protocol for coherent state. In Eq. (3.21) we have expressed the fidelity $\mathcal{F}$ as a function of the **CM** elements. $\mathcal{F}$, as w_{PHS} and w_{DUAN}, represents a robust signature of quantum properties for the state undergoing to a lossy transmission. In particular, in Fig. 3.11, we see that even in the high loss regime, $\mathcal{F}$ remains above the classical limit of 0.5 (see the inset for greater details). Thus proving that cv entangled state, as the one produced by our source, could, in principle, be though as the resource for realising teleportation protocol of coherent state, in principle, at an infinite distance.

Eventually we have retrieved, from our **CM**s, the value for the quantum mutual information $\mathcal{I}(\boldsymbol{\sigma})$ (Eq. (3.2)) and quantum discord $\mathcal{D}(\boldsymbol{\sigma})$ (Eq. (3.3)).
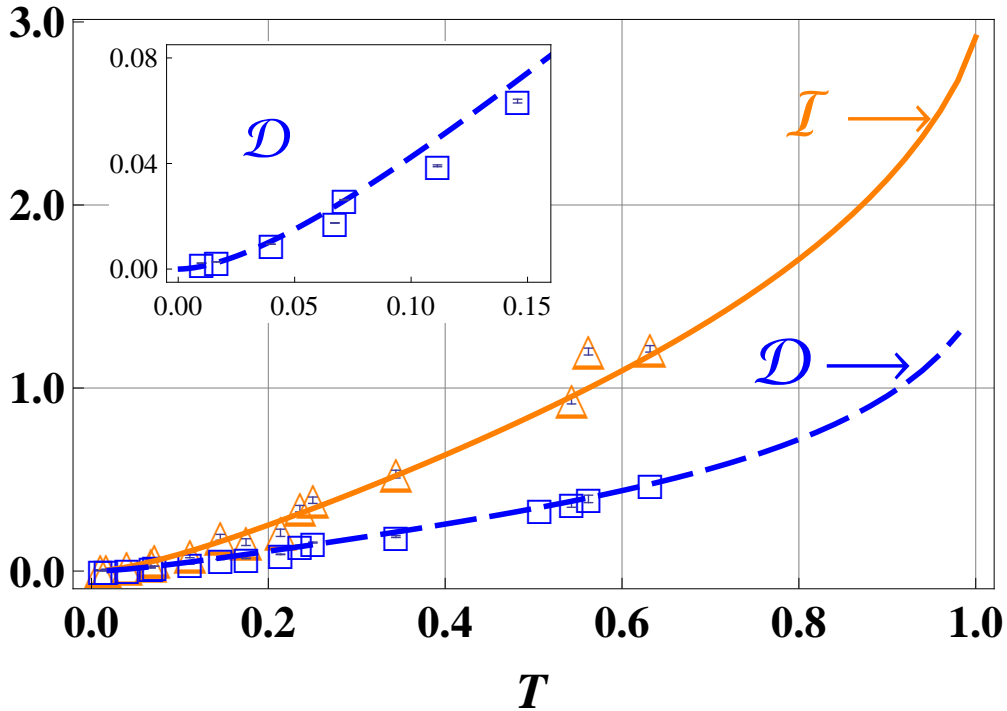
Figure 3.8: *(color online)* $\mathcal{I}$ and $\mathcal{D}$ vs.T. The full (*dark orange*) and dashed (*blue*) lines represent the expected behaviors calculated starting from the first experimental point we have measured ($T = 0.63$) for $\mathcal{I}$ and $\mathcal{D}$ respectively. The inset is a magnification of the plot of $\mathcal{D}$ in the high loss regime ($T < 0.15$). We note the persistence of a true quantum correlation even in presence of strong decoherence (high loss).

In Fig. 3.12 we report the experimental data together with the expected behaviors, as usually calculated considering the less decohered matrix as a reference, for $\mathcal{I}$ and $\mathcal{D}$ vs.T. As it can be seen the quantum discord follows very well its *theoretical* line while quantum mutual information is a little more scattered around it.

Moreover, our data prove that even in presence of strong decoherence, it is possible to evaluate that $\mathcal{D}$ keeps > 0, within the experimental indeterminacies, all the way down to an highly absorbed state. We note that Gaussian quantum discord is attracting, very recently, a lot of experimental interest [60, 61, 62]. In particular, in Ref. [60], the authors give an operational significance to quantum discord as the possibility of encoding quantum information in separable states. In Ref. [61] the optimal strategy for evaluating $\mathcal{D}(\boldsymbol{\sigma})$ in homodyne measurement is presented. It is interesting to compare our experimental plot with the one reported in Ref. [62] where the authors analyse the quantum discord under the lossy transmission of one of the two sub–systems. We note that in their case the scattering of the experimental points around the theoretical curve is almost equivalent for $\mathcal{I}$ and $\mathcal{D}$ while in our case there is a clear difference.

3.7 Experimental results in the range $0.01 \leq T < 0.25$

In this section we report the results obtained investiganting more carefully the strong dechoerence regime. The total losses we have measured span the interval $75 - 99\%$ ($0.01 \leq T < 0.25$).

In Fig. 3.9 we report the behaviour vs. T of the averaged correlation term $c = (|c_{1,T}| + |c_{2,T}|)/2$ and of the averaged diagonal element $\widetilde{n}_T = (n_T + m_T)/2$. As expected the correlation between the two sub–systems degrades linearly toward 0 with the total loss T, while the diagonal element goes to 0.5, the variance of the vacuum state.

In Fig. 3.10 we have plotted w_{PHS} and w_{DUAN} vs T. We can see that, even if the analysed state, for $T = 0.01$, is very close to a two mode vacuum (the total average number of photon $((n + m - 1)/2)$ reduce to 0.02 ± 0.01), it is still experimentally possible to prove that the state is non–separable. For $T = 0.99$, $w_{PHS} = -0.008 \pm 0.001$ while $w_{DUAN} = -0.018 \pm 0.001$ so that the distances from the classical limit are respectively 8 and 18 times the experimental indeterminacies. Thus, in the very high loss regime it becomes more reliable to assess entanglement using the latter than the former.

Observing Fig. 3.11, we confirm that the fidelity $\mathcal{F}$ is a robust signature of quantum properties for the state undergoing to a lossy transmission. In particular we see that even in the high loss regime, $\mathcal{F}$ remains above the classical limit of 0.5, proving that CV entangled state, as the one produced by our source, could be used as resource for realising teleportation protocol of coherent state, in principle, at an infinite distance. For $T = 0.01$, $\mathcal{F} = 0.5023 \pm 0.0002$ so that the distance from the classical limit is still 12 times the experimental indeterminacy.

Eventually we have retrieved the values for quantum mutual information $\mathcal{I}(\boldsymbol{\sigma})$ (Eq. (3.2)) and discord $\mathcal{D}(\boldsymbol{\sigma})$ (Eq. (3.3)).

In Fig. 3.12 we report the experimental data together with the expected behaviours, as usually calculated considering the less decohered matrix as a ref-
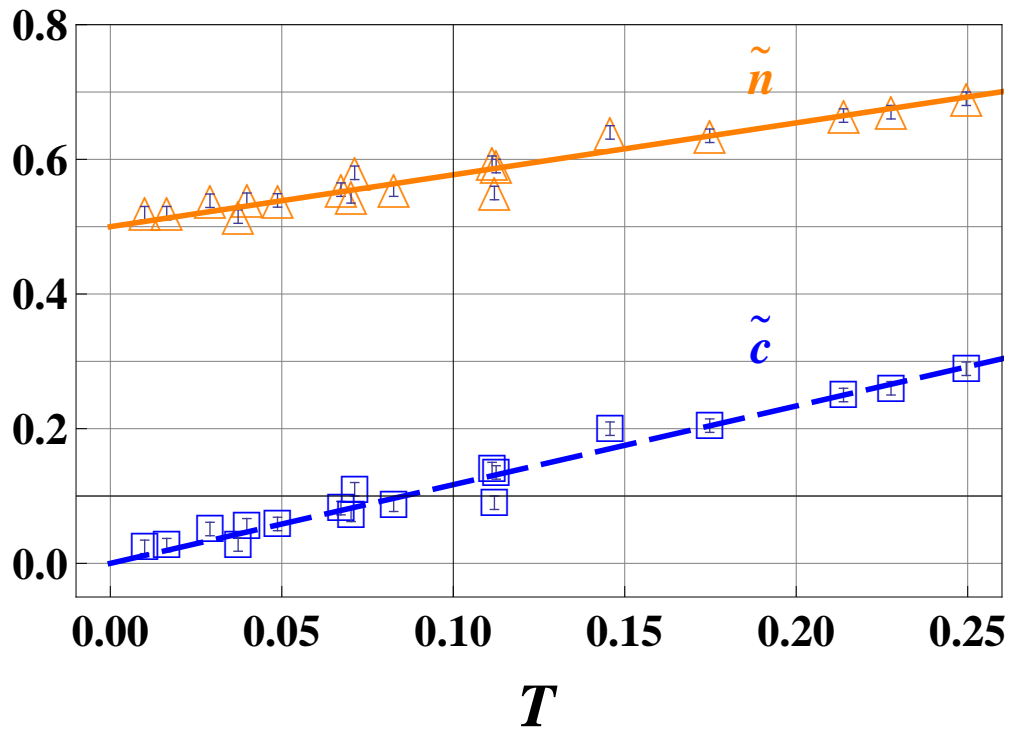
Figure 3.9: *(color online)* Behaviour of the averaged correlation term $|c_{1,T}| + |c_{2,T}|/2$ and of the averaged diagonal element $\widetilde{n}_T = (n_T + m_T)/2$ in Eq. (3.24). As expected the first reduces linearly with T. The straight (full and dashed) lines represent the expected behaviours calculated setting the less absorbed **CM** as the reference state. Error bars are smaller than data points and amount to ± 0.01.
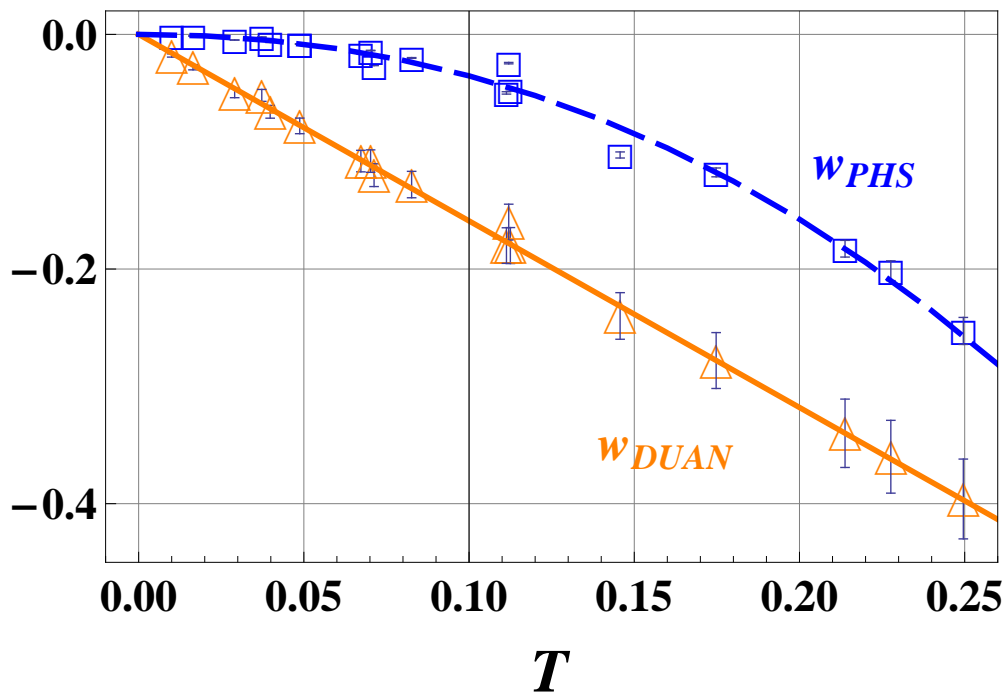
Figure 3.10: *(color online)* w_{PHS} and w_{DUAN} vs. T. The full *dark orange* (lower) and the *blue* (upper) lines represent the expected behaviour of w_{PHS} and w_{DUAN} respectively. Error bars range between 10^{-4} and 0.1.
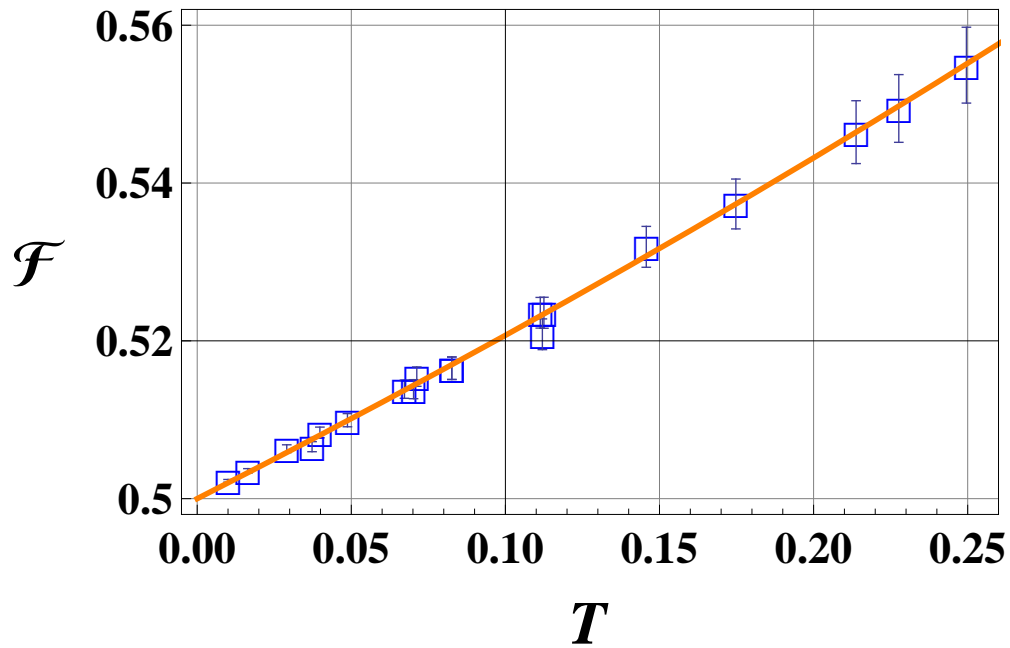
Figure 3.11: *(color online)* $\mathcal{F}$ vs. T. The full *(dark orange)* line represents the expected behaviour. Error bars, obtained by propagating the experimental indeterminacies in Eq. (3.21), range between 10^{-5} and 0.01. It si worth noting that even for $T = 0.99$ the experimental point lies inside the quantum region ($\mathcal{F} = 0.5023 \pm .0.0002$).
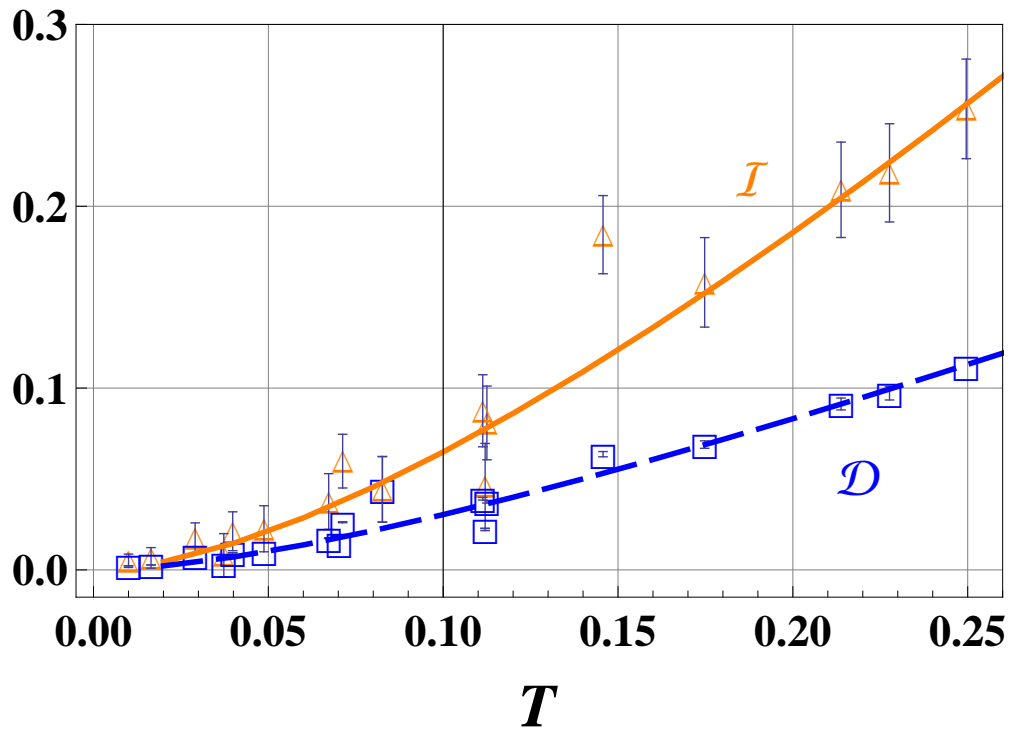
Figure 3.12: *(color online)* $\mathcal{I}$ and $\mathcal{D}$ vs.T. The full (*dark orange*) and dashed (*blue*) lines represent the respective expected behaviours. Error bars respectively, range between 3×10^{-3} and 0.02 for $\mathcal{I}$ and 10^{-4} and 0.03 for $\mathcal{D}$. Note that the data for $\mathcal{I}$ scatters more from the expected behaviour may be signalling extra classical correlations.

erence, for $\mathcal{I}$ and $\mathcal{D}$ vs. T. As it can be seen the quantum discord follows its *theoretical* line better than the mutual information. The latter is a little more scattered around it. Moreover, our data prove that even in presence of strong decoherence, it is possible to evaluate that $\mathcal{D}$ keeps > 0, within the experimental indeterminacies, all the way down to an highly absorbed state. In particular, for $T = 0.01$, $\mathcal{D} = 0.0022 \pm 0.0001$ so that the distance from the classical limit is 22 times the experimental indeterminacy.

CHAPTER 4

BELL'S INEQUALITY VERSUS PURITY AND ENTANGLEMENT FOR GAUSSIAN STATES

In this chapter, we want to analyze the violation of Bell's inequality, for Gaussian bipartite states, in terms of the covariance matrix, and to present a new handy relation that describe in a simple way the linking among entanglement, purity and Bell's non-locality. To achieve our aim we follow the approach of Banaszek and Wodkiewicz [14]. Although there has been a small controversy regarding the use of such a method[1], it provides an immediate physical significance about the nature of the analyzed state. In fact, as we saw in § 2.7.4, it is possible to extract informations about the nonlocality of the state simply observing its representation in the phace space, since the Wigner function can be expressed as Eq. (2.33).

4.1   CHSH inequality in the space phace for Gaussian states

In this section we consider a Gaussian state, described by the covariance matrix σ Eq. (3.14) and we evaluate the quantity (2.35) $\mathcal{B}$ in terms of the following displacement amplitudes [14]: $\alpha_1 = 0$, $\alpha_2 = \sqrt{\mathcal{I}}$, $\beta_1 = 0$, $\beta_2 = -\sqrt{\mathcal{I}}$. In this circumstance $\mathcal{B}$ reads

$$
\begin{aligned}
\mathcal{B}\left(\mathcal{I}, n, c\right) &= \frac{1 + 2\exp\left\{-\frac{n}{n^2-c^2}\mathcal{I}\right\} - \exp\left\{-\frac{n+c}{n^2-c^2}2\mathcal{I}\right\}}{4\left(n^2-c^2\right)} \\
&= \mu\left[1 + 2e^{-4n\mu\mathcal{I}} - e^{-8(n+c)\mu\mathcal{I}}\right]
\end{aligned}
\tag{4.1}
$$

with $\mu = \frac{1}{4(n^2-c^2)}$. The maximal violation in respect to the displacement amplitude is given by

$$
\mathcal{B}_{\widetilde{\mathcal{I}}}\left(n, c\right) \equiv \max_{\mathcal{I}} \mathcal{B}\left(\mathcal{I}, n, c\right).
$$

We obtain the maximal value of $\mathcal{I}$, corresponding to the maximal violation of the inequality (2.36), by the derivative of $\mathcal{B}$, that gives $\widetilde{\mathcal{I}} = \frac{1}{4\mu(n+2c)}\ln\left[\frac{n+c}{n}\right]$. So $\mathcal{B}_{\widetilde{\mathcal{I}}}$ reads

$$
\begin{aligned}
\mathcal{B}_{\widetilde{\mathcal{I}}}\left(n, c\right) &= \mu\left[1 + 2e^{-4n\mu\widetilde{\mathcal{I}}} - e^{-8(n+c)\mu\widetilde{\mathcal{I}}}\right] \\
&= \mu\left[1 + 2\left(\frac{n}{n+c}\right)^{\frac{n}{n+c}} - \left(\frac{n}{n+c}\right)^{2\frac{n+c}{n+2c}}\right]
\end{aligned}
\tag{4.2}
$$

---

[1]In [44], the authors define *an unsatisfactory feature* the fact that the magnitude of the violation of the Bell's inequality depends on the displacement in the phase space, and not only by the "dichotomic" parity operator

It is possible to express $\mathcal{B}_{\widetilde{\mathcal{I}}}$ in terms of the subsystem's purity μ_s and the correlation strength $\mathcal{C}_{a|b}$ between the two subsystems a and b,

$$\mathcal{C}_{a|b} \equiv \frac{\langle \Delta X_a X_b \rangle}{\sqrt{\langle \Delta X_a^2 \rangle \langle \Delta X_b^2 \rangle}},$$

obtaining

$$\mathcal{B}_{\widetilde{\mathcal{I}}}\left(\mu_s, \mathcal{C}_{a|b}\right) = \frac{\mu_s^2}{1 - \mathcal{C}_{a|b}^2}\left[1 + \Upsilon\left(\mathcal{C}_{a|b}\right)\right] \tag{4.3}$$

with

$$\Upsilon\left(\mathcal{C}_{a|b}\right) = \left(1 + 2\mathcal{C}_{a|b}\right)\left(1 + \mathcal{C}_{a|b}\right)^{-2\left(1 + \mathcal{C}_{a|b}\right)/\left(1 + 2\mathcal{C}_{a|b}\right)}.$$

As already announced, our aim is to analyze the relationship among inequality's violation, entanglement and purity. Precisely for this reason we prefer not to refer to a specific measure of entanglement (unique only for pure states), rather we use the witness w_{DUAN} Eq. (3.16) for evaluating the entanglement. Indeed, as we saw in the previous chapter, the Duan criterion is a necessary and sufficient condition to assert the presence of entanglement in diagonal states Eq. (3.14).

It is easy to see that also w_{DUAN} can be written as function of μ_s and $\mathcal{C}_{a|b}$. By Eq. (3.16), it reads

$$w_{DUAN} = \frac{(1 - \mathcal{C}_{a|b})}{\mu_s} - 1. \tag{4.4}$$

4.1.1 Bell's inequality violation for pure Gaussian states

We want to analyze the trend of $\mathcal{B}_{\widetilde{\mathcal{I}}}$ in terms of entanglement witness w_{DUAN} for pure states. To achieve our aim it is convenient to express $\mathcal{B}_{\widetilde{\mathcal{I}}}$ as a function of the purity μ of the overall system and, of course, of the w_{DUAN}.

Since Eq. (1.9) we have

$$\mu = \frac{\mu_s^2}{1 - \mathcal{C}_{a|b}^2},$$

that, in terms of w_{DUAN} Eq. (4.4), becomes

$$\mu = \frac{\mu_s^2}{1 - (\mu_s w_{DUAN} + \mu_s - 1)^2}.$$

Inverting it we obtain

$$\mu_s = \frac{2\mu(1 + w_{DUAN})}{1 + \mu(1 + w_{DUAN})^2} \tag{4.5}$$

Substituting the quantities $\mathcal{C}_{a|b}$ and μ_s Eqs. (4.4, 4.5) in Eq. 4.2, we find $\mathcal{B}_{\widetilde{\mathcal{I}}}(\mu, w_{DUAN})$, that is the relationship among the Bell's function $\mathcal{B}_{\widetilde{\mathcal{I}}}$, the purity μ and the entanglement witness w_{DUAN}. For pure states $\mathcal{B}_{\widetilde{\mathcal{I}}}^{pure}\left(w_{DUAN}\right) \equiv \mathcal{B}_{\widetilde{\mathcal{I}}}\left(1, w_{DUAN}\right)$ reads

$$\mathcal{B}_{\widetilde{\mathcal{I}}}^{pure}\left(w_{DUAN}\right) = 1 + \left[\frac{3 - (1 + w_{DUAN})^2}{2}\right]\left[\frac{1 + (1 + w_{DUAN})^2}{2}\right]^{\frac{4 - 3(1 + w_{DUAN})^2}{3(1 + w_{DUAN})^2}}.$$

(4.6)

where w_{DUAN} assumes values that are inclused in the codomain $[-1, 0]$. By Eq. (4.6) it is possible to see that $\mathcal{B}_{\widetilde{\mathcal{I}}}^{pure}(0) = 2$, i. e. the point $w_{DUAN} = 0$, that marks the border between separable and entangled states, providing the border point between the *hidden variable regime* and *quantum regime*. Moreover $\mathcal{B}_{\widetilde{\mathcal{I}}}^{pure}(-1) \simeq 2.19$, that coincides with the maximal value found in [14]. This maximal value can be optimized through a appropriate selection[2] of the displacement amplitudes in Eq. (2.35), but this is beyond our purposes. In fact, our aim is to find the relationship that links different quantum features regardless of the optimal value which $\mathcal{B}_{\widetilde{\mathcal{I}}}$ may assume.
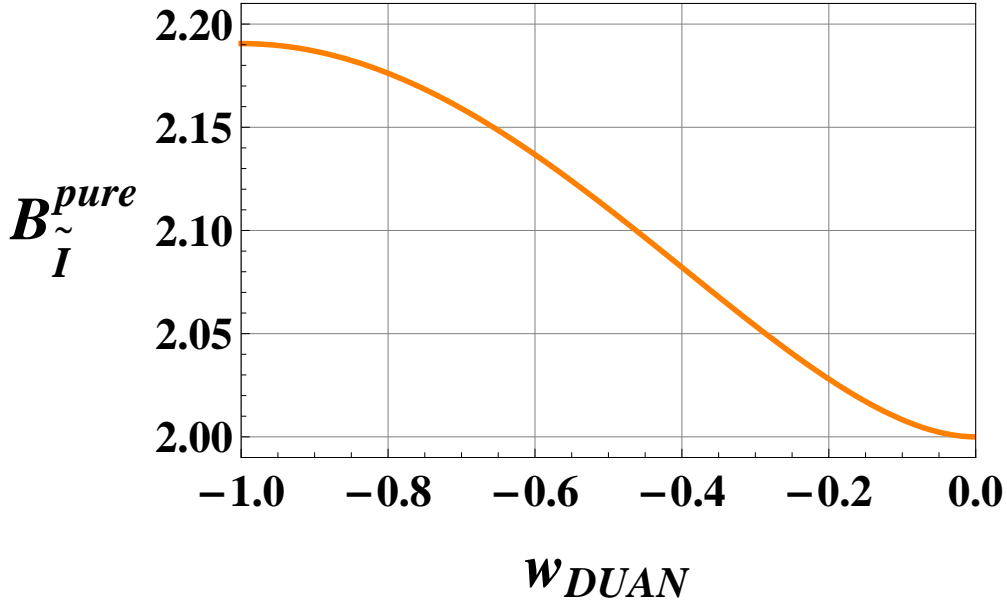
Figure 4.1: *(color online)* Behaviour of $\mathcal{B}_{\widetilde{\mathcal{I}}}^{pure}$ as a function of w_{DUAN}, throughout the range of values identified by the codomain $[-1, 0]$ of w_{DUAN}.

In the plot Fig 4.1 we report the behaviour of $\mathcal{B}_{\widetilde{\mathcal{I}}}^{pure}$ as a function of w_{DUAN}, throughout the range of values identified by the codomain of w_{DUAN}. We can see that $\mathcal{B}_{\widetilde{\mathcal{I}}}^{pure}$ is monotonic. Moreover it is greater than the limit 2 when the state is entangled, minor otherwise. In this sense, we can say that for pure Gaussian

---

[2]for example, in [46], Olivares at al. obtain a better violation, corresponding at $\mathcal{B}_{\widetilde{\mathcal{I}}} = 2.32$, searching the maximum of $\mathcal{B}$ Eq. (2.35) with the following displacement amplitudes: $\alpha_1 = \sqrt{\mathcal{I}}$, $\alpha_2 = -3\sqrt{\mathcal{I}}$, $\beta_1 = -\sqrt{\mathcal{I}}$, $\beta_2 = 3\sqrt{\mathcal{I}}$.

states $\mathcal{B}_{\widetilde{\mathcal{I}}}^{pure}$ can be considered an entanglement witness as w_{DUAN}. This outcome (obtained in the context of the continuous variables) confirms the results obtained by Popescu et al [63], in according to which any pure entangled bipartite state violates the Bell's inequality in the two and more dimensional Hilbert spaces.

Moreover, observing the relations Eqs. (4.3), (4.6) it is possible to establish the following equivalences:

$$\left\{\mathcal{C}_{a|b} > 0\right\} \Leftrightarrow \left\{w_{DUAN} < 0\right\} \Leftrightarrow \left\{\mathcal{B}_{\widetilde{\mathcal{I}}} > 2\right\}.$$

4.1.2 Bell's inequality violation for mixed Gaussian states

In the more general circumstances ($\mu \neq 1$), let $C_{a|b} > 0$, and

$$\mu_D = 1 - \mathcal{C}_{a|b},$$

$$\mu_B = \left[\frac{2(1 - \mathcal{C}_{a|b}^2)}{1 + (1 + 2\mathcal{C}_{a|b})(1 + \mathcal{C}_{a|b})^{-2\frac{1+\mathcal{C}_{a|b}}{1+2\mathcal{C}_{a|b}}}}\right]^{\frac{1}{2}},$$

$$\mu_F = \sqrt{1 - \mathcal{C}_{a|b}^2},$$

the entanglement and the Bell's violation depend by the purity. With reference to Eq. (4.3) we can distinguish three different regions. They are shown in Fig. 4.2.

The region I includes not entangled states, identified by the condition $\mu_s < \mu_D$; the region II, identified by the condition $\mu_D < \mu_s < \mu_B$ reports the entangled states, that are local for Bell (don't violate the inequality (2.35)); eventually, the region III, bordered by $\mu_B < \mu_s < \mu_F$, represents the entangled states that are also nonlocal. The existence of the region II, as also identified by Werner [65], makes the Bell's inequality a not too good entanglement witness for mixed states. Moreover it is a further confirmation of the existence of different forms of non-locality (see §2.6.2).

4.2 Gaussian noise breaks Bell's nonlocality, but not entanglement

In this Section we want to show that passive Gaussian noise (described in § 3.4) breaks the Bell's nonlocality. In particular we see that when a pure ($c = \sqrt{n^2 - 0.25}$), entangled ($w_{DUAN} > 0.5$) Bell's nonlocal (i.e. $\mathcal{B}_{\widetilde{\mathcal{I}}} > 2$) state evolves in a Gaussian channel, retains its entanglement, but looses its Bell's nonlocality. This mean that although, at the born, the state is pure, therefore, for it, the violation Bell's inequality and the presence of entanglement are the expression of the same type of non-classical correlations (in the previous section we have seen that the Bell's function becomes one kind of entanglement witness), the decoherence highlights the different nature of the two markers: the Gaussian state
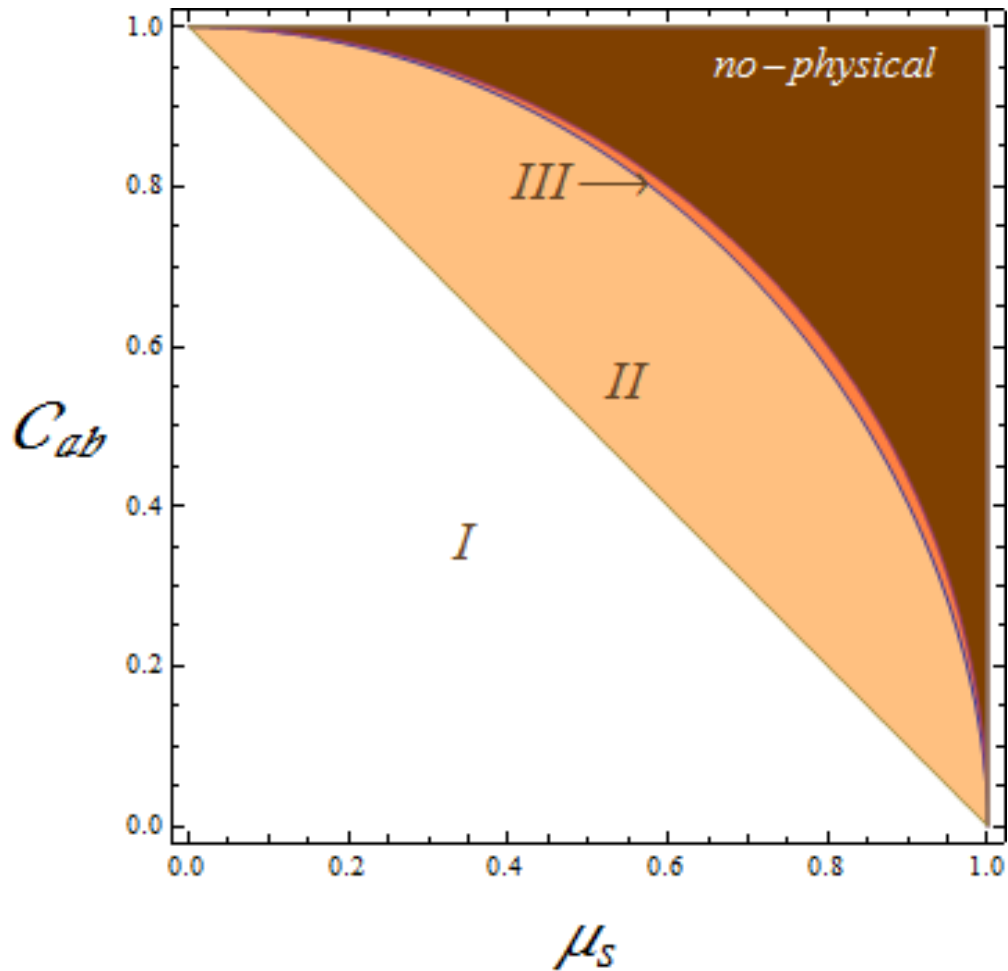
Figure 4.2: *(color online)* Region plot of different *nonlocality markers*. The region *I* includes not entangled states, identified by the condition $\mu_s < \mu_D$; the region *II* includes entangled states that are local for Bell (2.35), identified by the condition $\mu_D < \mu_s < \mu_B$; The region *III* represents the entangled states that are also nonlocal, bordered by $\mu_B < \mu_s < \mu_F$. See text for more details

becomes local (in according to Bell), i.e. it admits a description in terms of hidden variables, although it remains entangled. So the link that we have established in § (4.1.1) between entanglement and Bell's nonlocality for pure states is broken when the states undergo decoherence.
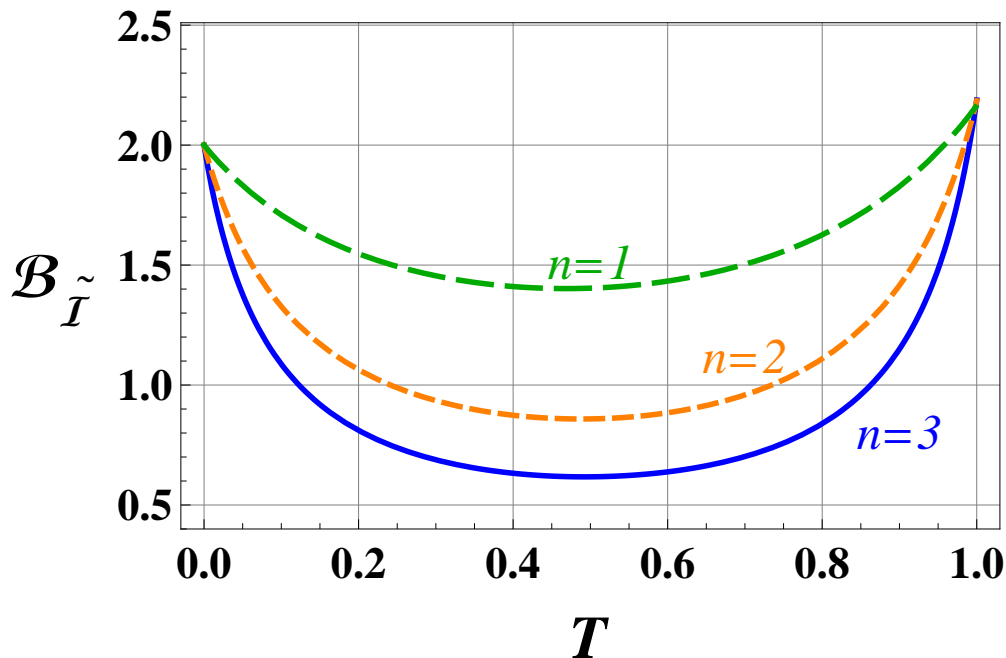
Figure 4.3: *(color online)* Behaviour of $\mathcal{B}_{\widetilde{\mathcal{I}}}$ as a function of transmission coefficient T, simulanting decoherence. We note that decoherence heavily affecst the Bell's nonlocality. In fact $\mathcal{B}_{\widetilde{\mathcal{I}}}$ violates Bell's inequality for a very little range of values of T.

In the plot Fig. 4.3, it is reported the behaviour of $\mathcal{B}_{\widetilde{\mathcal{I}}}$ as a function of transmission coefficient[3]

T for different values of the parameter n. The plot clearly shows that the decoherence acts immediately (for T very close to 1) making possible only a description in terms of hidden variables ($\mathcal{B}_{\widetilde{\mathcal{I}}} \leq 2$). Furthermore, a greater number of photons in the starting (pure) state corresponds to a larger starting ($T = 1$) value of $\mathcal{B}_{\widetilde{\mathcal{I}}}$, but also a steeper descent towards the transition from non-local to the local regime. This behavior is a confirmation of the circumstance [64] that the larger degree of the initial squeezing, the more rapidly the squeezed state loses its nonlocality.

---

[3]It is found with the help of Eqs (3.25).

Part III

Non-Gaussian Resources

CHAPTER 5

DEGAUSSIFIED STATES

From what we have seen in the chapter 3, Gaussian states are a quantum resource easy to implement and control and also robust against the decoherence.

In particular, we have analyzed the circumstance in which the Gaussian state is generated by parametric oscillators. These fields are widely used in quantum communication as resource states for teleportation protocols.

However we have also seen that for this class of states the fidelity of teleportation $\mathcal{F}$ is governed by the entanglement (see Eqs. (3.19), (3.22)) as the only free parameter, i.e. the success of such protocol is limited directly by the squeezing level. This circumstance suffers from two limitations.

The first limitation is technical: to produce a stable source that generates a twin beam with a high degree of squeezing. The parameter of squeezing increases as the non-linear process that generates the down conversion takes place close to the threshold. But, as the pump amplitude is approaching the threshold the impact of fluctuating parameters tends to explode. As discussed by Chaturvedi et al [73] the fields generated by the OPO contribute increasingly to the fluctuations of the mode of pump giving rise to a phase transition. Even if the latter develops for relative distances from the threshold of the order of 10^{-6}, for squeezing more than 10 dB, the impact of amplitude fluctuations must be brought to account. This means that increasing of r the state may be not more Gaussian, with a non-Gaussianity not easily controllable.

The second limitation is physical. As we saw in the first chapter thare are quantum constraints to the physicity of the states as the purity Eq.(1.3) and the Haisemberg principle Eq. (1.16). For Gaussian states, the constraint *purity* translates in a bound, Eq. (3.18), for the correlation term c. This term is related to the degree of entanglement of the state. Since $\mathcal{F}$, for Gaussian resources (even in the most desirable possible case: pure states) that teleporting a coherent state, has only one degree of freedom: the entanglement, it follows that the constraint on c is a constraint on the fidelity. As we saw in the previous chapter, in the limit of very high energies (tending to infinity) the constraint is negligible, but however, it exists. The constraints Eqs.(1.3), (1.16) concern both Gaussian and not Gaussian states. However, only for Gaussian resources the fidelity of teleportation $\mathcal{F}$ is governed by one free parameter.

For this reasons it appears very interesting to explore other classes of states. Naturally the non-Gaussian states are a too general class and it is not easy to establish the qualities that a state must have for beeing an useful resource to

Quantum Information.

In this chapter we describe a new class of states introduced, at first, by Dell'Anno et al. [4] in the year 2007. Moreover we study the nonlocal character of this class of states both through the method of pseudospin and in the phase space. The optimization of the Bell's function by a free parameter allows to identify the most nonlocal resource among all the states belonging to the class. The most nonlocal state has the same characteristics as identified by Dell'Anno et al [4] actually useful for quantum teleportation. It complies with all the three reasonable criteria, identified in [4], which help us to ascertain the features that a resource must have to ensure a teleportation fidelity better than that obtained by Gaussian resources.

The described results are reported in [10].

5.1 The Squeezed Bell states

In [4], Dell'Anno et al. investigated cv quantum teleportation using non-Gaussian states of the radiation field as entangled resources.

They introduced a class of two-mode squeezed Bell-like states with the free parameter δ: the squeezed Bell states $|\psi\rangle_{SB}$,

$$|\psi\rangle_{SB} = S_{12}(\zeta)\left\{\cos\delta\,|0,0\rangle_{12} + e^{i\theta}\sin\delta\,|1,1\rangle_{12}\right\},\tag{5.1}$$

where $S_{12}(\zeta) = e^{-\zeta a_1^\dagger a_2^\dagger + \zeta a_1 a_2}$ is the two-mode squeezing operator, $\zeta = re^{i\phi}$ is the squeezing parameter, $|m,m\rangle_{12}$ $m = 0, 1$ is a two-mode Fock state. The normalization of the state is guaranted by the relation $\cos^2\delta + \sin^2\delta = 1$. For completeness we have reported in Eq. (5.1) the relative phase θ. However, in [4], it was found that the inclusion of θ between the two terms inside the braces does not improve the performance of $|\psi\rangle_{SB}$. This state interpolates between and include as subcases different classes of degaussified resources. Indeed, in addition to the trivial case of

- the Gaussian s*queezed vacuum state*

$$|\psi\rangle_{VS} = S_{12}(\zeta)\,|0,0\rangle_{12},\tag{5.2}$$

  obtained for $\delta = 0$, we have that:

- the *squeezed photon number state*

$$|\zeta;1,1\rangle = S_{12}(\zeta)\,|1,1\rangle\tag{5.3}$$

  is recovered for $\delta = \pi/2$.

State	Definition
PS squeezed state	$N_{PS} \, a_1 a_2 S_{12}(\zeta)|0,0>_{12}$
PA squeezed state	$N_{PA} \, a_1^\dagger a_2^\dagger S_{12}(\zeta)|0,0>_{12}$
Squeezed number states	$S_{12}(\zeta)|1,1>_{12}$
Twin Beam	$S_{12}(\zeta)|0,0>_{12}$

Table 5.1: Theoretical (operatorial) definition of some Gaussian and degaussified states included in the SB class.

- The *photon added squeezed states*

$$\left| \zeta; 1^{(+)}, 1^{(+)} \right\rangle = \frac{S_{12}\left(\zeta \right)}{\sqrt{1 + \tanh^2 r}} \left\{ -e^{-i\phi} \tanh r \, |0,0\rangle_{12} + |1,1\rangle_{12} \right\}, \qquad (5.4)$$

is obtained for $\delta = \cos^{-1} \left(-\frac{e^{-i\phi} \tanh r}{\sqrt{1+\tanh^2 r}} \right)$; while we obtain

- the *photon subtracted squeezed states*

$$\left| \zeta; 1^{(-)}, 1^{(-)} \right\rangle = e^{i\phi} \frac{S_{12}\left(\zeta \right)}{\sqrt{1 + \tanh^2 r}} \left\{ -e^{i\phi} |0,0\rangle_{12} + e^{2i\phi} \tanh r \, |1,1\rangle_{12} \right\} \quad (5.5)$$

putting $\delta = \cos^{-1} \left(-\frac{e^{i\phi}}{\sqrt{1+\tanh^2 r}} \right)$.

For convenience we list in TABLE 5.1 the theoretical definitions of all the states obtained by Eq. (5.1).

As we seen by Eq. (5.1), the squeezed Bell state depends by the free parameter δ, that allows not only to recover the class of degaussified states, but also to tune suitably the coefficients in such a way as to optimize their performace according to the our purposes.

For example, in the next section, we will try the parameter δ that maximizes the violation of Bell's inequality. In this way we will identify the parameter that gives the most nonlocal state among all those obtained by Eq. (5.1).

5.2 Bell-CHSH's inequality for Squeezed Bell states

A given state does not have to violate all possible Bell's inequalities to be considered nonlocal [44]; it is nonlocal when it violates any Bell's inequality. Thus the nonlocality degree depends not only on the given quantum state, but also on the Bell operator considered (see § 2.7). In this section, we calculate the Bell's function $\mathcal{B}$ for the squeezed Bell states through the use of two different Bell operators: pseudospins and parity (the latter is linked to phase space approach). Our aim is to compare the nonlocality of all states obtainable by eq. (5.1). As

we seen this class includes the twin beam Eq. (5.2). For this reason we have neglected the homodyne approach.

All obtained results are reported in [10].

5.2.1 Pseudospin approach for the Squeezed Bell states

Following the strategy described in § 2.7.1 we calculate the quantity

$$
\begin{aligned}
E\left(\theta_1, \theta_2\right) &= \langle\psi_{TB}|\, s_{\theta_1}^{(1)} \otimes s_{\theta_2}^{(2)}\, |\psi_{TB}\rangle \\
&= \cos\theta_1 \cos\theta_2 \left\langle S_z^{(1)} \otimes S_z^{(2)}\right\rangle \\
&\quad + \cos\theta_1 \sin\theta_2 \left\langle S_z^{(1)} \otimes \left(S_+^{(2)} + S_-^{(2)}\right)\right\rangle \\
&\quad + \sin\theta_1 \cos\theta_2 \left\langle \left(S_+^{(1)} + S_-^{(1)}\right) \otimes S_z^{(2)}\right\rangle \\
&\quad + \sin\theta_1 \sin\theta_2 \left\langle \left(S_+^{(1)} + S_-^{(1)}\right) \otimes \left(S_+^{(1)} + S_-^{(1)}\right)\right\rangle.
\end{aligned}
$$

At first, we observe that the $|\psi_{SB}\rangle$ can be written as

$$
|\psi_{SB}\rangle = S_{12}\left(\zeta\right)\left[c_1 + c_2 a_1^\dagger a_2^\dagger\right]|00\rangle.
$$

Using the two-mode Bogoliubov transformations,

$$
\begin{aligned}
S_{12}\left(\zeta\right) a_1^\dagger S_{12}^\dagger\left(\zeta\right) &= S_{12}^\dagger\left(-\zeta\right) a_1^\dagger S_{12}\left(-\zeta\right) = c a_1^\dagger + e^{-i\phi} s a_2 \qquad (5.6) \\
S_{12}\left(\zeta\right) a_2^\dagger S_{12}^\dagger\left(\zeta\right) &= S_{12}^\dagger\left(-\zeta\right) a_2^\dagger S_{12}\left(-\zeta\right) = c a_2^\dagger + e^{-i\phi} s a_1, \qquad (5.7)
\end{aligned}
$$

we can write

$$
\begin{aligned}
|\psi_{SB}\rangle &= \left[c_1 + c_2\left(c a_1^\dagger + e^{-i\phi} s a_2\right)\left(c a_2^\dagger + e^{-i\phi} s a_1\right)\right] S_{12}\left(r\right)|00\rangle \\
&= \sum_{n=0}^{\infty}\left[c_1 C_n^{(TB)} + e^{-i\phi} c_2 c s\left(2n+1\right)\right]|n, n\rangle \\
&\quad + c_2 c^2 \sum_{n=0}^{\infty} C_n^{(TB)}\left(n+1\right)|n+1, n+1\rangle \\
&\quad + e^{-2i\phi} c_2 s^2 \sum_{n=0}^{\infty} C_n^{(TB)} n\, |n-1, n-1\rangle \\
&= \sum_{n=0}^{\infty}\left[c_1 C_n^{(TB)} + e^{-i\phi} c_2 c s C_n^{(TB)}\left(2n+1\right) + e^{-2i\phi} c_2 s^2 C_{n+1}^{(TB)}\left(n+1\right)\right. \\
&\quad \left. + c_2 c^2 C_{n-1}^{(TB)} n\left(1-\delta_{n,0}\right)\right]|n, n\rangle,
\end{aligned}
$$

where $C_n^{(TB)} = e^{in\phi}\frac{\tanh^n r}{\cosh r}$. So, through this transformation, $|\psi_{SB}\rangle$ reduces to the form

$$
|\psi_{SB}\rangle = \sum_{n=0}^{\infty} C_n^{(SB)}|n, n\rangle \qquad (5.8)
$$

where $\sum_{n=0}^{\infty} \left| C_n^{SB} \right|^2 = 1$ for the normalization, with

$$C_n^{(SB)} = c_1 C_n^{(TB)} + e^{-i\phi} c_2 cs \left(2n+1\right) + e^{-2i\phi} c_2 s^2 C_{n+1}^{(TB)} \left(n+1\right) + c_2 c^2 C_{n-1}^{(TB)} n \left(1 - \delta_{n,0}\right),$$

where $c_1 = \cos\delta$, $c_2 = \sin\delta$, and $\delta_{n,0}$ is Kronecker's delta function.

By the form Eq. (5.8) it is apparent that the terms $\left\langle S_z^{(1)} \otimes \left(S_+^{(2)} + S_-^{(2)}\right) \right\rangle$, $\left\langle \left(S_+^{(1)} + S_-^{(1)}\right) \otimes S_z^{(2)} \right\rangle$ vanish. Thus the function $E\left(\theta_1, \theta_2\right)$ becomes

$$
\begin{aligned}
E\left(\theta_1, \theta_2\right) &= \cos\theta_1 \cos\theta_2 \sum_{n=0}^{\infty} \left(\left| C_{2n+1}^{SB} \right|^2 + \left| C_{2n}^{SB} \right|^2 \right) & (5.9) \\
&\quad + \sin\theta_1 \sin\theta_2 \sum_{n=0}^{\infty} \mathrm{Re} \left[2 C_{2n}^{SB} C_{2n+1}^{SB*} \right] & (5.10) \\
&= \cos\theta_1 \cos\theta_2 + \sin\theta_1 \sin\theta_2 \sum_{n=0}^{\infty} \mathrm{Re} \left[2 C_{2n}^{SB} C_{2n+1}^{SB*} \right].
\end{aligned}
$$

We can see that the function $E\left(\theta_1, \theta_2\right)$ depends on the following free parameters: squeezing parameter r, the relative weight δ between the Fock states $|00\rangle$ and $|11\rangle$ of the SB state, and the angles of orientation θ_1, θ_2 of the measurements. So, by the computation of the Bell operator, Eq. (2.32), we obtain $\mathcal{B} = \mathcal{B}\left(r, \delta, \theta_1, \theta_2, \theta_1', \theta_2'\right)$.

In ref. [44], the authors choose some values of orientations $\theta_1, \theta_2, \theta_1', \theta_2'$:

$$
\begin{aligned}
\theta_1 &= 0 & \theta_1' &= \pi/2 & (5.11) \\
\theta_2 &= \theta & \theta_2' &= -\theta.
\end{aligned}
$$

Their aim is to find the maximal violation of the inequality using TB states. With the setting Eqs. (5.11) and $\delta = 0$, the Bell's function $\mathcal{B}$ results

$$\mathcal{B}\left(\theta_2\right) = 2\left(\cos\theta_2 + \tanh\left(2r\right)\sin\theta_2\right),$$

and maximizing with respect to θ_2, we have

$$
\begin{aligned}
\mathcal{B}_{\max}\left(r\right) &\equiv \max_{\theta_2} \mathcal{B}\left(\theta_2\right) \\
&= 2\sqrt{1 + \tanh^2\left(2r\right)},
\end{aligned}
$$

that is, obviously, the same result of [44]. We can deduce that the squeezed vacuum bipartite state ((5.8) with $C_n^{(SB)} = C_n^{(TB)}$) exhibits a violation of the inequality of Bell soon as the parameter of squeezing is different from zero ($r > 0$). This confirms the connection between entanglement and violation of Bell's inequality for pure states [63], [66]. The maximal violation is given by r tending to infinity.

In this case, in fact, the squeezed vacuum state tends to the EPR (maximally correlated) state.

We have studied the function $\mathcal{B}$ obtained in the general case Eq. (5.9) with the same chosen (5.11) for the angles of ref. [44], so we have a direct comparison with the Gaussian states. With the setting (5.11) we obtain the function $\mathcal{B} = \mathcal{B}(r, \delta, \theta)$. The maximization procedure of $\mathcal{B}$ is made on the parameters (δ, θ), i.e. $\mathcal{B}_{opt}(\delta^{(\max)}, \theta^{(\max)}) = \max_{\delta,\theta} \mathcal{B}(r, \delta, \theta)$.

Of course, we obtain the degaussified states PS, PA, PN and the Gaussian TB tuning suitably the parameter δ (according to ref. [4] (§5.4)).

In Fig. 5.1 is reported the behaviour of $\mathcal{B}_{opt}(\delta^{(\max)}, \theta^{(\max)})$ (blue solid line), i.e. the of optimized function $\mathcal{B}$, as function of r. It is compared with the $\mathcal{B}_{opt}(\delta^{(PS)}, \theta^{(\max)})$, obtained tuning δ so as to provide the PS state (green dot-dashed line), the TB state (orange dashed line), and PA state (purple dotted line). We can observe that the optimized SB state is more nonlocal than everyone else considered states. In particular, we note that $\mathcal{B}_{opt}$ reaches the maximum, $2\sqrt{2}$, for r tending to infinity, asymptotically, and for $r = 0$ with $\delta = \pi/2$, i.e. when the SB state becomes the well-known Bell state $\frac{1}{\sqrt{2}}(|00\rangle + |11\rangle)$. However, for $r \to \infty$ all states approach the same value of violation.
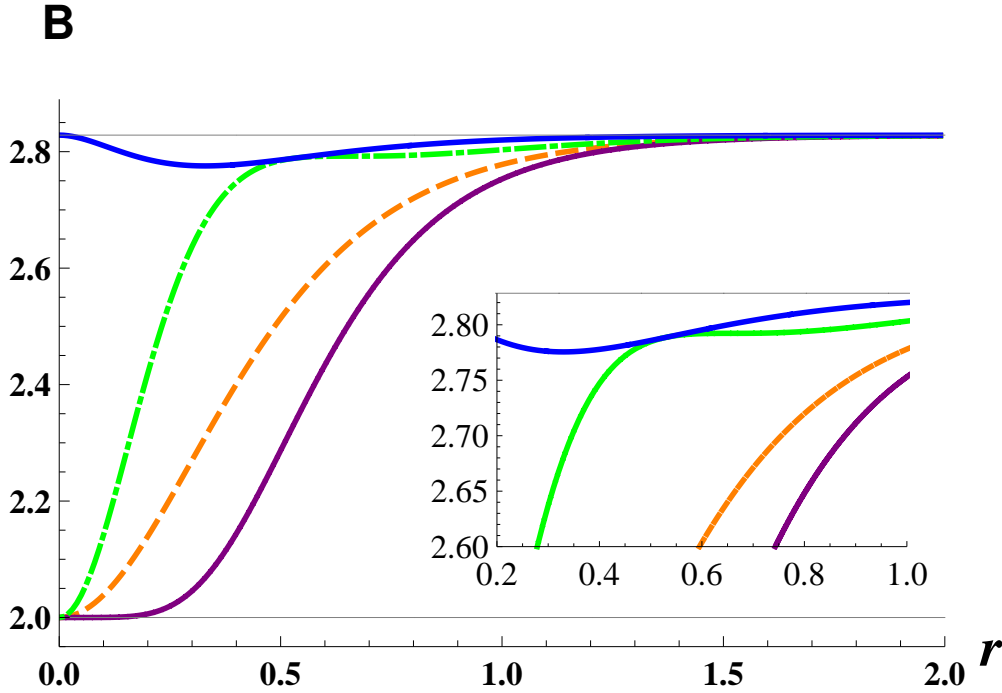
Figure 5.1: *(color online)*—Plot of the Bell function for the optimized state (*blue solid line*), for the PS state (*green dot-dashed line*), for the TB state (*orange dashed line*), and for the PA state (*purple dotted line*) for r ranging from 0 to 2. The inset is a magnification of the trends for $r \in [0.2, 1.0]$.

5.3   Appropriate non-Gaussianity for cv quantum teleportation

It has been demonstrated [67] that the fidelity of teleportation can be improved by exploiting the suitable deguassifications of Gaussian resources. Schemes of degaussification produce enhancing of the entanglement of the output state. However, when the resource is non-Gaussian, entanglement isn't only free degree conditioning the teleportation fidelity. There are other properties that play a crucial role in the success of teleportation. It is well known that the Gaussian twin beam, in the limit of infinite squeezing, realizes exactly the cv version of the maximally entangled Bell state (qubit). We have seen, in the previous chapter, that in the limit of r tending to infinity the Gaussian twin beam allows perfect quantum teleportation with unitary fidelity. Therefore, [4] any efficient resource for cv quantum information tasks should enjoy a further property, i.e. resemble the form of a two-mode squeezed vacuum state, as much as possible, in the large r limit, while retain its non-Gaussian character, Eqs. (1.11), (1.12). The squeezed-vacuum affinity $\mathcal{G}$ can be quantified by the following maximized overlap:

$$\mathcal{G} = \max_{s} |\ _{12}\langle -s|\ \psi_{res}\rangle_{12}\ |^2, \tag{5.12}$$

where $|-s\rangle$ is a two-mode squeezed vacuum state with real parameter of squeezing $-s$ and $|\psi_{res}\rangle$ is any entangled two-mode resource.

It is possible to see [4] that at sufficiently large squeezing the *photon-added squeezed* and *photon-subtracted squeezed* resources have high entanglement and, moreover, possess strong non-Gaussianity. Nevertheless, as we'll see in the next section, they aren't the best resource of teleportation, they don't satisfy the propriety of squeezed-vacuum affinity. It is the optimal interplay of these three proprierties: entanglement, non-Gaussianity and squeezed-vacuum affinity, that allows to obtain the optimal non-Gaussian resource for cv quantum teleportation [4].

5.4   cv quantum teleportation with non-Gaussian resources

The authors of ref.s [4], [5] analyzed the teleportation fidelity $\mathcal{F}$ Eq. (2.40) obtained using $|\psi\rangle_{SB}$ as resource for different Gaussian (coherent, squeezed) and non-Gaussian (single photon, photon added coherent) single mode input states. For each given input state, the analytical expression of $\mathcal{F}$ is a function of the independent parameters r, ϕ, δ and θ, i. e. $\mathcal{F} = \mathcal{F}(r, \phi, \delta, \theta)$. Maximizing $\mathcal{F}$, at fixed r, the optimal fidelity,

$$\mathcal{F}_{opt} = \max_{\delta} \mathcal{F}(\widetilde{r}, \phi, \delta, \theta),$$

is obtained for values of δ, that are different for each input state, but that do not reproduce any of the states already known, Eqs. (5.2), (5.3), (5.4), (5.5). The investigation revealed that the optimal non-Gaussian resource, obtained tuning the parameter δ in $|\psi\rangle_{SB}$, realizes the simultaneous maximization of the content

of entanglement, of the degree of affinity with the two-mode squeezed vacuum (5.12), and of the, suitably measured, amount of non-Gaussianity Eqs. (1.11), (1.12).

The same results are obtained considering a realistic cv quantum teleportation [5].

CHAPTER 6

ENTANGLEMENT SWAPPING OF THE SQUEEZED BELL STATES

Quantum resources are fragile and are subject to decoherence by interaction with the environment. The unavoidable losses in the communication channel can lead to a deterioration of quantumness limiting the possible applications of these states to Quantum-Communication protocols. For this reason the performance of the squeezed Bell states was analyzed also in the presence of losses, mechanisms of decoherence and low efficency of detection. The analisys gaves the same results of the ideal case [5]. However, even if the squeezed Bell state turns out to be the best teleportation resource, compared to all those analyzed even in the presence of losses, the overall performance degrades.

As we saw in section (2.5) to restore the entanglement lost during propagation it is very useful to use the entanglement swapping protocol. It, e.g., plays a relevant role in the quantum repeaters implementation, because error probability is linked to the length of channel. The swapping protocol allows to distribute entanglement between the nodes of shorter segments, wherein the channel is been divided.

To determine which is the best resource of teleportation even in circumstances where the state undergoes a process of swapping before becoming a resource for teleportation we [11] have analyzed a cascaded quantum information scheme, including as first step either an ideal or realistic swapping protocol, and subsequently an ideal teleportation protocol. The cascaded scheme is structured as follows:

- Let ρ_{res} the initial resource. At first we apply the entanglement swapping protocol, using the formalism of the characteristic function (see section 2.5).

As we have said in the previous chapters, it is easy to produce Gaussian twin beam TB with finite degree of squeezing. On the contrary it is hard and more expensive to obtain non-Gaussian states. Therefore, following the idea of sticking to the availability of current technologies, we have assumed to have at disposal many copies of TB and few copies of SB states. With such a constraint, the most convenient approach would be to swap the non-Gaussian entanglement using the TB and the SB states as resources and input states of the swapping protocol, respectively. On the other hand, by removing the above constraint, one would have on-demand availability of SB states. In this desirable instance, one could use SB states both as input and as resources of the swapping protocol. Moreover, as we seen in the previous chapter, the SB can be tuned for giving the main

de-gaussified states. For all these reasons, we have chosen to swap the squeezed Bell states with all resources of interest so far considered.

- At second, we study the Vaidman-Braustein-Kimble (VKB) protocol (see § 2.8) for cv teleportation of a coherent state with non-Gaussian entangled swapped resources, obtaining a teleportation fidelity $\mathcal{F}$ Eq. (2.40) as function also of the states used in the swapping protocol. In terms of the quadratures, it reads

$$\mathcal{F} \rightarrow \mathcal{F}_{AswB} = \frac{1}{2\pi} \int dX_4 dY_4 \chi_{in}^{(coh)}(X_4, Y_4) \chi_{out}^{(telep)}(X_4, -Y_4),$$

  where $A, B = SB, PS, TB$ denote the inputs of the swapping protocol (see Fig. 2.1), $\chi_{in}^{(coh)}$ is the characteristic function of the coherent input state of the teleportation protocol and $\chi_{out}^{(telep)}$, given by

$$\chi_{out}^{(telep)}(X_4, Y_4) = \chi_{in}^{(coh)}(X_4, Y_4) \chi_{out}^{(swapp)}(X_4, -Y_4; X_4, Y_4),$$

  is the single mode output state of the teleportation protocol obtained using as resource the output state $\chi_{out}^{(swapp)}$ of the swapping protocol.

- The final teleportation fidelity is optimized tuning the controllable available free parameters P,

$$\mathcal{F}_{AswB}^{(opt)} = \max_P \mathcal{F}_{AswB}.$$

6.0.1 Teleportation fidelity with swapped resources

As explained above, we have computed the output characteristic function $\chi_{out}^{(swapp)}$ of the swapping protocol following the protocol described in section 2.5. We do not report the analytical expression as it is excessively long and cumbersome. Given $\chi_{out}^{(swapp)}$, it is then straightforward to compute the output characteristic function $\chi_{out}^{(telep)}(X_4, Y_4)$ of the subsequent ideal teleportation protocol

$$\chi_{out}^{(telep)}(x_4, p_4) = \chi_{in}^{(coh)}(x_4, p_4) \chi_{out}^{(swapp)}(x_4, -p_4; x_4, p_4), \tag{6.1}$$

We have derived the analytical expression for the teleportation fidelity $\mathcal{F}_{AswB}$ in the most general instance is $SBswSB$. It contains as particular cases all the fidelities of interest. Such a fidelity depends on the following parameters: the squeezing amplitudes r_{12}, r_{34} and the phases ϕ_{12}, ϕ_{34} and the angles fo *non-Gaussianity* δ_{12}, δ_{34} and phases θ_{12}, θ_{34} of the input states and of the resources in addition to the parameters associated with the experimental setup[1]. Before

---

[1] g_i, $i = 1, 4$, that is the gain associated with unitary displacements;
T_i (R_i), $i = 2, 3$ that is transmissivity (reflectivity) of beam splitters
Υ_i, $i = 1, 4$ that is damping factors
$n_{th,i}$, $i = 1, 4$, that is average number of thermal photons

proceeding in the analysis, we establishes some simplifications and assumptions. Without any loss of generality, as in Refs [4], [5] we fix the phases of the SB states as follows: $\theta_{12} = \theta_{34} = 0$ and the squeezing phases $\phi_{12} = \phi_{34} = \pi$. Due to such a choice, the dependence of the teleportation fidelity on the two gains g_i $(i = 1, 4)$ reduces to the unique parameter $\widetilde{g} = g_1 + g_2$.

We don't report the relation obtained for $\mathcal{F}_{SBswSB}$ (more cumbersome). However, free parameters available for optimization, that gives $\mathcal{F}^{opt}_{SBswSB}$, are $P = \{\delta_{12}, \delta_{34}, \widetilde{g}\}$.

In order to provide significant examples, we report the analytical expressions for $\mathcal{F}_{TBswTB}$ and $\mathcal{F}_{SBswTB}$. They are computed by letting $\delta_{12} = \delta_{34} = 0$ in the general analytical expression for $\mathcal{F}_{SBswSB}$ and related to ideal swapping protocol (i.e. $R_2 = R_3 = 0$, $\tau_1 = \tau_4 = 0$, see § 2.5). We obtain:

$$\mathcal{F}_{TBswTB} = \left\{ 1 + \frac{1}{4}(1 + \widetilde{g})^2(e^{-2r_{12}} + e^{-2r_{34}}) + \frac{1}{4}(1 - \widetilde{g})^2(e^{2r_{12}} + e^{2r_{34}}) \right\}^{-1}. \quad (6.2)$$

The optimal value $\widetilde{g}_{opt}$ obtained for fixed r_{12}, r_{34} reads

$$\widetilde{g}_{opt} = \frac{1 - e^{-2(r_{12}+r_{34})}}{1 + e^{-2(r_{12}+r_{34})}}.$$

We can see that, for growing values of the quantity $(r_{12} + r_{34})$, $\widetilde{g}_{opt}$ goes rapidly to one. The optimal fidelity, abtained by $\widetilde{g}_{opt}$, reads

$$\mathcal{F}^{(opt)}_{TBswTB} = \frac{1 + e^{-2(r_{12}+r_{34})}}{(1 + e^{-2r_{12}})(1 + e^{-2r_{34}})}.$$

It is invariant under exchange of r_{12} and r_{34}. In the limit of $r_{34} \to \infty$, we obtain the Eq.(3.19).

If we let $\delta_{34} = 0$ in $\mathcal{F}_{SBswSB}$ we get $\mathcal{F}_{SBswTB}$,

$$\mathcal{F}_{SBswTB} = \mathcal{F}_{TBswTB} \times \qquad\qquad\qquad\qquad\qquad (6.3)$$
$$\left\{ 1 + \frac{e^{-4r_{12}}}{8}\mathcal{F}^2_{TBswTB}\left[(1 + \widetilde{g})^2 - e^{4r_{12}}(1 - \widetilde{g})^2\right]\sin^2\delta_{12} \right.$$
$$+ \frac{e^{-2r_{12}}}{2}\mathcal{F}_{TBswTB}\left[(1 + \widetilde{g})^2(\cos\delta_{12} - \sin\delta_{12})\right. \qquad (6.4)$$
$$\left.\left. - e^{4r_{12}}(1 - \widetilde{g})^2(\cos\delta_{12} + \sin\delta_{12})\right]\sin\delta_{12} \right\},$$

where $\mathcal{F}_{TBswTB}$ is given by Eq. (6.2).

If we fix $\widetilde{g}$, the optimal fidelity $\mathcal{F}^{(opt)}_{SBswTB}$ is given by the optimal angle δ^{opt}_{12} such that

$$\tan 2\delta^{opt}_{12}$$
$$= \frac{\left[e^{-2r_{12}}\widetilde{g}^2_+ - e^{2r_{12}}\widetilde{g}^2_-\right]\left\{4e^{2(r_{12}+r_{34})} + (e^{2r_{12}} + e^{2r_{34}})\left[\widetilde{g}^2_+ + e^{2(r_{12}+r_{34})}(1 - \widetilde{g}^2)^2\right]\right\}}{\widetilde{g}^2_+\left[4e^{2r_{34}} + \widetilde{g}^2_+\right] + e^{2(r_{12}+r_{34})}\widetilde{g}^2_-\left[1 + 4e^{2r_{34}}\widetilde{g}^2_-\right] + (1 - \widetilde{g}^2)^2(e^{4r_{12}} + 4e^{2(r_{12}+r_{34})} + e^{4r_{34}})},$$

with $\widetilde{g}_+ = 1 + \widetilde{g}$, $\widetilde{g}_- = 1 - \widetilde{g}$. If we let $\widetilde{g} = 1$ and so $r_{34} \to \infty$ we obtain $2\delta_{12}^{opt} = [1 + e^{-2r_{12}}]$ associated with optimized teleportation of input coherent states with (non-swapped) SB states used as resources.

Finally the optimized fidelity $\mathcal{F}_{SBswTB}^{(opt)}$ is given by

$$\mathcal{F}_{SBswTB}^{(opt)} = \max_{\widetilde{g}} \mathcal{F}_{SBswTB}\Big|_{\delta_{12}=\delta_{12}^{opt}}.$$

Moreover, if δ_{12} is a specific fuction of r_{12}, such that $\cos\delta_{12} = \frac{\cosh r_{12}}{\sqrt{\cosh 2r_{12}}}$, the SB states reduce to PS states and the optimized fidelity is simply given by

$$\mathcal{F}_{PSswTB}^{(opt)} = \max_{\widetilde{g}} \mathcal{F}_{SBswTB}\Big|_{\delta_{12}=\cos^{-1}\left[\cosh r_{12}/\sqrt{\cosh 2r_{12}}\right]}.$$

The optimization over $\widetilde{g}$ is carried out numerically.

6.0.2 Results. Ideal swapping protocol:plots

In Fig. 6.1 we plot the optimized fidelities $\mathcal{F}_{SBswTB}^{(opt)}$, $\mathcal{F}_{PSswTB}^{(opt)}$ and $\mathcal{F}_{TBswTB}^{(opt)}$ as a function of r_{12}, at a fixed r_{34}. We compare them with the corresponding fidelities $\mathcal{F}_{SB}^{(opt)}$, $\mathcal{F}_{PS}^{(opt)}$ and $\mathcal{F}_{TB}^{(opt)}$ associated with the same non-swapped resources.

Figure 6.1: (Color online) Optimized fidelity of teleportation $\mathcal{F}_{AswTB}^{(opt)}$ with $A = SB$ (full line), PS (dashed line), and TB (dotted line), as a function of the squeezing parameter r_{12} of the swapped input state, and at fixed $r_{34} = 1.5$ of the swapping TB resource. For comparison, we also report the plots of the teleportation fidelities associated with the corresponding non-swapped resources (same plot style, but with tinier and lighter lines). While the fidelities associated with non-swapped resources saturate to one, the fidelities associated with swapped resources saturate to a lower level, depending on the swapping squeezing parameter r_{34}.

Obviously, for large value of the squeezing parameter r_{34}, the fidelities $\mathcal{F}_{A^{sw}TB}^{(opt)}$ tend to the ideal fidelities $\mathcal{F}_A^{(opt)}$. Indeed, the saturation level, exhibited for large values of the squeezing of the swapped resource r_{12}, is higher, and tends to the ideal value one, for growing r_{34}. In order to emphasize the improvement of the teleportation with non-Gaussian resources, in Ref. [4] it is introduced a suitable relative fidelity defined as:

$$\Delta\mathcal{F}_{SB}^{(A)} = \frac{\mathcal{F}_{SB}^{(opt)} - \mathcal{F}_A^{(ref)}}{\mathcal{F}_A^{(ref)}} \,, \tag{6.5}$$

where $\mathcal{F}_{SB}^{(opt)}$ is the optimized teleportation fidelity of teleportation associated with a SB resource, and $\mathcal{F}_A^{(ref)}$ is the reference (optimized) fidelity associated to a resource A. In order to quantify the enhancement in the teleportation performance when using (swapped) non-Gaussian SB resources with respect to reference swapped resources, we generalize Eq. (6.5) and define the following relative fidelity:

$$\Delta\mathcal{F}_{SBswA}^{(B^{sw}C)} = \frac{\mathcal{F}_{SBswA}^{(opt)} - \mathcal{F}_{BswC}^{(ref)}}{\mathcal{F}_{BswC}^{(ref)}} \,, \tag{6.6}$$

where $\mathcal{F}_{SBswA}^{(opt)}$ is the optimized fidelity of teleportation that we obtain using a SB resource swapped with a resource A, and $\mathcal{F}_{BswC}^{(ref)}$ is the reference (optimized) teleportation fidelity associated with a resource B swapped with a resource C. In particular, we analyze the behavior of $\Delta\mathcal{F}_{SBswTB}^{(TBswTB)}$ and $\Delta\mathcal{F}_{SBswTB}^{(PSswTB)}$. These quantities are plotted in Fig. 6.2 as functions of the squeezing parameter r_{12} of the swapped resource. It is worth noticing that the percentage improvement corresponding to swapped resources is practically equal to that corresponding to non-swapped resources. A high enhancement is obtained with respect to the Gaussian instance. Moreover, the swapped SB resources result better that the swapped PS resources too, especially for low values of r_{12}; however, a significant improvement is also evident for $r_{12} \in [1, 2]$. The Figs. 6.3 and 6.4 show the three-dimensional plots of $\Delta\mathcal{F}_{SBswTB}^{(BswTB)}$, with $B = TB$ and $B = PS$ respectively, as functions of r_{12} and r_{34}. $\Delta\mathcal{F}_{SBswTB}^{(TBswTB)}$, see Fig. 6.3, is monotone both as a function of r_{12} and as a function of r_{34}. However the performance supremacy of swapped SB resources is evident with respect to swapped TB resources for low values of r_{12} as $r_{34} \neq 0$. Looking at Fig. 6.4, i.e. $\Delta\mathcal{F}_{SBswTB}^{(PSswTB)}$, we see that the swapped SB resources are better than the swapped PS resources for low values of r_{12}; then the improvement, i.e. the relative fidelity, vanishes (as the resources coincide) for a specific value of r_{12}, depending on r_{34}; at last, for growing r_{12}, $\Delta\mathcal{F}_{SBswTB}^{(PSswTB)}$ exhibits a revival till it goes to zero for large r_{12}.

Let us now assume that also the swapping resource can be a non-Gaussian resource as well. Then, we consider the optimized fidelities $\mathcal{F}_{AswA}^{(opt)}$ with $A = SB, PS, TB$. Although we have computed the analytical expression for $\mathcal{F}_{AswA}$,
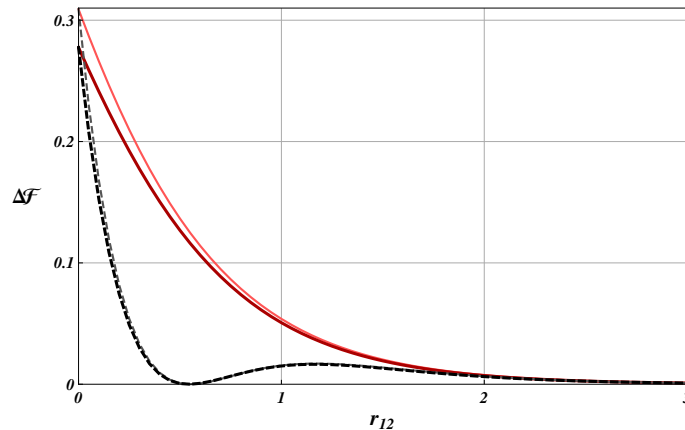
Figure 6.2: (Color online) Relative teleportation fidelities $\Delta\mathcal{F}_{SB^{sw}TB}^{(B^{sw}TB)}$ with $B = TB$ (full line) and $B = PS$ (dashed line), as a function of the squeezing parameter r_{12} of the swapped input state, and at fixed $r_{34} = 1.5$ of the swapping TB resource. For comparison, we also report the relative fidelities $\Delta\mathcal{F}_{SB}^{(A)}$ associated with the corresponding non-swapped resources (same plot style, but with tinier and lighter lines).

the optimization of these fidelities is carried out numerically. In Fig. 6.5, $\mathcal{F}_{AswA}^{(opt)}$ is plotted as a function of r_{12}, for a fixed value of r_{34}. As expected, a sensible enhancement of the teleportation fidelity can be observed for the fully non-Gaussian instances with respect to the fully Gaussian instance; such an improvement is more pronounced for the case of swapped SB resources. In Fig. 6.6, the relative teleportation fidelities $\Delta\mathcal{F}_{SBswSB}^{(TBswTB)}$ and $\Delta\mathcal{F}_{SBswSB}^{(PSswPS)}$ are plotted as functions of r_{12}. The relative fidelities clearly show a marked enhanced performance of swapped SB resources with respect to swapped PS and TB resources. Remarkably, in the fully non-Gaussian instance, the optimized (swapped) SB resources never collapse onto optimized (swapped) PS resources; correspondingly, the relative fidelity never vanishes.

6.0.3   Results. Realistic swapping protocol:plots

Let us now investigate the behavior of the swapped resources in the instance of realistic swapping protocol. We assume to know the values of the parameters associated with imperfections and decoherence effects. From an operational point of view, the knowledge of these parameters is equivalent to assume a control on the characteristics of the experimental apparatus, including the inefficiency of the photo-detectors and the length and damping rate of the noisy channels. Fixed the parameters associated with the experimental apparatus, the optimization of the fidelities is carried out numerically. In Fig. 6.7, we plot the optimized fidelities $\mathcal{F}_{AswB}^{(opt)}$ for several choices of the swapped resource A and of the swapping
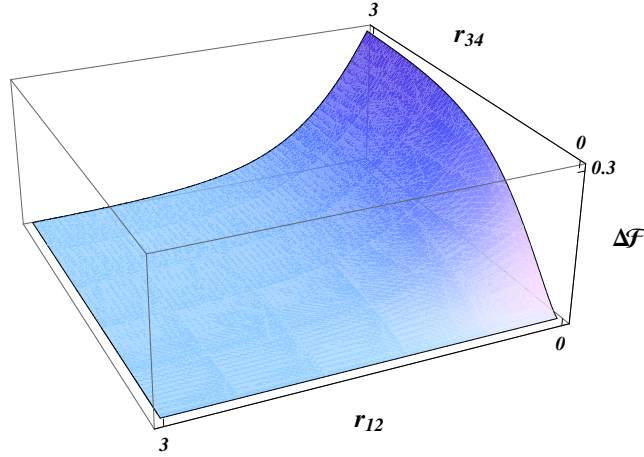
Figure 6.3: (Color online) Three-dimensional relative teleportation fidelity $\Delta\mathcal{F}_{SB^{sw}TB}^{(TB^{sw}TB)}$ as a function of the squeezing parameter r_{12} of the swapped input resource, and of the squeezing parameter r_{34} of the swapping TB resource. $\Delta\mathcal{F}_{SB^{sw}TB}^{(TB^{sw}TB)}$ is monotone in r_{12} and r_{34}.

resource B. We observe that the (swapped) SB resources perform better than the (swapped) PS and TB resources, even when they are swapped with TB resources. Indeed, $\mathcal{F}_{SBswSB}$ shows the best performance for any value of r_{12} (at fixed r_{34}). Furthermore, also $\mathcal{F}_{SBswTB}$ maintains above $\mathcal{F}_{PSswPS}$, $\mathcal{F}_{PSswTB}$, and $\mathcal{F}_{TBswTB}$ for any r_{12}. Let us notice that the PS resources perform better than the TB resources for low values of r_{12}, and as the squeezing parameter grows, both the fidelities $\mathcal{F}_{PSswPS}$ and $\mathcal{F}_{PSswTB}$ decrease going even below the fully Gaussian instance $\mathcal{F}_{TBswTB}$. In order to emphasize the percentage improvement obtained in the instance of SB input states and/or resources, in Fig. 6.8, we plot the relative fidelity $\Delta\mathcal{F}_{SBswX}^{(BswC)}$ for several choices of the swapping and swapped resources.

6.1 Conclusions

In this chapter, as in ref. [11], we have studied the efficiency of the cv quantum swapping protocol for the transmission of quantum states and entanglement, using a general class of non-Gaussian entangled resources. As a preliminary task, we have expressed the entanglement swapping protocol in the characteristic function representation. In order to evaluate the performance of the swapping protocol, we have exploited a criterion based on the ideal teleportation of input coherent states using swapped states as entangled resources; in particular, the teleportation fidelity has been assumed as convenient indicator to quantify the performance levels. We have showed that the non-Gaussian squeezed Bell resources allows for optimization procedures, yielding high values of the fidelities both in the ideal and the realistic instances.
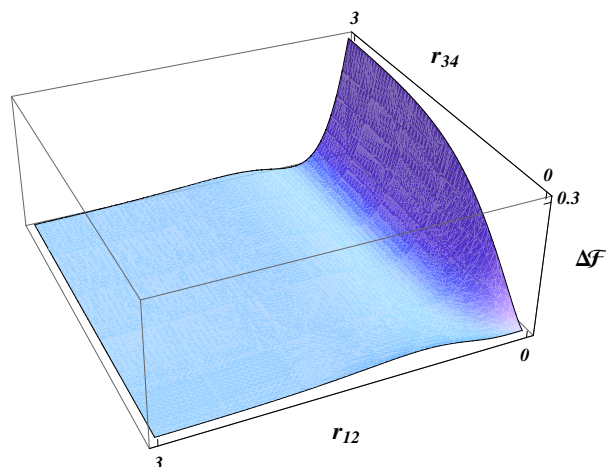
Figure 6.4: (Color online) Three-dimensional relative teleportation fidelity $\Delta\mathcal{F}_{SB^{sw}TB}^{(PS^{sw}TB)}$ as a function of the squeezing parameter r_{12} of the swapped input resource, and of the squeezing parameter r_{34} of the swapping TB resource.
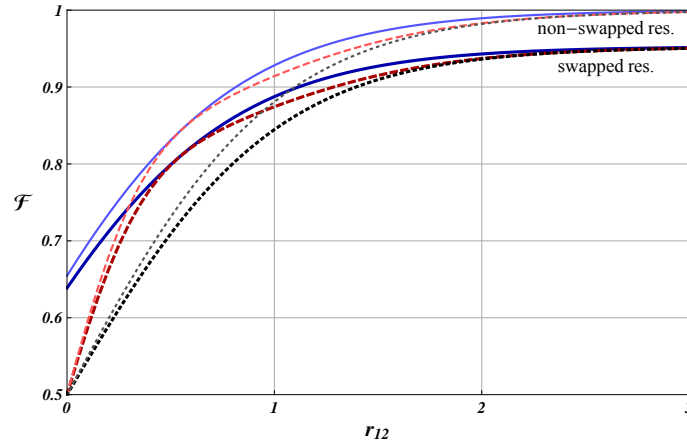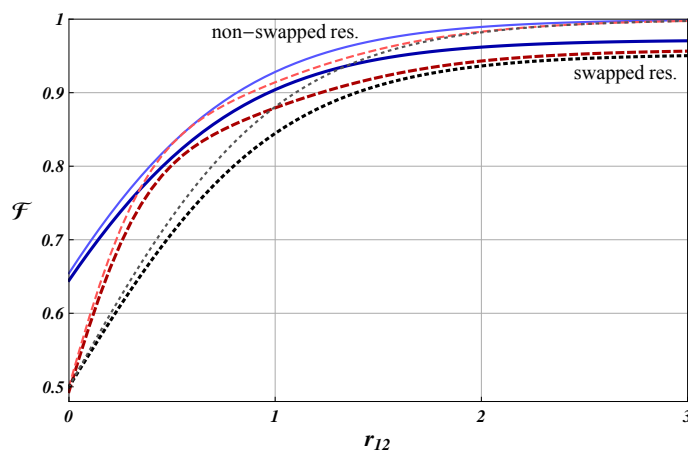

Figure 6.5: (Color online) Optimized fidelity of teleportation $\mathcal{F}_{A^{sw}A}^{(opt)}$ with $A = SB$ (full line) $A = PS$ (dashed line) and $A = TB$ (dotted line), as a function of the squeezing parameter r_{12} of the swapped input state, and at fixed $r_{34} = 1.5$ of the swapping resource. For comparison, we also report the plots of the teleportation fidelities associated with the corresponding non-swapped resources (same plot style, but with tinier and lighter lines). The swapped SB resources show a sensibly higher saturation level with respect to the swapped PS and TB resources.
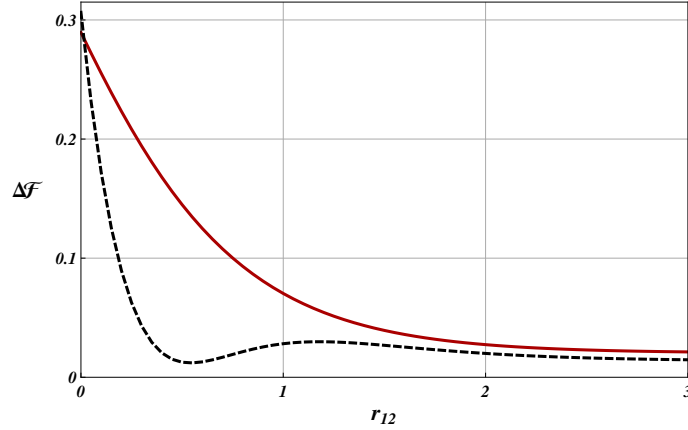
Figure 6.6: (Color online) Relative teleportation fidelities $\Delta\mathcal{F}^{(A^{sw}A)}_{SB^{sw}SB}$ with $A = TB$ (full line) and $A = PS$ (dashed line), as a function of the squeezing parameter r_{12} of the swapped input state, and at fixed $r_{34} = 1.5$ of the swapping resource. $\Delta\mathcal{F}^{(PS^{sw}PS)}_{SB^{sw}SB}$ never vanishes for any r_{12}.
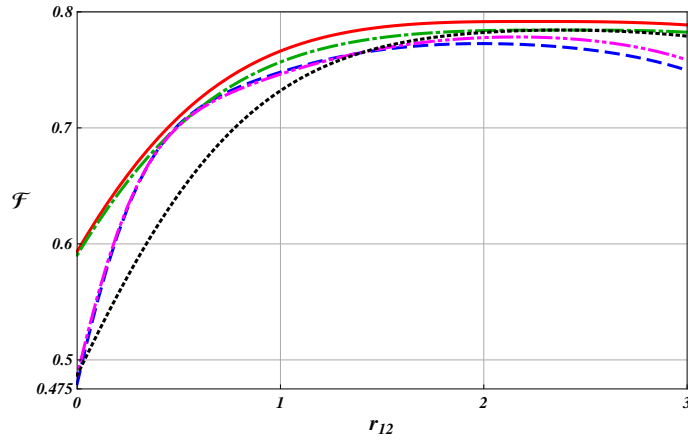
Figure 6.7: (Color online) Optimized fidelity of teleportation $\mathcal{F}^{(opt)}_{A^{sw}B}$ with $A = B = SB$ (full line), $A = B = PS$ (dashed line), $A = SB$, $B = TB$ (dot dashed line), $A = PS$, $B = TB$ (double-dot dashed line), and $A = B = TB$ (dotted line), as a function of the squeezing parameter r_{12} of the swapped input state, and at fixed $r_{34} = 1.5$ of the swapping resource. The parameters of the experimental apparatus are fixed as: $\tau_1 = 0.1$, $n_{th,1} = 0$, $\tau_4 = 0.2$, $n_{th,4} = 0$, $R_2 = \sqrt{0.05}$, $R_3 = \sqrt{0.05}$. The swapped SB resources show a sensibly higher saturation level with respect to the swapped PS and TB resources.
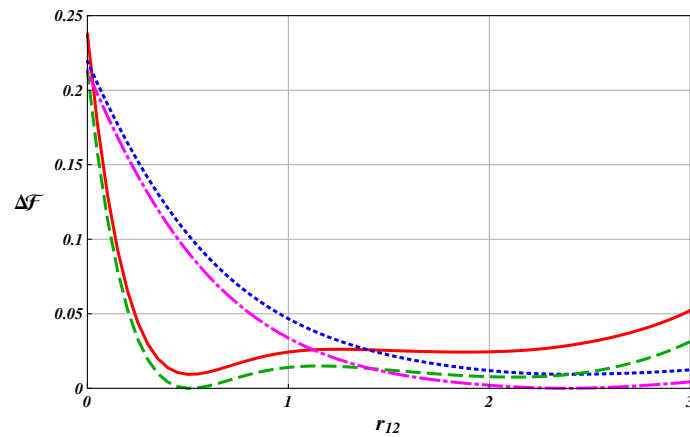
Figure 6.8: (Color online) Relative teleportation fidelities $\Delta\mathcal{F}_{SB^{sw}A}^{(B^{sw}C)}$ with $A = SB$, $B = C = PS$ (full line), $A = SB$, $B = C = TB$ (dotted line), $A = C = TB$, $B = PS$ (dashed line), $A = B = C = TB$ (dot-dashed line), as a function of the squeezing parameter r_{12} of the swapped input state, and at fixed $r_{34} = 1.5$ of the swapping resource. The parameters of the experimental apparatus are fixed as in Fig. 6.7.

CHAPTER 7

ENGINEERING OF THE SQUEEZED BELL STATES

As we seen in the chapter 5, the SB state, proposed in [4, 5], is

$$|\Psi>_{SB}\equiv S_{12}\left(-r\right)\left\{\cos\delta|0,0>_{12}+\sin\delta|1,1>_{12}\right\}. \qquad (7.1)$$

Tuning suitably the parameter δ we can obtain the PA state, the PS state, the PN state, and the TB [4], where addition/subtraction operations, as well as the number state, are referred to the case of 1 photon.

As we seen in chapters 5 e 6, $|\Psi>_{SB}$ constitutes an optimal resource of non locality, very useful for realizing the quantum teleportation and the swapping protocol with a very high efficiency. For this reason we proceeded to plan an experimental set up able to generate such state. In ref [12], we introduce the basic scheme of generation, and the preliminary analysis on the performance of the new resources will be performed. The experimental scheme introduced generates a new class of non-Gaussian resources that approximates, under both ideal and realistic conditions, the class of the (theoretically defined) SB states. The scheme has the advantage of being versatile, in the sense that a variation of the free experimental parameters allows the generation of all degaussified states, described in §5.1. Furthermore, the free experimental parameters can be exploited to optimize (as we have made in the previous chapters) in different situations, the performance in some quantum protocols.

In this chapter we report the results described in [12], in which we introduce (see §7.1), in two steps, the basic generation scheme of the new class of entangled states: at first, we consider a very ideal case of generation in order to emphasize the connection with the (theoretically defined) SB states, and, at second, we discuss the realistic instance.

The usefulness of the state is investigated in §6.5, estimating its performance as a resource for the quantum teleportation of a coherent state [49] (see § 2.8). Based on this criterion, we show that the optimized state, generated by our realistic scheme, provides, in a significant range of the parameters, a better performance than the other realistically generated states, including the PS state.

7.1 Scheme of generation of the new resources

The basic generation scheme is illustrated in Fig. 7.1.

In this scheme we exploit two (independently generated) Gaussian twin beams, $|\zeta>_{12}=S_{12}(\zeta)|0,0>_{12}$ and $|\xi>_{34}=S_{34}(\xi)|0,0>_{34}$, i. e. we start by the initial
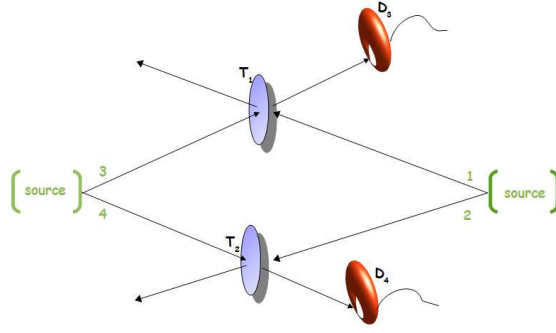
Figure 7.1: (Color online) the block-scheme of ideal setup for generating the class of states Eq. (7.4). Two indipendent twin beam $|\zeta\rangle_{12}$ and $|\xi\rangle_{34}$, are mixed into two beam splitters BS_I and BS_{II} of transmittivity T_1 and T_2, respectively. Two single photon detectors D_3 and D_4 realize simultaneous ddetections.

"proto-state"

$$|\zeta>_{12}|\xi>_{34}= S_{12}(\zeta)S_{34}(\xi)|\mathbf{0}>_{1234}, \tag{7.2}$$

where $|\mathbf{0}>_{1\ldots n}= \bigotimes_{k=1}^{n}|0>_k$ is the tensor product of n vacuum states. The twin beams feed the input ports of two beam splitters of transmissivity T_1 and T_2, respectively. Specifically, modes $1,3$ mix themselves at the beam splitter (BS_I), and modes $2,4$ at the beam splitter (BS_{II}). The resulting state is the four-mode entangled state $|\Phi>_{1234}$ described by:

$$\begin{aligned}|\Phi> {}_{1234} &= U_{13}(\kappa_1)U_{24}(\kappa_2)|\zeta>_{12}|\xi>_{34}\\ &= U_{13}(\kappa_1)U_{24}(\kappa_2)S_{12}(\zeta)S_{34}(\xi)|\mathbf{0}>_{1234}.\end{aligned} \tag{7.3}$$

Here the squeezing operators are given by $S_{ij}(\mu) = \exp\left\{-\mu\hat{a}_i^\dagger\hat{a}_j^\dagger + \mu^*\hat{a}_i\hat{a}_j\right\}$ $(\mu = \zeta, \xi)$ with complex squeezing parameters $\zeta = r\exp\left\{i\,\phi_\zeta\right\}$ $(i = 1, j = 2)$ and $\xi = s\exp\left\{i\,\phi_\xi\right\}$ $(i = 3, j = 4)$, respectively. Furthermore, the beam-splitter operators are given by $U_{lk}(\kappa_l) = \exp\left\{\kappa_l\left(a_l^\dagger a_k - a_l a_k^\dagger\right)\right\}$, where for the first one $l = 1, k = 2$, for the second one $l = 3, k = 4$, and where $\tan\kappa_l = \sqrt{(1 - T_l)/T_l}$.

The basic idea is that, starting by the four-mode state $|\Phi>_{1234}$, the conditional measurements provided by the simultaneous "cliks" of detectors D_3, D_4, and the restriction to suitable ranges of the beam-splitters parameters and of the squeezing parameters, will lead to the generation of two-mode states which well will approximate the theoretical SB states.

Now we proceed by steps. At first, in §7.1.1, we consider the ideal situation, i. e. *single-photon conditional measurements* without inefficiency and losses. This allows to describe the basic elements of the scheme and to understand the connection with the theoretical SB states (§7.1.2). Then, in §7.1.3, we discuss the full realistic instance, that includes detection inefficiency and losses, whose values are choosen as those currently accessible in actual experiments.

7.1.1 Single-photon conditional measurements

Simultaneous detections project the state of Eq. (7.3) onto the *tunable state* (T)

$$|\Psi_T> = \mathcal{N}_{34} < 1,1|U_{13}(\kappa_1)U_{24}(\kappa_2)S_{12}(\zeta)S_{34}(\xi)|\mathbf{0}>_{1234}, \qquad (7.4)$$

with $\mathcal{N}$ a normalization constant.

To make the calculations less complicated, we have described the strategy of post-selection in the formalism of the characteristic function. When a post-selection strategy is applied, the simultaneous detections of single photons in mode 3 and 4 project the density matrix $\rho_{1234} \equiv |\Phi>_{1234}{}_{1234}\langle\Phi|$ into

$$\rho_T^{(|1>)}$$

$$\equiv \frac{1}{\mathcal{N}_T^{(|1>)}}\mathrm{Tr}_{34}\left[\rho_{1234} \otimes {}_3|1><1|_3 \otimes {}_4|1><1|_4\right]$$

$$= \frac{1}{\mathcal{N}_T^{(|1>)}\pi^4}\int d^2\boldsymbol{\beta}_1 d^2\boldsymbol{\beta}_2 d^2\boldsymbol{\beta}_3 d^2\boldsymbol{\beta}_4$$

$$\times \boldsymbol{\chi}_{1234}\left(\boldsymbol{\beta}_1;\boldsymbol{\beta}_2;\boldsymbol{\beta}_3;\boldsymbol{\beta}_4\right)\hat{D}_1\left(-\beta_1\right)\hat{D}_2\left(-\beta_2\right)$$

$$\times \mathrm{Tr}_{34}\left[\hat{D}_3\left(-\beta_3\right)\hat{D}_4\left(-\beta_4\right){}_3|1><1|_3{}_4|1><1|_4\right]$$

$$= \frac{1}{\mathcal{N}_T^{(|1>)}\pi^2}\int d^2\boldsymbol{\beta}_1 d^2\boldsymbol{\beta}_2 \mathcal{M}\left(\boldsymbol{\beta}_1;\boldsymbol{\beta}_2\right)\hat{D}_1\left(-\beta_1\right)\hat{D}_2\left(-\beta_2\right)$$

where $\mathcal{M}\left(\boldsymbol{\beta}_1;\boldsymbol{\beta}_2\right)$ is given by:

$$\mathcal{M}\left(\boldsymbol{\beta}_1;\boldsymbol{\beta}_2\right) \equiv \frac{1}{\pi^2}\int d^2\boldsymbol{\beta}_3 d^2\boldsymbol{\beta}_4 \boldsymbol{\chi}_{1234}\left(\boldsymbol{\beta}_1;\boldsymbol{\beta}_2;\boldsymbol{\beta}_3;\boldsymbol{\beta}_4\right)$$

$$\times \chi_3^{(|1>)}\left(\boldsymbol{\beta}_3\right)\chi_4^{(|1>)}\left(\boldsymbol{\beta}_4\right),$$

and [1]

$$\chi_k^{(|1>)}\left(\boldsymbol{\beta}_k\right) = \mathrm{Tr}_k\left[\hat{D}_l\left(-\beta_l\right){}_3|1><1|_3\right]$$

$$= \left(1-|\beta_k|^2\right)e^{-|\beta_k|^2/2} \quad \text{for } k=3,4,$$

---

[1] $< m|D(-\alpha)|n> = \left(\frac{n!}{m!}\right)^{1/2}\alpha^{m-n}e^{-|\alpha|^2/2}L_n^{m-n}\left(|\alpha|^2\right)$, and $L_1^0(x) = L_1(x) = 1-x$.

is the characteristic function of the single-photon projector, $_k|1 >< 1|_k$, acting on the $k-$th mode. The normalization constant $\mathcal{N}_T^{(|1>)}$ is given by

$$\mathcal{N}_T^{(|1\rangle)} = \text{Tr}_{1234}\left[\rho_{1234} \otimes \ _3|1 >< 1|_3 \otimes \ _4|1 >< 1|_4\right].$$

In conclusion, we have

$$\begin{aligned}
\boldsymbol{\chi}_T^{(|1\rangle)}(\boldsymbol{\gamma}_1, \boldsymbol{\gamma}_2) &= \frac{1}{\mathcal{N}_T^{(|1\rangle)}}\text{Tr}_{12}\left[\rho_{12}\hat{D}_1(\gamma_1)\hat{D}_2(\gamma_2)\right] \\
&= \frac{1}{\mathcal{N}_T^{(|1\rangle)}\pi^2}\int d^2\boldsymbol{\beta}_1 d^2\boldsymbol{\beta}_2 \mathcal{M}(\boldsymbol{\beta}_1; \boldsymbol{\beta}_2) \\
&\quad \times \text{Tr}_{12}\left[\hat{D}_1(\gamma_1)\hat{D}_1(-\beta_1)\hat{D}_2(\gamma_2)\hat{D}_2(-\beta_2)\right] \\
&= \frac{1}{\mathcal{N}_T^{(|1\rangle)}}\mathcal{M}(\gamma_1; \gamma_2).
\end{aligned}$$

7.1.2 Tunable states similar to Squeezed Bell states

Varying the free parameters, κ_1, κ_2, r, s, ϕ_ζ, ϕ_ξ we can obtain different (Gaussian or degaussified) states. First of all, we fix $\phi_\zeta = \pi$; thus, $S_{12}(\zeta) \equiv S_{12}(-r)$. On the other hand, if we fix also $\phi_\xi = \pi$ (as it will be later forced by optimization, see next section) it is simple to see that, with this choice for the phases, the role of the two beam splitters inside the scheme become indistinguishable:

$$T_1 = T_2 \equiv T,$$

and thus $\kappa_1, \kappa_2 \equiv \kappa$. Obviously, we have also $\xi = -s$ and $S_{34}(\xi) \equiv S_{34}(-s)$. Indeed, we will see that this simplified instance is sufficient for our purposes. Furthermore, we will make the assumption that $\kappa^2 << 1$, and that the value of the strength $|\xi|(\equiv s)$ of the ancillary squeezing S_{34} is at most of the same order of κ^2 (this will be clarified by the procedure below). Therefore, we exploit beam splitters with a high transmissivity $T = \cos^2|k|$, and the ancillary squeezing S_{34} with a weak squeezing strength. As a consequence of such assumptions, the unitary operators $U_{13}(\kappa)$, $U_{24}(\kappa)$ can be expanded in power series and can be truncated to the order κ^2, while $S_{34}(\xi)$ can be truncated to the order $|\xi| \equiv s$.

Therefore, we have:

$$
\begin{aligned}
|\Phi\rangle_{1234} \approx \\
\left[1 + \kappa(a_1^\dagger a_3 - a_1 a_3^\dagger) + \frac{\kappa^2(a_1^\dagger a_3 - a_1 a_3^\dagger)^2}{2} + \mathcal{O}(\kappa^3)\right] \times \\
\left[1 + \kappa(a_2^\dagger a_4 - a_2 a_4^\dagger) + \frac{\kappa^2(a_2^\dagger a_4 - a_2 a_4^\dagger)^2}{2} + \mathcal{O}(\kappa^3)\right] \times \\
\left[1 + (s(a_3^\dagger a_4^\dagger - a_3 a_4) + \mathcal{O}(s^2))\right] \times \\
S_{12}(-r)|0,0,0,0\rangle_{1234}.
\end{aligned} \tag{7.5}
$$

Next, the postelection strategy is applied. Specifically, by using coincidence photodetection, the conditional measurements of simultaneous detections of single photons in mode 3 and 4 project the non-normalized state Eq. (7.5) onto $_{34}<1,1|\Phi>_{1234}$. Thus:

$$
_{34}<1,1|\Phi>_{1234} \approx (s + \kappa^2 a_1 a_2)S_{12}(-r)|0,0>_{12}. \tag{7.6}
$$

Due to our assumptions on the parameters κ^2 and $|\xi|$, in the above equation we have implicitly neglected terms proportional to $|\xi|\kappa^2$, i.e. contributions of the form $-s\kappa^2(a_1^\dagger a_1 + a_2^\dagger a_2)S_{12}(-r)|0,0>_{12}$, and of higher degree. Exploiting the (two-mode) Bogoliubov transformations

$$
S_{12}^\dagger(-r)\, a_i\, S_{12}(-r) = \cosh r\, a_i + \sinh r\, a_j^\dagger, \quad (i \neq j = 1,2), \tag{7.7}
$$

we obtain the non-normalized state:

$$
\begin{aligned}
S_{12}(-r)\, \Big\{ (s + \kappa^2 \sinh r \cosh r)|0,0\rangle_{12} \\
+ \kappa^2 \sinh^2 r|1,1>_{12}\Big\},
\end{aligned} \tag{7.8}
$$

whose form, apart from normalization, coincides with that of the squeezed Bell state (5.1). Introducing normalization factors, we obtain finally:

$$
\begin{aligned}
|\psi_T>_{12} &= S_{12}(-r)\, \{c_{00}|0,0>_{12} + c_{11}|1,1>_{12}\}, \\
c_{00} &= \frac{-\lambda + \sinh r \cosh r}{[(-\lambda + \sinh r \cosh r)^2 + (\sinh^2 r)^2]^{1/2}}, \\
c_{11} &= (1 - c_{00}^2)^{1/2},
\end{aligned} \tag{7.9}
$$
$$
\tag{7.10}
$$

where $\lambda = -s/\kappa^2$. Obviously, the state can be written in the form (5.1), where it is simple to see that

$$
\delta = \arctan\left(\frac{\kappa^2 \sinh^2 r}{s + \kappa^2 \sinh r \cosh r}\right). \tag{7.11}
$$

Note that, being the expression (7.8) of the state generated by the scheme of Fig. 7.1 practically identical to that of the theoretical state (5.1), the particular cases of the PA, PS, PN and TB states generated in this ideal instance can be obtained by choosing the experimental parameters in such a way that δ (Eq. (7.11)) is led to assume, from time to time, the corresponding special values described in [4]. It is to be noted that one could also consider further terms in the expansion, again obtaining states which approximate the theoretical SB states. For example, one can truncate at order κ^4 in the beam splitter operators, and one can truncate at order $|\xi|^3$ in the squeezing operator, by imposing the constraint that $|\xi|^2$ is at most of order κ^3. But, for our aims, this would be only an unnecessary complication.

The ideal instance here discussed allows to well understand the general idea, showing that the basic scheme can generate states similar to the theoretical SB states. On the other hand, the constraint that the shape of the generated states must be just that of the SB states is not strictly necessary for our aims, being the previous procedure only addressed to emphasize the connection with the theoretical SB states. In fact, we aim simply to generate states with a better performance than that of TB and of generated PS squeezed states. If our scheme, in some conditions, generates a state that is not of the SB form (5.1), but that satisfies this requirement, it is not a problem. Therefore, in the analysis of § 7.2, while retaining the condition $\kappa^2 << 1$, the parameter s will be free to assume any value.

We now move to discuss the inclusion of unavoidable experimental imperfections to gain insight on a realistic realization of our scheme.

7.1.3 Realistic generation

In realistic experimental conditions the state $|\Psi_T>$ takes trace of decoherence mechanisms which affect the squeezing sources: cavity output coupling, and losses during the propagation [55],[68].

In this context, the four-mode proto–state $|\zeta>_{12}|\xi>_{34}$, Eq. (7.2), becomes the four-mode squeezed thermal state described by the input density matrix (see appendix A)

$$\rho_{1234} = S_{12}(\zeta) S_{34}(\xi) \rho_{1234}^{th} S_{12}^{\dagger}(\zeta) S_{34}^{\dagger}(\xi), \tag{7.12}$$

where $\rho_{1234}^{th} = \bigotimes_{k=1}^{4} \rho_k^{th}$, with ρ_k^{th} is the density matrix of the thermal state associated to the k–mode. On the other hand, at typical temperatures (300 K), the thermal density matrix ρ_{1234}^{th} tends to the vacuum state, so that ρ_{1234} coincides pratically with the projection operator associated to the previous pure state $|\Phi>_{1234}$ (see the discussion in Appendix B).

A possible realistic scheme is sketched in Fig.7.2. The decoherence mechanisms are modelled by introducing four fictitious beam-splitters (one for every starting mode) with equal transmissivity $T_\ell (= 1 - R_\ell)$. Each beam-splitter has the empty port illuminated by a vacuum mode v_k. As already mentioned, at room temperature the thermal contribution to the decoherence is negligible, and
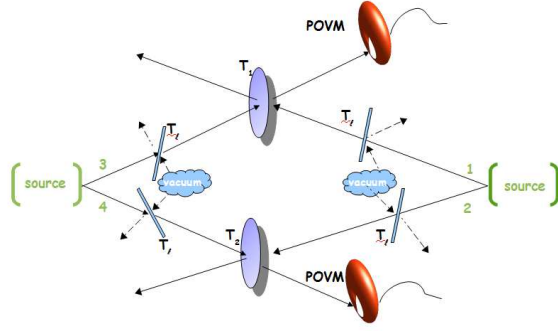
Figure 7.2: Realistic scheme (color online).(color online). At the ideal scheme (Fig. (7.1)), four fictitious beam splitters of transmittivity T_ℓ are introduced to mimic dechoerence mechanisms. Moreover, the single-photon detectors are replaced by POVMs ($\Pi_3^{(on)}$ and $\Pi_4^{(on)}$) with quantum efficiencies $\eta < 1$.

thus we must simply replace the state $|\Phi>_{1234}$ of Eq. (7.3) with the state

$$|\Phi'>_{1234} = \bigotimes_{k=1}^{4} \widehat{U}_k\left(T_\ell\right)|\Phi>_{1234}, \tag{7.13}$$

where the beam splitter operator that mixes mode $\hat{a}_k$ with the respective vacuum $\hat{v}_k$ is given by $U_k\left(T_\ell\right) = \exp\left\{\kappa_\ell \hat{a}_k^\dagger \hat{v}_k - \kappa_\ell^* \hat{a}_k \hat{v}_k^\dagger\right\}$, and κ_ℓ is such that $\tan\kappa_\ell = \sqrt{\left(1 - T_\ell\right)/T_\ell}$. Now we will proceed with the postselection procedure (see appendix A for further details). The detection associated to modes $k = 3, 4$ is now modeled by the POVM $\Pi_k^{(on)}(\eta_k)$, taking account simply of the threshold detection of $n \geq 1$ photons, that is given by

$$\Pi_k^{(on)}(\eta_k) = \mathbb{I}_k - \Pi_k^{(off)}(\eta_k), \tag{7.14}$$

where

$$\Pi_k^{(off)}(\eta_k) = \sum_{m=0}^{\infty} \left(1 - \eta_k\right)^m |m>_k\ {}_k<m|, \tag{7.15}$$

and η_k is the $k-$mode non-unit detection efficiency. So that the relative density matrix becomes

$$\rho_\mathbf{T}^{(on)}\left(T_\ell, \eta_3, \eta_4\right) = \frac{\mathrm{Tr}_{34}\left[\rho'_{1234} \otimes \Pi_3^{(on)}(\eta_k) \otimes \Pi_4^{(on)}(\eta_k)\right]}{\mathcal{N}_\mathbf{T}^{(on)}\left(\eta_3, \eta_4\right)}, \tag{7.16}$$

where ρ'_{1234} is the density matrix relative to the state $|\Phi'>_{1234}$, and the normalization constant

$$\mathcal{N}_{\mathbf{T}}^{(on)}(\eta_3,\eta_4) = \text{Tr}_{1234}\left[\rho_{1234}\otimes\Pi_3^{(on)}(\eta_k)\otimes\Pi_4^{(on)}(\eta_k)\right], \qquad (7.17)$$

that depends on η_3, η_4, represents the success rate in a real scenario. Applying this scheme, we can obtain, under a realistic situation of presence of losses ($T_\ell < 1$) and of not perfect quantum efficiencies ($\eta_3, \eta_4 < 1$), an approximated version of SB states, PS and TB states simply by inserting the values of the ancillary parameters which provide these states in the theoretical instance [4]:

$$\begin{aligned}
\rho_{PS}^{(on)}(T_\ell,\eta_3,\eta_4) &= \left.\rho_{\mathbf{T}}^{(on)}(T_\ell,\eta_3,\eta_4)\right|_{s=0,\kappa\simeq 0}, \\
\rho_{SB}^{(on)}(T_\ell,\eta_3,\eta_4) &= \left.\rho_{\mathbf{T}}^{(on)}(T_\ell,\eta_3,\eta_4)\right|_{s\simeq\kappa^2\ll 1,\phi=\pi}, \\
\rho_{TB}^{(on)}(T_\ell,\eta_3,\eta_4) &= \left.\rho_{\mathbf{T}}^{(on)}(T_\ell,\eta_3,\eta_4)\right|_{\xi=\zeta\equiv\varepsilon}.
\end{aligned}$$

It must be also remarked that, in addition to the other imperfections, it is to be considered a further practical restriction: due to decoherence, the effective value of the squeezing parameters is reduced. In fact, in appendix A, it is shown that the real squeezing parameter r' is related to the free-losses parameter r according to

$$r' = -\frac{1}{2}\ln\left[1 - T_\ell\left(1 - e^{-2r}\right)\right]. \qquad (7.18)$$

So, $e.g.$, if in the block scheme (Fig. 7.2) the squeezing is fixed at $r = 2$ ($\simeq 17.4$ dB), the realistic scheme, affected by 15% losses ($T_\ell = 0.85$), corresponds to a beam with r' of about 0.90 ($\simeq 7.81$ dB).

Once established the generation scheme, and the form of the generated states, the criterion that will be assumed in the next section to test their usefulness will be their efficiency (measured by fidelity) in implement quantum teleportation. However, we will compare only fidelities associated to optimized SB states, PS states and TB. In fact, the performance of the PA states and, even more, of the SN states when used as resources in quantum teleportation protocols is much worst than that of the Gaussian TB: the reason is that these resources do not satisfy the crucial requirement of Gaussian affinity [4].

7.2   The tunable resources for the teleportation protocol

Preliminaries – In this Section we seek to optimize the fidelity of the BKV teleportation protocol for a coherent state [49] using, as the bipartite entangled resource, the states generated by the proposed scheme. To this end, it is convenient to exploit the formalism of the characteristic function [69], particularly suited for the analysis of non-Gaussian states, because it simplifies the computational

strategies, expecially if the non-Gaussian state is used as a resource for the BKV teleportation protocol [4].

For a n-mode state described by the density matrix ρ the characteristic function is defined by

$$\chi(\beta_1, \beta_2, ..., \beta_n) = \text{Tr}[\rho D_1(\beta_1) D_2(\beta_2) \cdot D_n(\beta_n)], \qquad (7.19)$$

where $D_i(\beta_i)$ denotes the Glauber displacement operator for the mode i ($i = 1, ..., n$).

In Appendix B we show that, given a four–mode state represented by the characteristic function $\boldsymbol{\chi}_{1234}(\boldsymbol{\beta}_1; \boldsymbol{\beta}_2; \boldsymbol{\beta}_3; \boldsymbol{\beta}_4)$, the state achieved after conditional measurements on the two ancillaries modes (3 and 4) (depicted by detectors D in Fig. 7.1 is given by the characteristic function $\boldsymbol{\chi}_{\mathbf{T}}^{(D)}(\boldsymbol{\beta}_1; \boldsymbol{\beta}_2)$,

$$\begin{aligned} \boldsymbol{\chi}_{\mathbf{T}}^{(D)}(\boldsymbol{\beta}_1; \boldsymbol{\beta}_2) \;\; &= \;\; \frac{1}{\mathcal{N}\pi^2} \times \\ &\int d^2\boldsymbol{\beta}_3 d^2\boldsymbol{\beta}_4 \boldsymbol{\chi}_{1234}(\boldsymbol{\beta}_1; \boldsymbol{\beta}_2; \boldsymbol{\beta}_3; \boldsymbol{\beta}_4) \\ &\times \chi_3^{(D)}(\boldsymbol{\beta}_3) \chi_4^{(D)}(\boldsymbol{\beta}_4), \end{aligned} \qquad (7.20)$$

where $\boldsymbol{\beta}_k$ is a vector of the complex coherent amplitude, $d^2\beta_k = d\beta_k d\beta_k^*$, while $\boldsymbol{\chi}_{1234}(\boldsymbol{\beta}_1; \boldsymbol{\beta}_2; \boldsymbol{\beta}_3; \boldsymbol{\beta}_4)$ is the characteristic function of the initial state. It will correspond to $|\Phi>_{1234}$ (see Eq.(7.3)), for the ideal scheme, or to $|\Phi'>_{1234}$ (see Eq. (7.13)), for the realistic scheme. In the above formula, $\chi_k^{(D)}(\boldsymbol{\beta}_k)$ denotes the characteristic function of the conditional measurement realized by detectors D on the modes $k = 3, 4$ (its definition is provided in Appendix B).

We note now that we can consider the following states:

- *Theoretical states* – the ones given by their operatorial definition (see TABLE I) and not always exactly attainable by our scheme. Their performance has been considered in [4, 5].

- *Generated states: ideal case* – the ones generated by our scheme when we assume that losses are absent, detectors are perfectly photon-resolving, and projective measurements are performed.

- *Generated states: realistic case* – the ones generated by our scheme when losses are considered, and only on/off measurements are allowed, described by a non–ideal POVM.

In the next section we will discuss then at first the performance of the states generated in the ideal instance, by making also a comparison with the performance of the theoretical states. Later, we will discuss the performance of the states generated in realistic conditions. As announced, we will measure the performance

of a given state by considering the teleportation fidelity. In the formalism of the characteristic function, the teleportation fidelity is given by [69]

$$\mathcal{F} = \frac{1}{\pi} \int d^2\boldsymbol{\lambda}\chi_{in}(\boldsymbol{\lambda})\chi_{out}(-\boldsymbol{\lambda}), \tag{7.21}$$

where $\boldsymbol{\lambda}$ is the vector of the complex coherent amplitude for a generic state, and $d^2\lambda = d\lambda d\lambda^*$. Being the input state a coherent state $|\alpha>$, the characteristic function $\chi_{in} \equiv \chi_{coh}$ is

$$\chi_{coh}(\boldsymbol{\lambda}) = e^{-\frac{1}{2}|\lambda|^2+2i\Im[\lambda\alpha^*]}, \tag{7.22}$$

while the characteristic function χ_{out} of the output state is [4]

$$\chi_{out}(\boldsymbol{\lambda}) = \chi_{coh}(\boldsymbol{\lambda})\chi_{res}(\boldsymbol{\lambda}^*; \boldsymbol{\lambda}), \tag{7.23}$$

where $\chi_{res}(\boldsymbol{\lambda}^*; \boldsymbol{\lambda})$ denotes the characteristic function of the entangled state used as resource for the protocol. In order to determine the teleportation fidelity, We will exploit, from time to time, its specific form for each considered state.

However, before proceeding further, we recall that our proposal has been based on an approximation ($\kappa^2 << 1$), and on the possibility of an improvement provided by an optimization procedure. The only unconditioned parameter is the strength r of the squeezing operator $S_{12}(\xi)$; once fixed r, the fidelity of the state generated by our scheme will depend on the two squeezing parameters, and on transmissivities: thus, the optimization must be performed with respect to the phases of the two squeezing operators, to the transmissivities, and to the squeezing strength s of $S_{34}(\xi)$. In the following we will show that optimization with respect to phases and transmissivities is compatible with the assumptions exploited in order to generate SB states.

We have at first solved the optimization problem with respect to the squeezing phases; in fact, the analysis of several cases shows that the optimization procedure always returns $\phi_\zeta = \phi_\xi = \pi$, thus implying that the optimal building bricks for our scheme (see Fig. 7.1) are two independent two–mode squeezed states with $\zeta = -r$, and $\xi = -s$; this is in agreement with the position assumed *a priori* when we implemented our scheme in the previous section. From now on, thus, we will continue to use for the squeezing operators the notations: $S_{12}(-r), S_{34}(-s)$. As already remarked, this choice for the phases, that is forced by optimization, allows to take a common value T for the two transmissivities. The optimization with respect to T must take into account the role that the transmissivity plays in setting the distillation success rate (see Eq. (7.17)). Furthermore, the result of this analysis must be congruent with the assumption $\kappa^2 << 1$ (i. e. *high transmissivity* $T = \cos^2|k|$) that is needed for our generation scheme. We have found that the fidelity monotonically increases with T. The optimal value would be thus obtained for $T \to 1$, a limiting value that, however, leads the success rate to drop to zero. Therefore, we set, in all what follows, $T = 0.99$ (a value

experimentally obtainable), and we cancel the dependence on T. In this way, we satisfy the assumption $\kappa^2 \sim 0.01 << 1$ and, *de facto*, we achieve optimization with respect to transmissivity.

Finally, regarding optimization with respect to the ancillary parameter s, as we have announced in the previous section we allow that this parameter covers a wide range, and we identify, from time to time, the value of s that, at each given r, maximizes the fidelity. We will see that, when the ideal generation is considered, this value corresponds to SB states for not too large values of r, while for values of r which exceed a given threshold this is no more true; despite this, the states generated by the scheme and associated to the maximum fidelity provide a performance better than that of TB and PS states. In the realistic instance, obviously, we do not mind to compare the form of the optimized states with that of the theoretical SB states, but we focus our attention only on their performance.

7.2.1 Ideal case of the single-photon measurement

As a testbench for the proposed scheme, we have considered the teleportation fidelity for the most ideal case where the detectors D, Fig. 7.1, realize simultaneous projective single photon measurements, and the system is loss-free. The output state is, then, pure and described by the wave function given in Eq. (7.4).

Fig. 7.3 shows plots of the teleportation fidelity obtained using, as a resource, states that can be generated by the most ideal version of the proposed scheme. In particular, we have plotted the fidelity vs. the squeezing s ($\leq r$) of the ancillary modes $(3, 4)$ for eight different values of r ($= 0.6$, 0.8 , 1, 1.2, 1.4, 1.6, 1.8, and 2). For every curve, the value at $s = 0$ corresponds to the fidelity for a generated PS state, while $s = r$ corresponds to the fidelity obtained with a TB.

It can be seen that for every r there is a maximum in the fidelity that moves toward higher s when r increases; at the same time the maximum becomes less pronounced. We see that:

- For low values of the main squeezing the optimal resource is obtained for s close to 0. In particular, for the first lower values $r = 0.6, 0.8, 1$ the generated SB state, as approximated by our generation scheme, provides the best performance (the value of s does not exceed the order of magnitude of $\kappa^2 \sim 0.01$, see TABLE II).

- For values of r greater than 1 the state produced by the generation scheme and corresponding to the maximum fidelity, as r grows moves away increasingly from the SB state (the value of s exceeds sensibly the order of magnitude of $\kappa^2 \sim 0.01$, see TABLE II). However, this state still provides a better performance than that of a TB and of an (experimentally generated) PS state.
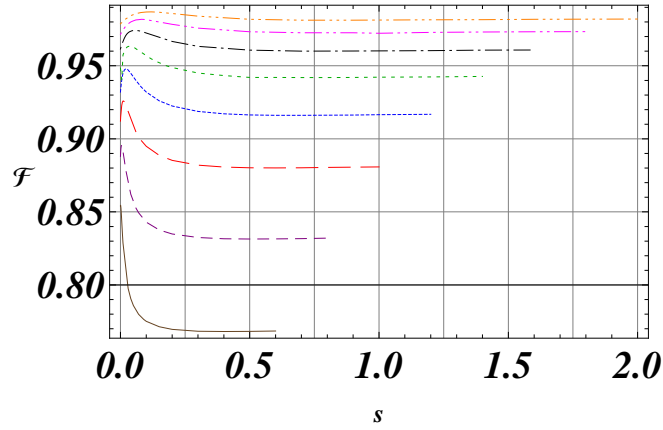
Figure 7.3: (Color on line) Fidelity of teleportation of the state generated from our scheme in the ideal instance (single-photon conditional measurements) plotted vs. the ancillary squeezing parameter s ($\leq r$) for different values of the main squeezing parameter r: (a) $r = 0.6$ (brown full line); (b) $r = 0.8$ (purple dashed line); (c) $r = 1$ (red large–dashed line); (d) $r = 1.2$ (blue dotted line); (e) $r = 1.4$ (green large–dotted line); (f) $r = 1.6$ (black dotted–dashed line); (g) $r = 1.8$ (magenta double dotted–dashed line); (h) $r = 2$ (orange triple dotted–dashed line). The point at $s = 0$ corresponds to the fidelity achieved with a PS squeezed state generated in ideal conditions, while at $s = r$ we obtain the fidelity achieved with a TB, generated as well in ideal conditions.

- In this same last region a TB state provides a better performance than that of the (experimentally generated) PS states and SB states.

Now we compare the optimal fidelity that can be obtained by the class of states here introduced, *i.e.* the value of the maximum in Fig. 7.3 with that of the *theoretical* states. In Fig. 7.4 it is plotted vs. r the optimal fidelity corresponding to states generated in the ideal case, and these values are compared with those of the fidelity obtained by exploiting the theoretical definition of TB, PS, and SB states. In the same figure it is also reported the fidelity of the PS states ($s = 0$) generated in the ideal case.

On one hand, we can see that, in this pretty ideal contest, the best fidelity of teleportation, for all the considered range of r, is achieved by exploiting the (optimized) theoretical SB states as found in Ref. [4]. On the other hand, the optimal fidelity for the class of states which we have introduced gets closer to that of the theoretical SB states when r increases. It has to be stressed that while the fidelities of the theoretical states and of the generated PS state can be analytically computed as functions of r, the optimal fidelity for the whole class of generated states must be computed numerically point by point, so that the plot of this optimized fidelity, if seen in greater details, looks as a broken line. In the

r	s
0.6	0.00057
0.8	0.0046
1.0	0.011
1.2	0.022
1.4	0.036
1.6	0.056
1.8	0.082
2.0	0.12

Table 7.1: Values of s corresponding to the maximum performance of the states generated by our scheme (in the ideal instance) for the considered values of r.

plot range $0 < r \lesssim 2$, representing experimentally feasible levels of squeezing, we can distinguish two different regimes:

a) $r \lesssim 0.5$ – the procedure of maximization Eq. (7.21) gives $s \simeq 0$, i.e. the best teleportation resource generated by the scheme is given by states that well approximate the experimentally generated PS states. On the other hand, the three curves corresponding to the optimal fidelity on generated states, to the fidelity of generated PS states and to to the fidelity of theoretical PS states, respectively, are superimposed and lie in between the fidelity of the optimized theoretical SB state (above) and the fidelity of a TB (below).

b) $r > 0.5$ – the performance of the optimized resource generated by the scheme overcomes both that of the generated PS state and that of the theoretical PS state, while offering a performance very close to that of the optimized theoretical SB state. In Fig. 7.5 we report the behaviours in the range $1 \leq r \leq 2$.

As an example, if we fix $r = 1.6$, we obtain the value 0.974 (at $s = 0.056$) for the optimized fidelity of the generated states. While, for the same r, the fidelities given by theoretical resources are 0.977 (optimized theoretical SB state), 0.965 (theoretical PS state), and 0.961 (TB). Therefore, in the framework of the ideal generation the performance of the generated states is very close to that of the theoretical ones.

7.2.2 Realistic lossy scenario

As pointed out previously, a realistic scenario for the generation of these class of states can be modeled by considering an inefficient photon detection and a lossy environment for the starting pair of two–mode squeezed states. In what follows we have considered the value $\eta = 0.15$ for the detection efficiency (that is the value currently obtainable in real experiments). Moreover, we remark that the values of the squeezing strength r which appear in the plots are referred to the original main squeezing, but the reduction to the effective squeezing r' has been
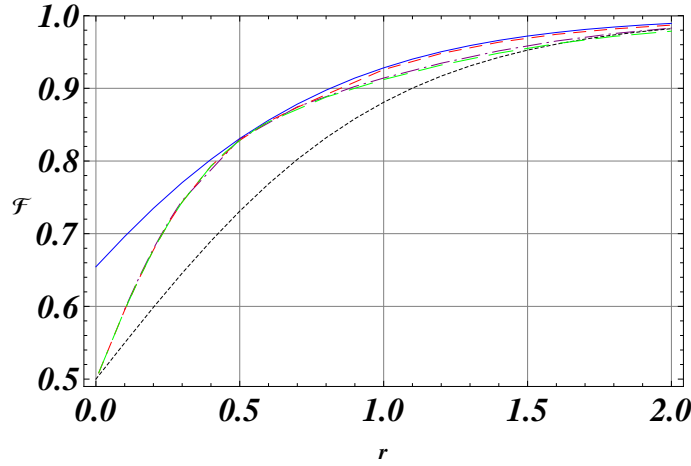
Figure 7.4: (Color online) Comparison among: the optimized fidelity on the class of generated states in the ideal instance of generation (red dashed), the fidelity of the PS squeezed state generated in the ideal instance (green large–dashed), the optimized fidelity of the theoretical SB states (cyan continuous), the fidelity of the theoretical PS squeezed states (purple dotted–dashed), and the fidelity of the theoretical TB (black dotted).

taken into account in order to obtain the final results.

In Fig. 7.6 we have plotted the optimized fidelity of teleportation associated to the generated states, (that depends on the squeezing strengths r, s) assuming at first an overall level of (fictitious) transmissivity $T_\ell = 0.85$ (i. e. a level of loss equal to 0.15) in Eq. (7.13). In the figure we have plotted the optimized fidelity as a function of the squeezing parameter s ($\leq r$), assuming for r the same values of Fig. 7.3. We can observe that:

a) the behavior of the fidelities does not change very much apart from a smoothing of the curves around their maximum;

b) as expected, the fidelities suffer a further deterioration due to the combined effect of non–ideal single photon detection processes, and of losses.

In this first plot the level of losses equal to 0.15 has been taken as a reference, being at present this level experimentally accessible by properly choosing optical components for the squeezing source. On the other hand, very recently an outstanding source with an overall loss of less than 0.08 has been reported [70]. In view of this result, we are led to investigate the behavior of the fidelities when the level of losses is varied. Therefore, we fix again the detection efficiency to be $\eta = 0.15$, we select for the squeezing parameter r the value $r = 1.6$, and we report, in Fig. 7.7, the optimized fidelity on the generated states as a function of the parameter of loss (denoted by ℓ). The plot is compared with the curves relative to the fidelity associated to the generated PS state, and to the fidelity associated to a TB, where also in these last two cases we have fixed $\eta = 0.15$, $r = 1.6$. As it
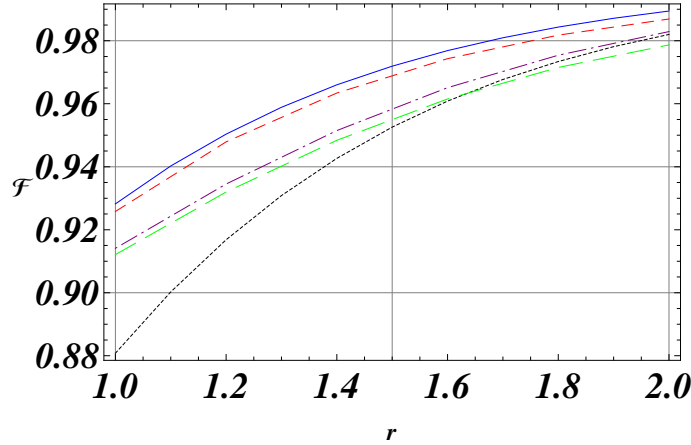
Figure 7.5: (Color online) Details of Fig. 7.4 in the range $1 \leq r \leq 2$ for: the optimized fidelity on the class of generated states in the ideal instance of generation (red dashed), the fidelity of the PS squeezed state generated in the ideal instance (green large–dashed), the optimized fidelity of the theoretical SB states (cyan continuous) the fidelity of the theoretical PS squeezed states (purple dotted–dashed), and the fidelity of the theoretical TB (black dotted).

can be seen, for losses up to $\ell = 0.30$ the optimized state obtained by our scheme of generation leads to the best fidelity. It has to be noted that, at a fixed r, the value of s corresponding to the maximum does not change very much. In the reported case this value is included in the interval $(0.048, 0.050)$.

Summing up, as remarked in point b) above the values of the fidelities in this realistic instance sensibly deteriorate. On the other hand, for values of r between 1.2 and 1.6 the optimized fidelities take again appreciable values which are better than those obtained when generated PS states and TB states are exploited. Furthermore, as we see by the Fig. 7.7, a (foreseeable) improving in the control of losses could improve the performance to levels comparable with those of the theoretical instance.

7.3 Conclusions

In this chapter [12], we have introduced a generation scheme that can produce a class of non-Gaussian tunable states which well approximates the class of SB states proposed in [4, 5]. A preliminary analysis shows that the state generated by our scheme is such that, used as a resource, provides the maximum fidelity of teleportation of a coherent state, i.e. ensures, in the most interesting range of the currently accessible experimental values of the main squeezing strength r, a better performance both with respect to a generated TB and with respect to a generated PS state (this last representing the best resource till now experimentally obtained). This is true both in ideal conditions and in realistic conditions.
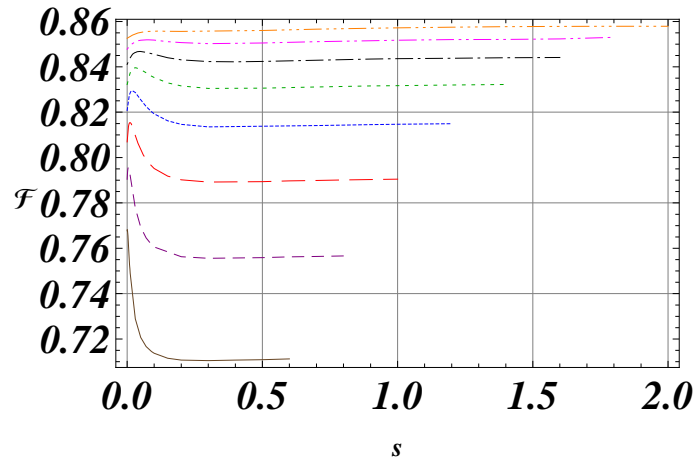
Figure 7.6: (Color online) Fidelity of teleportation in a realistic lossy scenario (level of losses equal to 0.15, i. e. $T_\ell = 0.85$, and $\eta = 0.15$). The fidelity depends on the squeezing parameters s, r, and has been plotted vs. s ($\leq r$) for the same values of r used in Fig. 7.3: (a) $r = 0.6$ (brown full line); (b) $r = 0.8$ (purple dashed line); (c) $r = 1$ (red large–dashed line); (d) $r = 1.2$ (blue dotted line); (e) $r = 1.4$ (green large–dotted line); (f) $r = 1.6$ (black dotted–dashed line); (g) $r = 1.8$ (magenta double dotted–dashed line); (h) $r = 2$ (orange triple dotted–dashed line).

In particular, in ideal conditions of generation (no losses, perfect photon-resolving detection) if $r > 0.5$ the performance of the optimal generated state lies very near to that of the optimized theoretical SB state. In realistic conditions (presence of losses, only on/off measurements allowed), obviously, the fidelities sensibly deteriorate, but, as remarked, the optimal generated state provides again, in a wide zone of interesting values of r, the best performance with respect to a generated TB state and with respect to a generated PS state.

It is interesting to note that also a slight improvement in reducing the level of losses and in increasing the detection efficiency leads to a relevant improvement in the performance of the optimal state generated in realistic conditions. Regarding the problem of improving the efficiency in photon-resolving, detectors based on superconducting wires could solve the problem in reasonable times. Once achieved these improvements, the efficiency of the realistically generated state would approach sensibly the remarkable efficiency of the optimal generated state in the ideal instance.

Anyway, our preliminary analysis shows that our scheme can generate non-Gaussian states with better performance than other generated states, including the PS state. In a forthcoming paper, the experimental set up needed to realize our scheme of generation will be designed. To this end, we will consider two possible instances: continuous wave and pulsed regime. In this second paper we
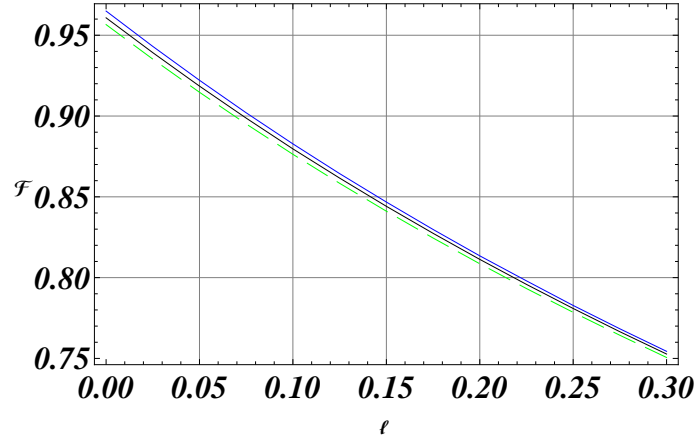
Figure 7.7: (Color online) Optimized fidelity of the states generated in realistic conditions (with $\eta = 0.15$) plotted as a function of the loss parameter ℓ, for $r = 1.6$ (blue full line). The plot is compared with those relative to the fidelity of the PS squezed states ($s = 0$, dark line)) and to the fidelity of the TB ($s = r$, green large–dashed line), when both are generated in realistic conditions with $\eta = 0.15$.

will face with the problem of a sufficiently effective detection in coincidence of two photons in the two different modes, as required by our scheme. In the same paper we will show how the generated states can be reconstructed by performing suitable homodyne detections.

Obviously, at the end of this route we aim to obtain our most ambitious goal, the actual realization of the experimental generation.

CHAPTER 8

NON LINEARITIES INDUCED BY FLUCTUATIONS IN THE OPTICAL PARAMETRIC OSCILLATOR

In the course of this Dissertation we have highligth that there are two main classes of quantum resources: Gaussian states and non-Gaussian states. We have seen that there are many benefits[1] from the use of these resources, but also that each of them suffers some limitations. For example, in the chapter 3, we have reported some experimental findings, showing that the quantum features of the Gaussian resources are very robust against the decoherence, but, in the chapter 5, we have described some technical and physical limitations afflicting this class of states. In particular we have stressed that we need of high squeezing parameter r for obtaing a very high teleportation fidelity. This means that the parametric process of down conversion, that generates the Gaussian squeezed states, must take place close to the critical point of threshold of the process. In such point the role of the fluctuating parameters of the system becomes critical. The generated state under this condition becomes an undesiderable, uncontrollable non-Gaussian state [71]. Moreover approching the threshold the fluctuating parameters tend to expolde.

On the other hand, it is possible to apply another strategy, that allows to better the performance of the resource without to approach the threshold of the down conversion process. In fact in the chapters 5 and 7 we have seen that starting from Gaussian states, as generated by the OPO under stable conditions[2], and applying some nonlinear operations -for expample a single photon detection- we obtain non-Gaussian states, that offer performances better than Gaussian states. In this case the non-Gaussianity isn't undesired and uncontrollable, but it is intentional.

To be fair we have to say that also the latter strategy suffers some limitations. To degaussify a two-mode Gaussian state is a non trivial experimental operation. In fact the conditioning measures must take place simultaneously on both modes of the state. This condition is not easy to obtain, also due to the low efficiency of the single photon detectors. So we can note that the scheme proposed in the chapter 7 presents some experimental diffulty. For this reason we studied extensively the feasibility conditions deducting that it is achievable (see chapter 7).

However, at the same time, we looked for other possible *sources* of non-Gaussianity.

In this chapter we present a preliminary study, conducted in collaboration with Prof. S. Solimeno and Dr A. Porzio, at the University of Naples Federico II,

---

[1] different for each class
[2] far from the threshold.

about a new way to obtain non-Gaussian states: to transform the undesiderable fluctuations of an OPO close to threshold in controllable tools for producing an optimal non-Gaussian resource. In this way, the non linearity for trasforming a Gaussian state in a non-Gaussian one isn't in the detection-step, but it is in the generation-step. Unfortunately this study is still at an early stage. However, as there seems to be very interesting, we consider appropriate to mention it in this Dissertation. The chapter is structured so as to provide an analysis of the role of fluctuations in a type–II OPO (see chapter 3). In particular we look at the modifications induced, by the fluctuations, onto the state, by the analisys of the characteristic function, and onto the covariance matrix. Eventually we study the ability of this state to act as a resource in a teleportation protocol. We prove that extra noise source can induce an improvement in the teleportation fidelity.

8.1 Graham-Haken-Langevin system

From what has been said in the previous chapters, we can deduce that the optical parametric oscillators are most used source of continuous variable entanglement. They are currently exploited for producing both Gaussian states and as source for degaussified states. Type II OPOs rely on parametric down–conversion: a strong *pump* beam at frequency ω_p interacts in a non–linear crystal with the vacuum fields thus generating two mutually orthogonal beams, *signal* and *idler*, at frequency $\omega_s = \omega_i = \frac{1}{2}\omega_p$ respectively [72],[73]. The three OPO cavity modes a_k (a_0 pump at frequency ω_p, a_s and a_i respectively signal and idler) evolve under the action of the Hamiltonian

$$H_{int} = i\hbar 2\chi \left(b_s b_i b_0^\dagger - b_0 b_s^\dagger b_i^\dagger \right) + i\hbar \left(\mathcal{E}^* b_0 - \mathcal{E} b_0^\dagger \right) \tag{8.1}$$

where χ is the coupling parameter proportional to the crystal second order susceptibility $\chi^{(2)}$. The pump field $\mathcal{E} = e^{-i\phi_p} \epsilon \left(1 + \mu_p \right)$ is treated in the rotating frame $e^{-i\omega_p t}$ as a complex quantity with a constant amplitude ϵ, that we assume modulated by a fluctuating factor $1 + \mu_p(t)$ ($\langle \mu_p \rangle = 0$) times a phase factor $e^{-i\phi_p}$, where $\phi_p(t)$ is a slowly diffusing phase, i.e. in accordance with the usual laser theory $\left\langle \left(\phi_p(t) - \phi_p(t') \right) \right\rangle^2 = 2\Delta y_\ell |t - t'|$ with Δ_ℓ the laser linewidth [74]. In particular $\frac{d}{dt}\phi_p = \varpi_p$ a stationary Gaussian process with $\langle \varpi_p(t) \varpi_p(t') \rangle = 2\Delta_\ell \delta(t - t')$. $\mu_p(t)$ will be treated as a stationary Gaussian process. Analogously a_s, a_i are defined in the frame $e^{-i\omega_p t/2}$.

The cavity modes are characterized by damping factor $\gamma_j = \gamma_{j,M} + \gamma_{j,x}$, with $\gamma_{j,M}, \gamma_{j,x}$ due respectively to the output mirror (M) and the other loss mechanisms (x: crystal absorption and scattering, absorption of the two mirrors, etc.). Modes are assumed to be slightly detuned by $\delta\varpi_j = \frac{\pi c}{L_j} \left[L_j \frac{\omega_j}{\pi c} \right] - \omega_j$, $[x]$ standing for the closest integer to x. $L_j = \bar{L}_j + \delta L_j$ with $\bar{L}_j$ the average OPO cavity optical length at frequency ω_j while δL_j is due to the mirror position fluctuations.

In OPO, the degree of correlation in the output fields is a function of the distance from the threshold oscillation. To have higher degree of correlation means to drive the OPO close to the oscillation threshold, in a regime where the OPO dynamic departs from the ideal case and the output fields are influenced by all the noise sources. The OPO dynamic can be described by a set of Langevin equations.

The evolution of the cavity mode operators is rooted in the theory of Langevin equations with quantum sources developed by Graham-Haken [72]. Namely it is described by the Graham-Haken Langevin equations (GHLE).

We introduce the quadratures

$$X_\varsigma = \frac{E}{2\sqrt{2}g_{\bar{\chi}}} \left(e^{i\phi_p/2} a_\varsigma + e^{-i\phi_p/2} a_\varsigma^\dagger \right) \tag{8.2}$$

$$Y_\varsigma = \frac{E}{2\sqrt{2}g_{\bar{\chi}}} \left(-i e^{i\phi_p/2} a_\varsigma + i e^{-i\phi_p/2} a_\varsigma^\dagger \right)$$

where the subscript $\varsigma = +, -$ distinguishes idler and signal, E is a parameter that quantifies the distance by the threshold, $g_{\bar{\chi}}$ is an adimensional parameter, of the order of 10^{-6}, describing the non-linear interaction strength $\bar{\chi}$ of the OPO crystal,

$$g_{\bar{\chi}} = \frac{2 |\bar{\chi}|}{\sqrt{2\gamma_0 \gamma}}.$$

In terms of the quadratures (8.2) the GHLEs become

$$\dot{\mathbf{\Psi}}_\varsigma = -\mathbf{H} \cdot \mathbf{\Psi}_\varsigma + \mathbf{N}_\varsigma \tag{8.3}$$

$$\dot{\mathbf{\Psi}}_0 = -\mathbf{H}_0 \cdot \mathbf{\Psi}_0 + \mathbf{N}_0 \tag{8.4}$$

where

$$\mathbf{\Psi}_0 = \begin{bmatrix} X_0 \\ Y_0 \end{bmatrix}, \quad \mathbf{N}_0 = \begin{bmatrix} \hat{\gamma}_0 \mu_p + \hat{X}_{R_0} \\ \hat{\varpi} + \hat{Y}_{R_0} \end{bmatrix},$$

and

$$\mathbf{H}_\varsigma = \begin{bmatrix} \lambda_\varsigma & 0 \\ 0 & \lambda_{\bar{\varsigma}} \end{bmatrix} + \begin{bmatrix} \varsigma E \left(X_0 + \delta\chi \right) & -\frac{\hat{\varpi}}{2} - \varsigma E Y_0 \\ \frac{\hat{\varpi}}{2} - \varsigma E Y_0 & -\varsigma E \left(X_0 + \delta\chi \right) \end{bmatrix} = \mathbf{H}_\varsigma^{(0)} + \varepsilon \mathbf{W}_\varsigma$$

$$\mathbf{H}_0 = -\hat{\gamma}_0 \mathbf{1} + \hat{\varpi} \begin{bmatrix} 0 & -1 \\ 1 & 0 \end{bmatrix} = \mathbf{H}_\varsigma^{(0)} + \varepsilon \mathbf{W}_0$$

We note that X_0, Y_0 are the quadratures relative to the pump, while $\hat{X}_{R_\varsigma}, \hat{Y}_{R_\varsigma}, \hat{X}_{R_0}, \hat{Y}_{R_0}$ are the vacuum fluctuating quadratures, such that

$$\left\langle \hat{X}_{R_\varsigma}(\tau) \hat{X}_{R_\varsigma}(\tau') \right\rangle = \left\langle \hat{Y}_{R_\varsigma}(\tau) \hat{Y}_{R_\varsigma}(\tau') \right\rangle = \delta(\tau - \tau')$$

$$\left\langle \hat{X}_{R_0}(\tau) \hat{X}_{R_0}(\tau') \right\rangle = \left\langle \hat{Y}_{R_0}(\tau) \hat{Y}_{R_0}(\tau') \right\rangle = \hat{\gamma}_0^2 \delta(\tau - \tau').$$

Moreover $\hat{\varpi} = \hat{\varpi}_s + \hat{\varpi}_i + \hat{\varpi}_p = 2\hat{\varpi}_s + \hat{\varpi}_p$, $\lambda_\varsigma = 1 - \varsigma E$.

We can see, by Eqs (8.3), that the OPO analyzed is characterized by four classical fluctuating parameters μ_p, ϖ_p, $\delta\nu$ and $\delta\chi$. These four terms, together determine the OPO dynamics. For typical operating conditions, ($\sigma_{\mu_p} \simeq 10^{-3} \div 10^{-2}, g_{\bar{\chi}} \simeq 10^{-6}$, $\gamma \simeq 10 \div 20$ MHz, $\sigma_{\varpi_p} \simeq 1 \div 1000$ Hz, $\sigma_T \simeq 1 \div 10$ mK, $\partial n/\partial T \approx 10^{-6} \div 10^{-4}$ and $\sigma_\chi \approx 10^{-5} \div 10^{-4}$) so that $\sigma_{\hat{\varpi}_p}$ and $\sigma_{\hat{\nu}}$ respectively range in the intervals $10^{-6} \div 10^{-4}$ and $10^{-5} \div 10^{-3}$.

We note that the presence of phase noises (ϖ_p and $\delta\nu$) physically implies that the dynamic of the X quadrature is coupled to the dynamic of Y. This physical aspect, has a strong consequence in the form of the fluctuating covariance matrix for the downconverted fields switching cross–correlations that are absent in an ideal system.

8.2 Integration of the GHL system

Integrating (8.4) yields

$$
\begin{aligned}
X_0(\tau) &= \int_{-\infty}^{\tau} e^{-\hat{\gamma}_0(\tau-\tau')} \times \\
&\quad \left[\cos\varphi(\tau,\tau') \left(\hat{\gamma}_0 \mu_p(\tau') + \hat{X}_{R_0}(\tau') \right) - \sin\varphi(\tau,\tau') \left(\hat{\varpi}(\tau') + \hat{Y}_{R_0}(\tau') \right) \right] d\tau' \\
Y_0(\tau) &= \int_{-\infty}^{\tau} e^{-\hat{\gamma}_0(\tau-\tau')} \times \\
&\quad \left[\cos\varphi(\tau,\tau') \left(\hat{\varpi}(\tau') + \hat{Y}_{R_0}(\tau') \right) + \sin\varphi(\tau,\tau') \left(\hat{\gamma}_0 \mu_p(\tau') + \hat{X}_{R_0}(\tau') \right) \right] d\tau'
\end{aligned}
$$

with $\varphi(\tau,\tau') = \int_{\tau'}^{\tau} \hat{\varpi} d\tau''$.

Analogously we have

$$
\boldsymbol{\Psi}_\varsigma(\tau) = \int_{-\infty}^{\tau} \mathbf{G}_\varsigma(\tau,\tau') \cdot \mathbf{N}_\varsigma(\tau')
$$

with

$$
\mathbf{G}_\varsigma(\tau,\tau') = \hat{T} e^{-\int_{\tau'}^{\tau} \mathbf{H}_\varsigma d\tau''} = 1 - \int_{\tau'}^{\tau} \mathbf{H}_\varsigma d\tau'' + \int_{\tau'}^{\tau} \mathbf{H}_\varsigma d\tau'' \int_{\tau'}^{\tau''} \mathbf{H}_\varsigma d\tau''' - \cdots
$$

$\hat{T}$ being the time ordering operator. Next $\mathbf{G}_\varsigma(\tau,\tau')$ can be expanded in a power series in ε :

$$
\mathbf{G}_\varsigma(\tau,\tau') = \mathbf{G}_\varsigma^{(0)}(\tau,\tau') + \varepsilon \mathbf{G}_\varsigma^{(1)}(\tau,\tau') + \varepsilon^2 \mathbf{G}_\varsigma^{(2)}(\tau,\tau')
$$

where

$$\frac{d}{d\tau}\mathbf{G}_\varsigma^{(0)}\left(\tau,\tau'\right) = -\mathbf{H}_\varsigma^{(0)}\cdot\mathbf{G}_\varsigma^{(0)}$$

$$\frac{d}{d\tau}\mathbf{G}_\varsigma^{(1)}\left(\tau,\tau'\right) = -\mathbf{H}_\varsigma^{(0)}\cdot\mathbf{G}_\varsigma^{(1)}+\mathbf{W}_\varsigma\cdot\mathbf{G}_\varsigma^{(0)}$$

$$\frac{d}{d\tau}\mathbf{G}_\varsigma^{(2)}\left(\tau,\tau'\right) = -\mathbf{H}_\varsigma^{(0)}\cdot\mathbf{G}_\varsigma^{(2)}+\mathbf{W}_\varsigma\cdot\mathbf{G}_\varsigma^{(1)}$$

that is

$$\mathbf{G}_\varsigma^{(0)}\left(\tau,\tau'\right) = e^{-\int_{\tau'}^{\tau}\mathbf{H}_\varsigma^{(0)}d\tau''}$$

$$\mathbf{G}_\varsigma^{(1)}\left(\tau,\tau'\right) = \int_{\tau'}^{\tau}\mathbf{G}_\varsigma^{(0)}\left(\tau,\tau''\right)\cdot\mathbf{W}_\varsigma\left(\tau''\right)\cdot\mathbf{G}_\varsigma^{(0)}\left(\tau'',\tau'\right)d\tau''$$

$$\mathbf{G}_\varsigma^{(2)}\left(\tau,\tau'\right) = \int_{\tau'}^{\tau}\mathbf{G}_\varsigma^{(1)}\left(\tau,\tau''\right)\cdot\mathbf{W}_\varsigma\left(\tau''\right)\cdot\mathbf{G}_\varsigma^{(1)}\left(\tau'',\tau'\right)d\tau''$$

Averaging the quantity

$$\boldsymbol{\Psi}_\varsigma\left(\tau\right)\boldsymbol{\Psi}_\varsigma^{T}\left(\tau\right) = \int_{-\infty}^{\tau}d\tau'\int_{-\infty}^{\tau}d\tau''\mathbf{G}_\varsigma\left(\tau,\tau'\right)\cdot\mathbf{N}_\varsigma\left(\tau'\right)\mathbf{N}_\varsigma^{T}\left(\tau'\right)\cdot\mathbf{G}_\varsigma^{T}\left(\tau,\tau''\right)$$

with respect to the quantum noise $\mathbf{N}_\varsigma\left(\tau'\right)$ yields the covariance matrix

$$\boldsymbol{\sigma}_\varsigma\left(\tau\right) = \int_{-\infty}^{\tau}\mathbf{G}_\varsigma\left(\tau,\tau'\right)\cdot\rho_{th}\cdot\mathbf{G}_\varsigma^{T}\left(\tau,\tau'\right)$$

with

$$\rho_{th} = \left\langle\mathbf{N}_\varsigma\left(\tau'\right)\mathbf{N}_\varsigma^{T}\left(\tau'\right)\right\rangle$$

the density matrix of the quantum noise entering the cavity.

From (8.2) it descends for the covariance matrix [75] $\sigma_{\varsigma ij}$ averaged with respect to the quantum noise sources $\hat{X}_{R_\varsigma},\hat{Y}_{R_\varsigma}$

$$\sigma_{\varsigma xx}\left(\tau\right) = \left\langle X_\varsigma^2\left(\tau\right)\right\rangle = \sigma_{\bar\varsigma yy}\left(\tau\right) = \left\langle Y_{\bar\varsigma}^2\left(\tau\right)\right\rangle$$

$$= \int_{-\infty}^{\tau}\left[e^{2\lambda_\varsigma\tau'}G_{\varsigma xx}^2\left(\tau,\tau'\right)+e^{2\lambda_{\bar\varsigma}\tau'}G_{\varsigma xy}^2\left(\tau,\tau'\right)\right]d\tau'$$

$$\sigma_{\varsigma xy}\left(\tau\right) = \left\langle X_\varsigma\left(\tau\right)Y_\varsigma\left(\tau\right)\right\rangle = \left\langle Y_\varsigma\left(\tau\right)X_\varsigma\left(\tau\right)\right\rangle$$

$$= \int_{-\infty}^{\tau}\left[-e^{2\lambda_\varsigma\tau'}G_{\varsigma xx}\left(\tau,\tau'\right)G_{\bar\varsigma xy}\left(\tau,\tau'\right)+e^{2\lambda_{\bar\varsigma}\tau'}G_{\varsigma xy}\left(\tau,\tau'\right)G_{\bar\varsigma xx}\left(\tau,\tau'\right)\right]d\tau'$$

In particular the variance $\left\langle X_{\theta\varsigma}^2\right\rangle = \sigma_{\theta\varsigma}$ of $X_{\theta\varsigma} = X_\varsigma\cos\theta + Y_\varsigma\sin\theta$ reads

$$\sigma_{\theta\varsigma}\left(\tau\right) = \sigma_{\varsigma xx}\left(\tau\right)\cos^2\theta + 2\sigma_{\varsigma xy}\left(\tau\right)\sin 2\theta + \sigma_{\varsigma yy}\left(\tau\right)\sin^2\theta$$

Depending $X_\varsigma(\tau), Y_\varsigma(\tau)$ on the Gaussian quantum processes $\hat{X}_{R_\varsigma}(\tau'), \hat{Y}_{R_\varsigma}(\tau')$ we have more in general

$$\left\langle X_{\theta_\varsigma}^{2n}(\tau) \right\rangle = \begin{cases} (2n-1)!!\sigma_{\theta_\varsigma}^n(\tau) \\ 0 \text{ othervise} \end{cases} \tag{8.5}$$

Therefore, we obtain

$$\begin{aligned}
\sigma_{\varsigma xx}(\tau) &= \frac{2g_{\tilde{\chi}}}{E^2} \frac{2\langle n(\tau)\rangle + 1}{2} \left[\cosh(2r(\tau)) - \sinh(2r(\tau))\cos 2\varphi(\tau)\right] \\
\sigma_{\varsigma xy}(\tau) &= \frac{2g_{\tilde{\chi}}}{E^2} \frac{2\langle n(\tau)\rangle + 1}{2} \sinh(2r(\tau))\sin 2\varphi(\tau) \\
\sigma_{\varsigma yy}(\tau) &= \frac{2g_{\tilde{\chi}}}{E^2} \frac{2\langle n(\tau)\rangle + 1}{2} \left[\cosh(2r(\tau)) + \sinh(2r(\tau))\cos 2\varphi(\tau)\right],
\end{aligned}$$

from which it is possible to reconstruct the quantum state. In fact, the Weyl characteristic function

$$\chi(\xi_\varsigma; t) = Tr[\hat{D}(\xi_\varsigma)\rho(t)],$$

can be found starting from the set of moments $\left\langle X_{\theta_\varsigma}^{2n}(\tau)\right\rangle$ and using Eq.(8.5). We obtain

$$\begin{aligned}
&\chi(\xi_\varsigma; \tau) \\
&= \left\langle \exp\left[-\left(\sigma_{\varsigma xx}(\tau)u_\varsigma^2 + (\sigma_{\varsigma xy}(\tau) + \sigma_{\varsigma yx}(\tau))u_\varsigma v_\varsigma + \sigma_{\varsigma yy}(\tau)v_\varsigma^2\right)\right]\right\rangle_{\text{fluctuating parameters}}
\end{aligned} \tag{8.6}$$

where

$$\begin{aligned}
u_\varsigma &= \frac{\varsigma u_1 + u_2}{\sqrt{2}}, \tag{8.7} \\
v_\varsigma &= \frac{\varsigma v_1 + v_2}{\sqrt{2}}.
\end{aligned}$$

$\chi(\xi_\varsigma; \tau)$ is averaged with respect the classical processes ϖ_p, ν, and χ and depending on time through the fluctuation induced by the pump amplitude in $\boldsymbol{\sigma}(\tau)$.

At zeroth order of the expansion $\chi(\xi_\varsigma; \tau)$ reduces to

$$\chi(\xi_\varsigma; \tau) = \left\langle \exp\left[-\left(\frac{A_{\bar{\varsigma}}(\tau)}{E_{\bar{\varsigma}}}u_\varsigma^2 + \frac{A_\varsigma(\tau)}{E_\varsigma}v_\varsigma^2\right)\right]\right\rangle_\mu \tag{8.8}$$

where

$$A_\varsigma(\tau) = E_\varsigma \int_{-\infty}^\tau e^{-E_\varsigma(\tau-\theta)-\varsigma 2g_{\tilde{\chi}}\int_\theta^\tau X_0^{(0)}(\tau'')d\tau''} d\theta \tag{8.9}$$

and

$$E_\varsigma = 2(1 + \varsigma E),$$

Consequently, by $\chi\left(\xi_\varsigma;\tau\right)$ we can obtain the Wigner function,

$$W\left(X_\varsigma,Y_\varsigma\right)=\frac{1}{\det\boldsymbol{\sigma}_\varsigma\left(\tau\right)}\left\langle\exp\left[-\left(\frac{X_\varsigma^2}{\sigma_{\varsigma xx}\left(\tau\right)}+2\frac{X_\varsigma Y_\varsigma}{\sigma_{\varsigma xy}\left(\tau\right)}+\frac{Y_\varsigma^2}{\sigma_{\varsigma yy}\left(\tau\right)}\right)\right]\right\rangle_{\text{fluctuating parameters}}.$$

Now, we can observe that purity μ Eq (1.2) is given by

$$\mu=Tr\left[\rho^2\right]=\left\langle\frac{1}{\sqrt{\det\boldsymbol{\sigma}_\varsigma\left(\tau\right)}}\right\rangle_{\varpi_p,\chi}$$

It has been proved in [75] that the covariance matrix of the mixed state $\boldsymbol{\sigma}_\varsigma$, at the output of non fluctuating OPO, propagating through a noisy channel is:

$$\boldsymbol{\sigma}_\varsigma\left(\tau\right)=\boldsymbol{\sigma}_\infty\left(1-e^{-\Gamma\tau}\right)+\boldsymbol{\sigma}_\varsigma\left(0\right)e^{-\Gamma\tau}\tag{8.10}$$

with $\boldsymbol{\sigma}_\infty$ the asymptotic covariance matrix

$$\boldsymbol{\sigma}_\infty=\left[\begin{array}{cc}\frac{2N+1+2M_1}{2}&M_2\\M_2&\frac{2N+1-2M_1}{2}\end{array}\right]$$

and $M=M_1+iM_2$ is the correlation function of the bath, while N is a phenomenological parameter related to the purity of the asymptotic state. Then we have that, in the circumstances in which fluctuating parameters are considered, Eq. (8.10) becomes

$$\boldsymbol{\sigma}_\varsigma\left(\tau\right)=\left[\begin{array}{cc}\frac{2N_{eff}+1+2M_{1eff}}{2}&M_{2eff}\\M_{2eff}&\frac{2N_{eff}+1-2M_{1eff}}{2}\end{array}\right]$$

where

$$\begin{aligned}N_{eff}&=&N+\frac{\sigma_{\varsigma xx}\left(0\right)+\sigma_{\varsigma yy}\left(0\right)-2N-1}{2}e^{-\Gamma\tau}\\M_{1eff}&=&M_1+\frac{\sigma_{\varsigma xx}\left(0\right)-\sigma_{\varsigma yy}\left(0\right)-2N-1}{2}e^{-\Gamma\tau}\\M_{2eff}&=&M_2+\left(\sigma_{\varsigma xy}\left(0\right)-M_2\right)e^{-\Gamma\tau}\end{aligned}$$

8.3   Teleportation fidelity

We want to calculate the teleportation fidelity $\mathcal{F}$ of a coherent state $|\beta\rangle$, described by the characteristic function

$$\chi_{in}\left(x,v\right)=\exp\left[-\frac{1}{2}\left|\alpha\right|^2+\left[\left(x+iv\right)\beta^*-\left(x-iv\right)\beta\right]/\sqrt{2}\right],$$

with Eq.(8.6) used as resourse. We have

$$\mathcal{F} = \frac{1}{2\pi} \int du_2 dv_2 \chi_{in}\left(u_2, v_2\right) \chi_{out}\left(-u_2, -v_2\right), \tag{8.11}$$

where χ_{out} is the characteristic function of the teleported state,

$$\chi_{out}\left(u_2, v_2\right) = \chi_{in}\left(u_2, v_2\right) \chi_{res}\left(u_2, -v_2; u_2, v_2\right). \tag{8.12}$$

and

$$\chi_{res}\left(u_1, v_1; u_2, v_2\right) = \chi\left(u_+, v_+; t\right)\chi\left(u_-, v_-; t\right),$$

where $\chi\left(u_+, v_+; t\right)$ is given in Eq.((8.6). Therefore,

$$\chi_{out}\left(u_2, v_2; \tau\right) = \chi_{in}\left(u_2, v_2\right) \exp\left[-\frac{E^2}{4g_{\bar{\chi}}}\left(\sigma_{+xx}\left(\tau\right) u_2^2 + \sigma_{-yy}\left(\tau\right) v_2^2\right)\right].$$

The fidelity $\mathcal{F}$ Eq.(8.11), is given by averaging on the time-dependent quantities

$$\mathcal{F} \equiv \overline{f\left(\tau\right)},$$

where

$$
\begin{aligned}
f\left(\tau\right) &= \frac{1}{2\pi} \int du_2 dv_2 \chi_{in}\left(u_2, v_2; \tau\right) \chi_{out}\left(-u_2, -v_2; \tau\right) \\
&= \frac{1}{\sqrt{\left(\frac{E^2}{2g_{\bar{\chi}}}\sigma_{+xx}\left(\tau\right) + 1\right)\left(\frac{E^2}{2g_{\bar{\chi}}}\sigma_{-yy}\left(\tau\right) + 1\right)}}
\end{aligned}
\tag{8.13}
$$

Expanding in terms of the fluctuating quantities $\sigma_{+xx}\left(\tau\right)$ and $\sigma_{-yy}\left(\tau\right)$, and retaining only even non–zero moments, we have

$$\mathcal{F} = \sum_{k=0}^{\infty} \mathcal{F}^{(k)}$$

with

$$
\begin{aligned}
\mathcal{F}^{(k)} &= \sum_{\substack{n: \\ n+m=k}} \frac{\delta_{k,0}}{\sqrt{\left(\frac{E^2}{2g_{\bar{\chi}}}\overline{\sigma_{+xx}} + 1\right)\left(\frac{E^2}{2g_{\bar{\chi}}}\overline{\sigma_{-yy}} + 1\right)}} \\
&+ \frac{\delta_{m,0}\Sigma_{+xx}^{(n-1)}}{\sqrt{\frac{E^2}{2g_{\bar{\chi}}}\overline{\sigma_{-yy}} + 1}} + \frac{\delta_{n,0}\Sigma_{-yy}^{(m-1)}}{\sqrt{\frac{E^2}{2g_{\bar{\chi}}}\overline{\sigma_{+xx}} + 1}} + \Sigma_{+xx}^{(n-1)}\Sigma_{-yy}^{(m-1)}
\end{aligned}
$$

where

$$\Sigma_{\varsigma qq}^{(\ell)} = \Theta\left[\ell\right] \frac{(2\ell)!!\,(4\ell+3)!!}{(4\ell+4)!!} \frac{\left(\frac{E^2}{2g_{\bar{\chi}}}\right)^{2(\ell+1)}\left(\overline{\sigma_{\varsigma qq}^2\left(\tau\right)} - \overline{\sigma_{\varsigma qq}}^2\right)^{\ell+1}}{\left(\frac{E^2}{2g_{\bar{\chi}}}\overline{\sigma_{\varsigma qq}} + 1\right)^{(4\ell+5)/2}}.$$

The parameters $\Sigma_{\varsigma qq}^{(\ell)}$ are the averages of the fluctuating quantities $\sigma_{\varsigma qq}^2(\tau)$. In particular, we have

$$\mathcal{F}^{(0)} = \frac{1}{\sqrt{\left(\frac{E^2}{2g_{\bar{\chi}}}\overline{\sigma_{+xx}} + 1\right)\left(\frac{E^2}{2g_{\bar{\chi}}}\overline{\sigma_{-yy}} + 1\right)}} \ , \tag{8.14}$$

$$\begin{aligned}\mathcal{F}^{(1)} &= \frac{\Sigma_{+xx}^{(0)}}{\sqrt{\frac{E^2}{2g_{\bar{\chi}}}\overline{\sigma_{-yy}} + 1}} + \frac{\Sigma_{-yy}^{(0)}}{\sqrt{\frac{E^2}{2g_{\bar{\chi}}}\overline{\sigma_{+xx}} + 1}} \\[2mm] &= \frac{3}{8}\mathcal{F}^{(0)}\left(\frac{\left(\overline{\sigma_{+xx}^2(\tau)} - \overline{\sigma_{+xx}}^2\right)}{\left(\overline{\sigma_{+xx}} + \frac{2g_{\bar{\chi}}}{E^2}\right)^2} + \frac{\left(\overline{\sigma_{-yy}^2(\tau)} - \overline{\sigma_{-yy}}^2\right)}{\left(\overline{\sigma_{-yy}} + \frac{2g_{\bar{\chi}}}{E^2}\right)^2}\right)\end{aligned} \tag{8.15}$$

$$\begin{aligned}\mathcal{F}^{(2)} &= \frac{\Sigma_{+xx}^{(1)}}{\sqrt{\frac{E^2}{2g_{\bar{\chi}}}\overline{\sigma_{-yy}} + 1}} + \frac{\Sigma_{-yy}^{(1)}}{\sqrt{\frac{E^2}{2g_{\bar{\chi}}}\overline{\sigma_{+xx}} + 1}} + \Sigma_{+xx}^{(0)}\Sigma_{-yy}^{(0)} \tag{8.16} \\[2mm] &= \frac{35}{64}\mathcal{F}^{(0)}\left(\frac{\left(\overline{\sigma_{+xx}^2(\tau)} - \overline{\sigma_{+xx}}^2\right)^2}{\left(\overline{\sigma_{+xx}} + \frac{2g_{\bar{\chi}}}{E^2}\right)^4} + \frac{\left(\overline{\sigma_{-yy}^2(\tau)} - \overline{\sigma_{-yy}}^2\right)^2}{\left(\overline{\sigma_{-yy}} + \frac{2g_{\bar{\chi}}}{E^2}\right)^4}\right. \\[2mm] &\quad \left. + \frac{9}{64}\frac{\left(\overline{\sigma_{+xx}^2(\tau)} - \overline{\sigma_{+xx}}^2\right)^2\left(\overline{\sigma_{-yy}^2(\tau)} - \overline{\sigma_{-yy}}^2\right)^2}{\left(\overline{\sigma_{+xx}} + \frac{2g_{\bar{\chi}}}{E^2}\right)^4\left(\overline{\sigma_{-yy}} + \frac{2g_{\bar{\chi}}}{E^2}\right)^4}\right) \tag{8.17}\end{aligned}$$

It is worth noting that the even moments all have positive coefficients so that any fluctuation of $\sigma_{+xx}(\tau)$ and $\sigma_{-yy}(\tau)$ will improve the overall fidelity.

CHAPTER 9

CONCLUSIONS

The purpose of this Dissertation was to investigate the quantum properties of the electromagnetic field of light radiation. These properties make it possible to ascertain the characteristics that a quantum state must have to be a good resource of teleportation.

We have dedicated part of the dissertation to the study of Gaussian bipartite states. They are one of the most renown resources for implementing of cv quantum communication protocols such as cv teleportation of coherent states. In the chapter 3, we have discussed in detail the relationship between three different entanglement criteria used in the cv framework and linked them to the teleportation fidelity. The latter evaluates the ability of this class of states in quantum teleportation protocol.

Then, in the same chapter, we have experimentally analyzed how the decoherence affects different entanglement criteria and quantum markers for a cv bipartite state outing a subthreshold type-II OPO. The decoherence is been experimentally introduced by transmitting the quantum state through a variable attenuator. Our experimental findings prove that the Lindblad approach for describing lossy transmission is valid all the way down to strongly decohered states. Moreover, we have proved that the particular class of states we have analyzed keeps, within the experimental indeterminacies, its main quantum signatures, i.e. the possibility of realizing quantum teleportation of coherent states with a fidelity above 0.5 and a quantum discord above 0 for a total loss of $\sim 99\%$. So it can, in principle, to realize quantum teleportation over an infinitely long Gaussian channel. From the analysis of the behaviour of the quantum discord and mutual information under decoherence, we interestingly found that the scattering of the points around the theoretical curve is significantly more evident for the quantum mutual information, which may be signaling that a key role, in our case, is played by unexpected classical correlations [6], [7], [8]. This point will be the subject of further theoretical and experimental investigations.

In the Chapter 4 we have shown that when a Gaussian bipartite state evolves in a Gaussian channel, retains its entanglement, but looses its Bell's nonlocality. This mean that although, at the born, the state is pure, therefore, for it, the violation Bell's inequality and the presence of entanglement are the expression of the same type of non-classical correlations, the decoherence highlights the different nature of the two markers: the Gaussian state becomes local (in according to Bell), i.e. it admits a description in terms of hidden variables, although it remains

entangled. We have analyzed the behaviour of the Bell function $\mathcal{B}_{\widetilde{\mathcal{I}}}$ under decoherence for different values of the **CM** element n (see Eq. (1.8)). We have seen that the decoherence immediately allows a description in terms of hidden variables ($\mathcal{B}_{\widetilde{\mathcal{I}}} \leq 2$). Furthermore, a greater number of photons in the starting (pure) state corresponds to a larger starting value of $\mathcal{B}_{\widetilde{\mathcal{I}}}$, but also a steeper descent towards the transition from non-local to the local regime [9]. This behavior is a confirmation of the circumstance that the larger degree of the initial squeezing, the more rapidly the squeezed state loses its nonlocality [64].

In the second part of this Dissertation, we have reported the study of non-Gaussian resources.

We have considered a general class of non Gaussian states, the Squeezed Bell states SB [4]. We have analyzed efficiency of this class in the cv quantum swapping protocol (chapter 6) for the transmission of quantum states and entanglement [11]. In order to ease the calculations, we have re-written the entanglement swapping protocol in the characteristic function formalism. In order to evaluate the performance of the state subjected to the swapping, we have used it as entangled resource for the ideal teleportation of input coherent state. The teleportation fidelity has been assumed as convenient indicator to quantify the performance levels. We have showed that the non-Gaussian squeezed Bell resources allow for optimization procedures, yielding high values of the fidelities both in the ideal and the realistic instances.

We have also shown that the Squeezed Bell states are the most nonlocal states among all the states of the same class [10] (chapter 5).

Attracted by these very positive results we have looked for engineering this type of resource. Actually, we have found a generation scheme (chapter 7) that produces a class of non-Gaussian tunable states. It is not exactly the Squeezed Bell class. However it well approximates the SB states proposed in [4, 5]. In fact, in the currently accessible experimental values of squeezing r, the state, that can be generated by our scheme, used as a resource, provides the maximum fidelity of teleportation of a coherent state with respect to a generated TB (representing the more feasible resource till now experimentally obtained) and with respect to a generated PS state (representing the best resource till now experimentally obtained). This is true both in ideal conditions and in realistic conditions, but obviously in realistic conditions (presence of losses, only on/off measurements allowed) the overall fidelities sensibly deteriorate [12].

However, we consider the introduced scheme a very good proposal for both the current technologies and the future technological improvements.

In fact it is sufficient a slight improvement in reducing the level of losses and in increasing the detection efficiency for improving clearly the performance of the optimal state generated in realistic conditions. These encouraging results lead us to design, in more details, our scheme of generation. In particular, in a forthcoming paper, we will consider two possible instances: continuous wave and

pulsed regime. In this second paper we will face with the problem of a sufficiently effective detection in coincidence of two photons in the two different modes, as required by our scheme. In the same paper we will show how the generated states can be reconstructed by performing suitable homodyne detections.

Eventually we have studied another class of non Gaussian states (chapter 8), obtained analyzing the fluctuating parameters of an type II-OPO. In this new model, the non linearity for trasforming a Gaussian state in a non-Gaussian one isn't in the detection-step (as in the previous scheme), but it is in the generation-step. This study is still at the preliminary stage. Our hope is to transform the undesiderable non-Gaussianity (producted by fluctuating OPO parameters) in controllable tools for producing an optimal non-Gaussian resource.

CHAPTER 10

APPENDIX A

10.1 PHS criterion and distillability

As we said in §2.4.1, entanglement criterion PHS does not always provide the same type of information (logical implication). At first, Peres [76] provided a necessary condition for separability, then Horodechi [31] showed that such condition is also sufficient in 2×2 and 2×3 Hilbert spaces. His proof is based on the operation of partial transposition. In fact, he demonstrated that:

Theorem 5 *If $(\rho^A)^T \geq 0$ in spaces of dimensions 2×2 and 2×3 then ρ_{AB} Eq. (2.10) is separable.*

So we can easily deduce that there exist PPT states, which are not separable in $M \times N$ spaces, with $M = 2$, $N \geq 4$ or $M \geq 3$. They are called *bound entangled states* to distinguish them from the *free entangled states*.

Once again we come to the conclusion that there are different forms of non-locality. More specifically, in this particular context we see that there are different forms of entanlgement [77]. However, although bound entangled states are entangled states, they are not distillable states, so they are not actually useful to Quantum Information protocols

10.2 Signatures of Entanglement

In §2.4.1 we have reported two particular entanglement criteria (PHS criterion and Duan one). Even if they reach the same conclusion[1], the starting point is different. The processing allowing to develop PHS criterion starts to definition of bipartite state Eq. (2.10) and discusses the properties that a density matrix must satisfy in order to represent a quantum state. The second criterion, instead, starts from the analysis of the properties that the (characterizing quantum state) observables must have. In the following we see in more details the latter approach.

Let $\{A_i\}$ the set of the Hermitian operators describing the observables of the system. The measure of A_i is affected by a statistical uncertainty ΔA_i,

$$\Delta A_i^2 = \left\langle A_i^2 \right\rangle - \left\langle A_i \right\rangle^2 .$$

If the quantum state is an eigenstate of the observable A_i, then $\Delta A_i = 0$. When it does not exist an simultaneous eigenstate of all operators $\{A_i\}$, then there is a non

---

[1]In [33], Duan et al showed that the Duan criterion becomes a necessary and sufficient condition for the entanglement, when the covariance matrix is positive semidefinite.

trivial limit $U > 0$ for the sum uncertainty (as it is obvious from the uncertainty principle),

$$\sum_i \Delta A_i^2 \geq U.$$

Now we consider a bipartite system, described by the quantum state ρ_{AB}, in which each subsystem (A, B) is characterized by a set of observables, $\{A_i\}$ and $\{B_i\}$, with local uncertainties such that

$$\sum_i \Delta A_i^2 \geq U_A, \quad \sum_i \Delta B_i^2 \geq U_B.$$

The operator proprierties $A_i + B_i$ of the joint system can be determinated by local measurements A_i, B_i respectively. For product state $\rho_{AB} = \rho_A \otimes \rho_B$ the values of the local measurements (made on the single subsystems) are uncorrelated, so the uncertainties of $A_i + B_i$ are equal to the sums of the local uncertainty,

$$\Delta \left(A_i + B_i \right)^2 = \Delta A_i^2 + \Delta B_i^2.$$

More in general, for mixture of product states, $\rho_{AB} = \sum_m p_m \rho_{m,A} \otimes \rho_{m,B,}$ we have

$$\sum_i \Delta \left(A_i + B_i \right)^2 \geq U_A + U_B. \tag{10.1}$$

Any violation of this uncertainty limit implies that the state cannot be separated into a mixture of product states.

The violation of any local uncertainty relation of the form Eq. (10.1) is therefore a sufficient condition for the existence of entanglement [78].

When the observables A_i and B_i are precisely the quadrature operators Eq. (1.6), we obtain Duan criterion.

CHAPTER 11

APPENDIX B

Characteristic function formalism – Here we describe in some details the proposed state in terms of the characteristic function. In such formalism, at the overall density operator ρ_{1234} relative to the product state[1] Eq.(7.2) $|\zeta>_{12} |\xi>_{34}$ is associated the following characteristic function

$$\boldsymbol{\chi}''\left(\boldsymbol{\alpha}''\right) = \boldsymbol{\chi}_{12}\left(\boldsymbol{\alpha}''_{12}\right)\boldsymbol{\chi}_{34}\left(\boldsymbol{\alpha}''_{34}\right),$$

where

$$\boldsymbol{\alpha}'' = \left(\boldsymbol{\alpha}''_{12}; \boldsymbol{\alpha}''_{34}\right) = \left(\alpha''_1, \alpha''^*_1; \alpha''_2, \alpha''^*_2; \alpha''_3, \alpha''^*_3; \alpha''_4, \alpha''^*_4\right),$$

$$\boldsymbol{\chi}_{ij}\left(\boldsymbol{\alpha}''_{ij}\right) = \exp\left\{-\frac{1}{2}\left(|\varsigma_i|^2 + |\varsigma_j|^2\right)\right\},$$

and $\varsigma_{i,j} = \alpha''_{i,j}\cosh|\lambda| + \alpha''^*_{j,i}e^{i\phi_\lambda}\sinh|\lambda|$, with $\lambda = \zeta$ if $i = 1 \wedge j = 2$, and $\lambda = \xi$ if $i = 3 \wedge j = 4$. For simulating the effect of decoherence in Fig. 7.2, we imagine four thermal beam splitters TBS (one for every beam), with transmissivity $T_{th}(= 1 - R_{th})$, in which each second port is occupied by the thermal state described by the following characteristic function

$$\boldsymbol{\chi}^{th}_k\left(\boldsymbol{\tau}'_k\right) = \exp\left\{-\frac{1}{2}\left(2\bar{n}^{th}_k + 1\right)|\tau'_k|^2\right\},$$

where $\boldsymbol{\tau}'_k = \left(\tau'_k, \tau'^*_k\right)$ and $\bar{n}_{th}$ is the average number of thermal quanta at the equilibrium in the $k-$th mode

$$\bar{n}^{th}_k = \left(e^{\hbar\omega/k_B T} - 1\right)^{-1}.$$

The overall characteristic function before of the thermal beam splitters, $\boldsymbol{\chi}_{preTBS}$, describes a eight-mode state given by

$$\boldsymbol{\chi}_{preTBS}\left(\boldsymbol{\alpha}''; \boldsymbol{\tau}'\right) = \boldsymbol{\chi}''\left(\boldsymbol{\alpha}''\right)\boldsymbol{\chi}_{th}\left(\boldsymbol{\tau}'\right), \tag{11.1}$$

where $\boldsymbol{\chi}_{th}\left(\boldsymbol{\tau}'\right) = \prod_{k=1}^4 \boldsymbol{\chi}^{th}_k\left(\boldsymbol{\tau}'_k\right)$. The beam splitters act on the state through a $SU(2)$ transformation, that yields the following relation among the variables of the input and output modes of the beam splitter

$$\begin{cases} \boldsymbol{\alpha}' = \sqrt{T_{th}}\boldsymbol{\alpha}'' + \sqrt{R_{th}}\boldsymbol{\tau}', \\ \boldsymbol{\tau} = \sqrt{T_{th}}\boldsymbol{\tau}' - \sqrt{R_{th}}\boldsymbol{\alpha}''. \end{cases}$$

---

[1]describing a pair of two indipendent two-mode squeezing states.

So the input modes are related at the output modes by the simple transformation

$$\begin{cases} \boldsymbol{\alpha}'' = \sqrt{T_{th}}\boldsymbol{\alpha}' - \sqrt{R_{th}}\boldsymbol{\tau}, \\ \boldsymbol{\tau}' = \sqrt{T_{th}}\boldsymbol{\tau} + \sqrt{R_{th}}\boldsymbol{\alpha}'. \end{cases} \tag{11.2}$$

Using the trasformations (11.2), the characteristic function (11.1), after the four thermal beam splitters BS_{th}, depend on $\boldsymbol{\alpha}'$ and $\boldsymbol{\tau}$, and it becomes

$$\boldsymbol{\chi}_{postTBS}\left(\boldsymbol{\alpha}';\boldsymbol{\tau}\right) = \boldsymbol{\chi}''\left(\sqrt{T_{th}}\boldsymbol{\alpha}' - \sqrt{R_{th}}\boldsymbol{\tau}\right)$$
$$\times \boldsymbol{\chi}_{th}\left(\sqrt{T_{th}}\boldsymbol{\tau} + \sqrt{R_{th}}\boldsymbol{\alpha}'\right).$$

Tracing out the thermal state by putting $\boldsymbol{\tau} = \boldsymbol{0}$, we have

$$\begin{aligned} \boldsymbol{\chi}'\left(\boldsymbol{\alpha}'\right) &= \boldsymbol{\chi}_{postTBS}\left(\boldsymbol{\alpha}';\boldsymbol{0}\right) \\ &= \boldsymbol{\chi}''\left(\sqrt{T_{th}}\boldsymbol{\alpha}'\right)\boldsymbol{\chi}_{th}\left(\sqrt{R_{th}}\boldsymbol{\alpha}'\right). \end{aligned} \tag{11.3}$$

The photon losses are introduced through other four beam splitters, VBS (V for "vacuum"), with transmissivity[2] $T_\ell\,(=1-R_\ell)$, in which each second port is occupied by the vacuum,

$$\boldsymbol{\chi}_k^{vac}\left(\boldsymbol{v}_k'\right) = \exp\left\{-\frac{1}{2}|v_k'|^2\right\}, \tag{11.4}$$

with $\boldsymbol{v}_k' = (v_k', v_k^{*\prime})$. So the overall vacuum characteristic function is $\boldsymbol{\chi}_{vac}\left(\boldsymbol{v}'\right) = \prod_{k=1}^4 \boldsymbol{\chi}_k^{vac}\left(\boldsymbol{v}_k'\right)$. The overall characteristic function before of the vacuum beam splitters, $\boldsymbol{\chi}_{preVBS}$, is given by

$$\boldsymbol{\chi}_{preVBS}\left(\boldsymbol{\alpha}';\boldsymbol{v}'\right) = \boldsymbol{\chi}'\left(\boldsymbol{\alpha}'\right)\boldsymbol{\chi}_{vac}\left(\boldsymbol{v}'\right). \tag{11.5}$$

In this case, the $SU(2)$ transformation gives the relations:

$$\begin{cases} \boldsymbol{\alpha} = \sqrt{T_\ell}\boldsymbol{\alpha}' + \sqrt{R_\ell}\boldsymbol{v}', \\ \boldsymbol{v} = \sqrt{T_\ell}\boldsymbol{v}' - \sqrt{R_\ell}\boldsymbol{\alpha}', \end{cases} \tag{11.6}$$

$$\begin{cases} \boldsymbol{\alpha}' = \sqrt{T_\ell}\boldsymbol{\alpha} - \sqrt{R_\ell}\boldsymbol{v}, \\ \boldsymbol{v}' = \sqrt{T_\ell}\boldsymbol{v} + \sqrt{R_\ell}\boldsymbol{\alpha}, \end{cases} \tag{11.7}$$

so, at the output of the beam splitters VBS, under the traformations (11.7) the characteristic function (11.5) becomes

$$\boldsymbol{\chi}_{postVBS}\left(\boldsymbol{\alpha};\boldsymbol{v}\right)$$
$$= \boldsymbol{\chi}'\left(\sqrt{T_\ell}\boldsymbol{\alpha} - \sqrt{R_\ell}\boldsymbol{v}\right)\boldsymbol{\chi}_{vac}\left(\sqrt{T_\ell}\boldsymbol{v} + \sqrt{R_\ell}\boldsymbol{\alpha}\right).$$

---

[2]For $T_\ell = 1$ we obtain the ideal state.

Tracing out the vacuum state $(\boldsymbol{v} = \boldsymbol{0})$, we have

$$
\begin{aligned}
\boldsymbol{\chi}(\boldsymbol{\alpha}) &= \boldsymbol{\chi}'\left(\sqrt{T_\ell}\boldsymbol{\alpha}\right)\boldsymbol{\chi}_{vac}\left(\sqrt{R_\ell}\boldsymbol{\alpha}\right) \\
&= \boldsymbol{\chi}''\left(\sqrt{T_{th}T_\ell}\boldsymbol{\alpha}\right)\boldsymbol{\chi}_{th}\left(\sqrt{R_{th}T_\ell}\boldsymbol{\alpha}\right) \\
&\qquad\qquad\qquad\qquad\qquad \times \boldsymbol{\chi}_{vac}\left(\sqrt{R_\ell}\boldsymbol{\alpha}\right)
\end{aligned}
$$

Considering the transformation by BS_I and BS_{II} for the complex variables $\boldsymbol{\alpha} = (\boldsymbol{\alpha}_1; \boldsymbol{\alpha}_2; \boldsymbol{\alpha}_3; \boldsymbol{\alpha}_4)$ (see Fig. 7.2)

$$
\begin{cases}
\boldsymbol{\alpha}_1 = \sqrt{T_1}\boldsymbol{\beta}_1 - \sqrt{R_1}\boldsymbol{\beta}_3, \\
\boldsymbol{\alpha}_3 = \sqrt{T_1}\boldsymbol{\beta}_3 + \sqrt{R_1}\boldsymbol{\beta}_1,
\end{cases}
$$
$$
\begin{cases}
\boldsymbol{\alpha}_2 = \sqrt{T_2}\boldsymbol{\beta}_2 - \sqrt{R_2}\boldsymbol{\beta}_4, \\
\boldsymbol{\alpha}_4 = \sqrt{T_2}\boldsymbol{\beta}_4 + \sqrt{R_2}\boldsymbol{\beta}_2,
\end{cases}
$$

the characteristic function $\boldsymbol{\chi}(\boldsymbol{\alpha})$ of the four modes $1, 2, 3, 4$, is given by

$$
\begin{aligned}
&\boldsymbol{\chi}_{1234}\left(\boldsymbol{\beta}_1; \boldsymbol{\beta}_2; \boldsymbol{\beta}_3; \boldsymbol{\beta}_4\right) \\
&= \boldsymbol{\chi}\left(\sqrt{T_1}\boldsymbol{\beta}_1 - \sqrt{R_1}\boldsymbol{\beta}_3; \sqrt{T_2}\boldsymbol{\beta}_2 - \sqrt{R_2}\boldsymbol{\beta}_4;\right. \\
&\qquad\quad \left.\sqrt{T_1}\boldsymbol{\beta}_3 + \sqrt{R_1}\boldsymbol{\beta}_1; \sqrt{T_2}\boldsymbol{\beta}_4 + \sqrt{R_2}\boldsymbol{\beta}_2\right).
\end{aligned} \tag{11.8}
$$

The density matrix of the characteristic function $\boldsymbol{\chi}_{1234}\left(\boldsymbol{\beta}_1; \boldsymbol{\beta}_2; \boldsymbol{\beta}_3; \boldsymbol{\beta}_4\right)$ is thus given by

$$
\begin{aligned}
\rho_{1234} \\
&= \frac{1}{\pi^4}\int d^2\boldsymbol{\beta}_1 d^2\boldsymbol{\beta}_2 d^2\boldsymbol{\beta}_3 d^2\boldsymbol{\beta}_4 \boldsymbol{\chi}_{1234}\left(\boldsymbol{\beta}_1; \boldsymbol{\beta}_2; \boldsymbol{\beta}_3; \boldsymbol{\beta}_4\right) \\
&\qquad\qquad\qquad \times \hat{D}_1\left(-\beta_1\right)\hat{D}_2\left(-\beta_2\right)\hat{D}_3\left(-\beta_3\right)\hat{D}_4\left(-\beta_4\right).
\end{aligned}
$$

However, we note that, at the optical frequency, $\hbar\omega$ is always in the range 1.5 to $2.5eV$, so at the enviroment temperature $T \simeq 300K$, the average number $\bar{n}_{th}$ is about 10^{-30}. The value of the $\bar{n}_{th}$ is very smaller compared at the the average number of photons introduced by the other operators involved. For this reason, we have neglected the thermal contribute to decoherence.

CHAPTER 12

APPENDIX C

Postselection: single-photon projector

When a post-selection strategy is applied by using coincidence photodetection, in the ideal case the conditional measurements of simultaneous detections of single photons in mode 3 and 4 project the density matrix ρ_{1234} into

$$\rho_T^{(|1><1|)}$$

$$\equiv \frac{1}{\mathcal{N}_T^{(|1><1|)}} \text{Tr}_{34} \left[\rho_{1234} \otimes {}_3|1><1|_3 \otimes {}_4|1><1|_4 \right]$$

$$= \frac{1}{\mathcal{N}_T^{(|1><1|)} \pi^4} \int d^2\boldsymbol{\beta}_1 d^2\boldsymbol{\beta}_2 d^2\boldsymbol{\beta}_3 d^2\boldsymbol{\beta}_4$$

$$\times \boldsymbol{\chi}_{1234} (\boldsymbol{\beta}_1; \boldsymbol{\beta}_2; \boldsymbol{\beta}_3; \boldsymbol{\beta}_4) \hat{D}_1 (-\beta_1) \hat{D}_2 (-\beta_2)$$

$$\text{Tr}_{34} \left[\hat{D}_3 (-\beta_3) \hat{D}_4 (-\beta_4)_3 |1><1|_{3\ 4}|1><1|_4 \right]$$

$$= \frac{1}{\mathcal{N}_T^{(|1><1|)} \pi^2} \int d^2\boldsymbol{\beta}_1 d^2\boldsymbol{\beta}_2 \mathcal{M} (\boldsymbol{\beta}_1; \boldsymbol{\beta}_2) \hat{D}_1 (-\beta_1) \hat{D}_2 (-\beta_2)$$

where

$$\mathcal{M} (\boldsymbol{\beta}_1;\ \boldsymbol{\beta}_2)$$

$$\equiv \frac{1}{\pi^2} \int d^2\boldsymbol{\beta}_3 d^2\boldsymbol{\beta}_4 \boldsymbol{\chi}_{1234} (\boldsymbol{\beta}_1; \boldsymbol{\beta}_2; \boldsymbol{\beta}_3; \boldsymbol{\beta}_4)$$

$$\times \chi_3^{(|1>)} (\boldsymbol{\beta}_3) \chi_4^{(|1>)} (\boldsymbol{\beta}_4),$$

and[1]

$$\chi_k^{(|1><1|)} (\boldsymbol{\beta}_k) = \text{Tr}_k \left[\hat{D}_l (-\beta_l)_3 |1><1|_3 \right]$$

$$= \left(1 - |\beta_k|^2 \right) e^{-|\beta_k|^2/2} \quad \text{for } k = 3, 4,$$

is the characteristic function of the single-photon projector, $_k|1><1|_k$, acting on the $k-$th mode. The normalization constant $\mathcal{N}_T^{(|1><1|)}$ is given by

$$\mathcal{N}_T^{(|1\rangle\langle1|)} = \text{Tr}_{1234} \left[\rho_{1234} \otimes {}_3 |1\rangle \langle1|_3 \otimes {}_4 |1\rangle \langle1|_4 \right].$$

---

[1] $< m|D (-\alpha) |n > = \left(\frac{n!}{m!} \right)^{1/2} \alpha^{m-n} e^{-|\alpha|^2/2} L_n^{m-n} \left(|\alpha|^2 \right)$, and $L_1^0 (x) = L_1 (x) = 1 - x$.

In conclusion, we have

$$
\begin{aligned}
\boldsymbol{\chi}_T^{(|1\rangle\langle 1|)}\left(\boldsymbol{\gamma}_1, \boldsymbol{\gamma}_2\right) &= \frac{1}{\mathcal{N}_T^{(|1\rangle\langle 1|)}} \mathrm{Tr}_{12}\left[\rho_{12}\hat{D}_1\left(\gamma_1\right)\hat{D}_2\left(\gamma_2\right)\right] \\
&= \frac{1}{\mathcal{N}_T^{(|1\rangle\langle 1|)}\pi^2}\int d^2\boldsymbol{\beta}_1 d^2\boldsymbol{\beta}_2 \mathcal{M}\left(\boldsymbol{\beta}_1; \boldsymbol{\beta}_2\right) \\
&\times \mathrm{Tr}_{12}\left[\hat{D}_1\left(\gamma_1\right)\hat{D}_1\left(-\beta_1\right)\hat{D}_2\left(\gamma_2\right)\hat{D}_2\left(-\beta_2\right)\right] \\
&= \frac{1}{\mathcal{N}_T^{(|1\rangle\langle 1|)}}\mathcal{M}\left(\gamma_1; \gamma_2\right).
\end{aligned}
$$

Postselection: realistic on/off operator (POVM)

A realistic on/off detector is described by a positive operator-valued measure (POVM), Eq.(7.16). The detection $on-$POVM gives

$$
\begin{aligned}
\rho_T^{(on)} &= \frac{\mathrm{Tr}_{34}\left[\rho_{1234}\otimes\hat{\Pi}_3^{(on)}\left(\eta_3\right)\otimes\hat{\Pi}_4^{(on)}\left(\eta_4\right)\right]}{\mathcal{N}_T^{(on)}} \\
&= \frac{1}{\mathcal{N}_T^{(on)}\pi^4}\times \\
\int d^2\boldsymbol{\beta}_1 d^2\boldsymbol{\beta}_2 d^2\boldsymbol{\beta}_3 d^2\boldsymbol{\beta}_4 &\boldsymbol{\chi}_{1234}\left(\boldsymbol{\beta}_1; \boldsymbol{\beta}_2; \boldsymbol{\beta}_3; \boldsymbol{\beta}_4\right)\hat{D}_1\left(-\beta_1\right)\hat{D}_2\left(-\beta_2\right)\times \\
\mathrm{Tr}_{34}&\left[\hat{D}_3\left(-\beta_3\right)\hat{D}_4\left(-\beta_4\right)\hat{\Pi}_3^{(on)}\left(\eta_3\right)\hat{\Pi}_4^{(on)}\left(\eta_4\right)\right] \\
&= \frac{1}{\mathcal{N}_T^{(on)}\pi^4}\int d^2\boldsymbol{\beta}_1 d^2\boldsymbol{\beta}_2 \mathcal{M}\left(\boldsymbol{\beta}_1; \boldsymbol{\beta}_2\right)\times \hat{D}_1\left(-\beta_1\right)\hat{D}_2\left(-\beta_2\right),
\end{aligned}
$$

where

$$
\mathcal{M}\left(\boldsymbol{\beta}_1; \boldsymbol{\beta}_2\right) = \frac{1}{\mathcal{N}_T^{(on)}\pi^2}\int d^2\boldsymbol{\beta}_3 d^2\boldsymbol{\beta}_4 \boldsymbol{\chi}_{1234}\left(\boldsymbol{\beta}_1; \boldsymbol{\beta}_2; \boldsymbol{\beta}_3; \boldsymbol{\beta}_4\right)\times\chi_3^{on}\left(\boldsymbol{\beta}_3\right)\chi_4^{on}\left(\boldsymbol{\beta}_4\right).
$$

Here

$$
\chi_k^{on}\left(-\boldsymbol{\beta}_l\right) \equiv \mathrm{Tr}_k\left[\hat{D}_k\left(-\beta_k\right)\Pi_k^{(on)}\right] = \pi\delta^{(2)}\left(\beta_k\right)-\frac{1}{\eta_k}\exp\left\{-\frac{2-\eta_k}{2\eta_k}|\beta_k|^2\right\} = \chi_k^{on}\left(\boldsymbol{\beta}_k\right)
$$

is the characteristic function of the POVM of the photodetector of the modes $k = 3, 4$, and

$$
\mathcal{N}_T^{(on)} = \mathrm{Tr}_{1234}\left[\rho_{1234}\otimes\hat{\Pi}_3^{(on)}\left(\eta_3\right)\otimes\hat{\Pi}_4^{(on)}\left(\eta_4\right)\right].
$$

The characteristic function obtained by the density matrix $\rho_T^{(on)}$ is

$$\boldsymbol{\chi}_T^{(on)}\left(\boldsymbol{\gamma}_1;\boldsymbol{\gamma}_2\right)$$

$$= \frac{1}{\mathcal{N}_T^{(on)}}\mathrm{Tr}_{12}\left[\rho_{12}\hat{D}_1\left(\gamma_1\right)\hat{D}_2\left(\gamma_2\right)\right]$$

$$\frac{1}{\mathcal{N}_T^{(on)}\pi^2}\int d^2\boldsymbol{\beta}_1 d^2\boldsymbol{\beta}_2\mathcal{M}\left(\boldsymbol{\beta}_1;\boldsymbol{\beta}_2\right)\times\mathrm{Tr}_{12}\left[\hat{D}_1\left(-\beta_1\right)\hat{D}_2\left(-\beta_2\right)\hat{D}_1\left(\gamma_1\right)\hat{D}_2\left(\gamma_2\right)\right]$$

$$= \frac{1}{\mathcal{N}_T^{(on)}\pi^2}\mathcal{M}\left(\gamma_1;\gamma_2\right).$$

In terms of the $\boldsymbol{\beta}_1$ and $\boldsymbol{\beta}_2$, we have

$$\boldsymbol{\chi}_T^{(on)}\left(\boldsymbol{\beta}_1;\boldsymbol{\beta}_2\right)$$

$$= \frac{1}{\mathcal{N}_T^{(on)}\pi^2}\int d^2\boldsymbol{\beta}_3 d^2\boldsymbol{\beta}_4 \boldsymbol{\chi}_{1234}\left(\boldsymbol{\beta}_1;\boldsymbol{\beta}_2;\boldsymbol{\beta}_3;\boldsymbol{\beta}_4\right)$$

$$\times\chi_3^{on}\left(\boldsymbol{\beta}_3\right)\chi_4^{on}\left(\boldsymbol{\beta}_4\right)$$

$$= \frac{1}{\mathcal{N}_T^{(on)}}\left[\boldsymbol{\chi}_{1234}\left(\boldsymbol{\beta}_1;\boldsymbol{\beta}_2;\mathbf{0};\mathbf{0}\right)\right.$$

$$+\frac{1}{\pi}\int d^2\boldsymbol{\beta}_4\boldsymbol{\chi}_{1234}\left(\boldsymbol{\beta}_1;\boldsymbol{\beta}_2;\mathbf{0};\boldsymbol{\beta}_4\right)\mathcal{G}_4\left(\beta_4\right)$$

$$+\frac{1}{\pi}\int d^2\boldsymbol{\beta}_3\boldsymbol{\chi}_{1234}\left(\boldsymbol{\beta}_1;\boldsymbol{\beta}_2;\boldsymbol{\beta}_3;\mathbf{0}\right)\mathcal{G}_3\left(\beta_3\right)$$

$$\left.+\frac{1}{\pi^2}\int d^2\boldsymbol{\beta}_3 d^2\boldsymbol{\beta}_4\boldsymbol{\chi}_{1234}\left(\boldsymbol{\beta}_1;\boldsymbol{\beta}_2;\boldsymbol{\beta}_3;\boldsymbol{\beta}_4\right)\mathcal{G}_3\left(\beta_3\right)\mathcal{G}_4\left(\beta_4\right)\right],$$

where

$$\mathcal{G}_k\left(\beta_k\right) = -\frac{1}{\eta_k}\exp\left\{-\frac{2-\eta_k}{2\eta_k}|\beta_k|^2\right\}.$$
$$\left(k=3,4\right).$$

BIBLIOGRAPHY

[1] A. Einstein, B. Podolsky, and N. Rosen, Phys. Rev. 47 777 1935, *Can Quantum-Mechanical Description of Physical Reality Be Considered Complete?*;

[2] E. Schrodinger, Proc Cambridge Phylos. Soc 32, 446 (1936), *Probability relations between separated systems*;

[3] M. M. Wolf, G. Giedke, and J. I. Cirac, Phys. Rev. Lett. 96 (2006), *Extremality of Gaussian Quantum States*;

[4] F. Dell'Anno, S. De Siena, L. Albano, and F. Illuminati, Phys. Rev. A 76, 022301 (2007), *Continuous-variable quantum teleportation with non-Gaussian resources*;

[5] F. Dell'anno, S. De Siena, F. Illuminati, Phys. Rev. A 81, 012333 (2010), *Realistic continuous-variable quantum teleportation with non-Gaussian resources*;

[6] D. Buono, G. Nocerino, A. Porzio and S. Solimeno, Phys. Rev. A 86, 042308 (2012), *Experimental analysis of decoherence in continuous-variable bipartite system*;

[7] D. Buono, G. Nocerino, V. D'Auria, A. Porzio, S. Olivares, and M. G. A. Paris, J. Opt Soc. Am B 27, A110 (2010), *Quantum characterization of bipartite Gaussian states*;

[8] G.Nocerino, D. Buono, A. Porzio and S. Solimeno, Physica Scripta inpress. *Survival of continuous variable entanglement over long distances*;

[9] In preparation;

[10] In preparation;

[11] F. Dell'Anno, D. Buono, G, Nocerino, S. De Siena and F. Illuminati, next submission, *Realistic entanglement swapping with non-Gaussian resources*;

[12] D. Buono, G, Nocerino, F. Dell'Anno, S. De Siena, A. Porzio and F. Illuminati, next submission, *Tunable non Gaussian resources by ancillary squeezing and conditioning. I. Basic scheme of generation and preliminary analysis*;

[13] E. Progovecki, Can. J. Phys. 45, 2173 (1967), *On a theory of measurement of incompatible observables in quantum mechanics*;

[14] L. E. Ballentine, Rev. Mod. Phys. 42, 4, (1970), *The Statistical Interpretation of Quantum Mechanics.*

[15] H. J. Carmichael, Statistical Method in quantum optics 1, (Springer, Berlin, 1999);

[16] M. G. Genoni, M. G. A. Paris, Phys Rev A 82, 052341 (2010), *Quantifying non-Gaussianity for quantum information*;

[17] M. G. Genoni, M. G. A. Paris and K. Banaszek, Phys. Rev. A. 76, 042327 (2007), *Measure of the non-Gaussian character of a quantum state*;

[18] A. Serafini, F. Illuminati, M. G. A. Paris and S. De Siena, Phys. Rev. A 69, 022318 (2004*),Entanglement and purity of two-mode Gaussian states in noisy channels*;

[19] H.-P. Breur, F. Petruccione, *The Theory of open quantum systems*, Oxford University Press (2002);

[20] E. H. Kennard, ZZ. Phys. 44 326-52 (1927), *Zur quantenmechanik einfacher Bewegungstypen*;

[21] H. Weyl, Theory of Groups and quantum Mechanics (New York: Dutton), pp 77, 393-4, (1928);

[22] L. Mandelstam and I. Tamm, J. Physique (USSR) 9, 249-54, *The uncertainty relation between energy and time in nonrelativistic quantum mechanics*, (1945);

[23] A. Furusawa, J. L. Soresen, S. L. Braunstein, A. A. Fuchs, H. J. Kimble, E. S. Polzik, Science 282, 706 (1998), *Unconditional Quantum Teleportation*;

[24] H. Ollivier and. W. H. Zurek, Phys. Rev. Lett 88, n 1(2002), *Quantum Discord: A Measure of the Quantumness of Correlations*;

[25] W. H. Zurek, Ann. Phys. (Leipzig) 9 (2000), 855-864, *Einselection and Dechoerence from an Information Theory Perspecive*;

[26] M. Horodechi, Quantum Information and Computation, vol. 1, n 1 (2001), 3-26;

[27] Sandu Popescu, Daniel Rohrlich, Phys. Rev. A 56 (1997), 3319, *Thermodynamics and the measure of entanglement* ;

[28] I. Bengtsson and K. Zyczkowski, *Geometry of Quantum States*, Cambridge University Press, 2006;

[29] C. H. Bennett, D. P DiVincenzo, J. A. Smolin, and W. K. Wootters, Phys. Rev. A 54 3824 (1996), *Mixed-state entanglement and quantum error correction*; S. Popescu, and D. Rohrlich, Phys. Rev. A 56 3319 (1997), *Thermodynamics and the measure of entanglement*; V. Vedral, M. B. Plenio, M. A Rippin, and P. L. Knight, Phys. Rev. Lett. 78 2275 (1997), *Quantifying entanglement*; G. Vidal, J. Mod. Opt. 47 355 (2000), *Entanglement monotones*;

M. Horodecki, P. Horodecki, andR. Horodecki, Phys. Rev. Lett. 84: 2014 (2000), *Limits for entanglement measures*;

[30] G. Vidal, R. F. Werner, Phys Rev A 65 032314 (2002), *Computable Measurement of Entanglement*;

[31] P. Horodecki, Phys. Lett. A 232, 333 (1997), *Separability criterion and inseparable mixed states with positive partial transposition*;

[32] R. Simon, Phys Rev Lett, 84, 12 (2000), *Peres-Horodecki Separability Criterion for Continuous Variable Systems*;

[33] L- M Duan, G. Giedke, J. I. Cirac, and P. Zoller, Phys. Rev. Lett 84, 12, (2000), *Inseparability Criterion for Continuous Variable Systems*;

[34] U. Leonhardt and H. Paul, Phys. Rev. A **48**, 4598 (1993);

[35] D. Walls and G. Milburn, *Quantum Optics* (Berlin, Springer, 1994);

[36] A. Serafini, M. G. A. Paris, F. Illuminati, and S. De Siena, J. Opt. B: Quantum Semiclass. Opt. **7**, R19 (2005), *Quantifying decoherence in continuous variable systems*;

[37] W. P. Bowen, N. Treps, B. C. Buchler, R. Schnabel, T. C. Ralph, T. Symul, and P. K. Lam, IEEE J. Sel. Top. Quant. **9**, 1519 (2003);

[38] E. G. Cavalcanti, S. J. Jones, H. M. Wiseman, and M. Reid, Phys Rev Aa 80 032112 (2009), *Experimental criteria for steering and Einstein-Podolsky-Rosen paradox*;

[39] M. D. Reid, Phys Rev. A 40, n.2 (1989), *Demonstration of the Einstein-Podolsky-Rosen paradox using nondegenerate prametric amplification*;

[40] J. Bell, Physics 1, 195 (1964), *On the Einstein Poldoski Rosen Paradox*;

[41] H. M. Wiseman, S. J. Jones, and A. C. Doherty, Phys. Rev. Lett. 98 140402 (2007), *Steering, Entanglement, Nonlocality, and the Einstein-Podolsky-Rosen Pradox*;

[42] D. Bohm, *Quantum Theory*, Chapter 22, Prentice-Hall, Englewood Cliffs, NJ, 1951;

[43] J. F. Clauser, M. A. Horne, A. Shimony and R. A. Holt, ,*Proposed experiment to test local hidden-variable theories*;

[44] Zeng-Bing Chen, Jian-Wei Pan, Guang Hou, and Yong-De Zhang, Phys. Rev. Lett 88 (2002), *Maximal Violation of Bell's Inequalitues for Continuous Variable Systems*;

[45] Stefano Olivares and Matteo Paris, J. Opt. B: Quantum Semiclass. Opt 7 S392 (2005), *Photon subtracted states and enhancement of nonlocality in the presence of noise*;

[46] Stefano Olivares and Matteo Paris, Phys. Rev. A 70, 032112 (2004), *Enhancement of nonlocality in phase space*;

[47] J. S. Bell, *Speakable and Unspeakable in Quantum Mechanics*, Cambridge University Press, Cambridge, England, 1987), chap. 21;

[48] K. Banaszek and K. Wodkievicz, Phys. Rev. A 58, 4345 (1998), *Nonlocality of the Einstein-Podolsky-Rosen state in the Wigner representation*;

[49] L. Vaidman, Phys. Rev. A **49**, 1473 (1994), *Teleportation of quantum states*; S. L. Braunstein and H. J. Kimble, Phys. Rev. Lett. **80**, 869 (1998), *Teleportation of Continuous Quantum Variables*;

[50] S. Pirandola and S. Mancini, Laser Physics 16, 10 2006, *Quantum Teleportation with Continuous Variables: A Survey*;

[51] M. Horodecki, P. Horodecki, R. Horodecki, Phys Lett.A 223 (1996), *Separability of mixed state: necessary and sufficient conditions*;

[52] V. Vedral and M. B. Plenio, Phys. Rev. A **57**, 1619 (1998), *Entanglement measures and purification procedures*;

[53] Gerardo Adesso, Alessio Serafini, and Fabrizio Illuminati, **92**, 087901 (2004), *Determination of continuous variable entanglement by purity measurements*;

[54] V. D'auria, S. Fornaro, A. Porzio, E.A. Sete, and S. Solimeno, Appl. Phys. B **91**, 309 (2008), C*haracterization of Gaussian bipartite entangled states by a single homodyne detector*;

[55] Virginia D'Auria, Antonino Chiummo, Martina De Laurentis, Alberto Porzio, and Salvatore Solimeno, Opt. Express **13**, 948 (2005), T*omographic characterization of OPO sources close to threshold*;

[56] Virginia D'Auria, Alberto Porzio, Salvatore Solimeno, Stefano Olivares, and Matteo G A Paris, J. Opt. B: Quantum Semiclass. Opt. **7** S750 (2005), *Characterization of bipartite states using a single homodyne detector*;

[57] Alberto Porzio, Virginia D'Auria, Salvatore Solimeno, Stefano Olivares, and Matteo G.A. Paris, Int. J. .Quantum Information, **5**, 63 (2007), *Homodyne Characterization of Continuous Variable Bipartite States*;

[58] V. D'Auria, S. Fornaro, A. Porzio, S. Solimeno, S. Olivares, and M.G.A. Paris, Phys. Rev. Lett. **102**, 020502 (2009), *Full Characterization of Gaussian Bipartite Entangled States by a Single Homodyne Detector*;

[59] J. Řeháček, S. Olivares, D. Mogilevtsev, Z. Hradil, M. G. A. Paris, S. Fornaro,

V. D'Auria, A. Porzio, and S. Solimeno, Phys. Rev A **79**, 032111 (2009), *Effective method to estimate multidimensional Gaussian states*;

[60] M. Gu, H. M. Chrzanowski, S. M. Assad, T. Symul, K. Modi, T. C. Ralph, V. Vedral, and P. K. Lam, Nat. Physics **8**, 671 (2012), *Observing the operational significance of discord consumption*;

[61] Rémi Blandino, Marco G. Genoni, Jean Etesse, Marco Barbieri, Matteo G.A. Paris, Philippe Grangier, and Rosa Tualle-Brouri, arXiv:1203.1127v3 [quant-ph] 11 Jun 2012, *Homodyne estimation of Gaussian quantum discord*;

[62] L. S. Madsen, A. Berni, M. Lassen, and U. L. Andersen, Phys. Rev. Lett. **109**, 030402 (2012), *Experimental Investigation of the Evolution of Gaussian Quantum Discord in an Open System*;

[63] S. Popescu, D. Rohrlich, Phys. Lett. A 166 (1992), 293-297, *Generic quantum nonlocality*;

[64] H. Jeong, J. Lee, and M. S. Kim, Phys Rev A 61 052101, *Dynamics of nonlocality for two-mode squeezed state in a thermal enviroment*;

[65] R. F. Werner, Phys Rev A 40, 4277 (1989), *Quantum states with Einstein-Podolsky-Rosen correlations admitting a hidden-variable model*;

[66] N. Gisin, and A. Peres, Phys Rev A 162, 15 (1998), *Maximal violation of Bell's inequality for arbitrarily large spin*;

[67] S. Olivares, M. G. A. Paris, and R. Bonifacio, Phys. Rev. A 67, 032314 (2003), *Teleportation improvement by inconclusive photon subtraction*;

[68] V D'Auria, C de Lisio, A Porzio, S Solimeno and Matteo G A Paris, J. Phys. B **39**, 1187 (2006), T*ransmittivity measurements by means of squeezed vacuum light*;

[69] P. Marian and T. A. Marian, Phys. Rev. A 74, 042306 (2006), *Continuous-variable teleportation in the characteristic-function description*;

[70] Sebastian Steinlechner, Jöran Bauchrowitz, Tobias Eberle, Roman Schnabel, *Strong continuous variable EPR-steering with a detection efficiency above 96%* arXiv:1112.0461 (2011).

[71] V. D'Auria, C. de Lisio, A. Porzio, S. Solimeno, J. Anwar, M. G. A. Paris, Phys. Rev. A 81, 033846 (2010), *Non-Gaussian states produced by close-to-threshold optical parametric oscillators:role of classical and quantum fluctuations*;

[72] R. Graham and H. Haken, Z. Phys. **210**, 276 (1968), *The quantum-fluctuations of the Optical Parametric Oscillator I*; R. Graham, Z. Phys. **210**, 319 (1968), *The quantum-fluctuations of the Optical Parametric Oscillator II*;

[73] S. Chaturwedi, K. Dechoum and P. D. Drummond, Phys. Rev. A **65**, 033805 (2002), *Limits to squeezing in the degenerate optical parametric oscillator*; P. D. Drummond, K. Dechoum, S. Chaturwedi, Phys. Rev. A **65**, 033806 (2002), *Critical quantum fluctuations in the degenerate parametric oscillator*; K. Dechoum, P. D. Drummond, S. Chaturvedi, M. D. Reid, Phys. Rev. A 70, 053807 (2004), *Critical fluctuations and entanglement in the nondegenerate parametric oscillator*;

[74] M. D. Reid and P. D. Drummond, Phys. Rev. Lett. **60**, 2731 (1988); M. D. Reid and P. D. Drummond, Phys. Rev. A **40**, 4493 (1989), *Correlations in nondegenerate parametric oscillation: Squeezing in the presence of phase diffusion*; P. D. Drummond and M. D. Reid, Phys. Rev. A **41**, 3930 (1990), *Correlations in nondegenerate parametric oscillation. II. Below threshold results*;

[75] M. G. A. Paris, F. Illuminati, A. Serafini and S. De Siena, Phys. Rev. A 68, 0123144 (2003), *Purity of Gaussian states: Measurement schemes and time evolution in noisy channels*;

[76] A. Peres, Phys. Rev Lett. 77, 1413 (1998), *Separability Criterion for Density Matrices*;

[77] M. Lewenstein, D. Bruss, J. I. Cirac, B. Kraus, M. Kus, J. Samsonowicz, A. Sanpera, R. Tarrach, Journal of Modern Optics, 47, 2841 (2000), *Separability and distillability in composite quantum systems -a primer-*;

[78] H. F. Hofmann and S. Takeuchi, Phys. rev. A 68, 032103 (2003), *Violation of local uncertainty relations as a signature of entanglement*;